THESIS FOR THE DEGREE OF DOCTOR OF PHILOSOPHY

Colors of Life and Optoelectronics: Zinc Porphyrins for Light-Emitting Electrochemical Cells and Organic Photodetectors

MARIZA MONE

Department of Chemistry and Chemical Engineering

CHALMERS UNIVERSITY OF TECHNOLOGY

Gothenburg, Sweden 2020

Colors of Life and Optoelectronics: Zinc Porphyrins for Light-Emitting Electrochemical Cells and Organic Photodetectors

MARIZA MONE
ISBN 978-91-7905-401-4

Doktorsavhandlingar vid Chalmers tekniska högskola
Ny serie nr 4868
ISSN 0346-718X

Department of Some Subject or Technology
Chalmers University of Technology
SE-412 96 Gothenburg
Sweden
Telephone + 46 (0)31-772 1000

Cover:
Two hands are shown in the cover, which represent the light and the darkness. Between those hands a porphyrin is placed; since in this thesis porphyrin derivatives were used both for the emission of light as well as for its detection.

Chalmers Reproservice
Gothenburg, Sweden 2020

Colors of Life and Optoelectronics: Zinc Porphyrins for Light-Emitting Electrochemical Cells and Organic Photodetectors

MARIZA MONE

Department of Chemistry and Chemical Engineering
Chalmers University of Technology

Abstract

The field of organic optoelectronics constitutes an interdisciplinary field that covers chemistry, physics, materials science and biology. The technological promises of the organic materials over their inorganic counterparts include a lower production cost and the feasibility to be processed through solution-based techniques on large-area and/or flexible substrates. Among organic optoelectronic devices, two technologies are discussed in this thesis. Those are light emitting electrochemical cells (LECs) and photomultiplication (PM) type organic photodetectors (OPDs). The LEC is a light emitting technology that has attracted a lot of scientific interest due to its simple device architecture and fabrication. A category of LECs that is of high interest, are those LECs consisting of materials emitting near-infrared (NIR) light. This specific field is highly alluring, due to the unique applications NIR light can generate in a wide range of fields from medicine to optical communications. However, organic NIR emitters are inherently of lower efficiency when compared to other wavelengths, thus posing a challenge in material design. Hereof, an attempt was made in the context of this work to design and synthesize emitters that will produce light in the deep NIR region and in a functional LEC. The problem of high aggregation of NIR emitters was tackled by blending with appropriate host materials. On the other side, PM type OPDs aim in sensing and not in the production of light. The characteristic of this special category of OPDs is the possibility of enhancing the received weak signal without the need of external components in the device, like photomultiplier tubes. However, since this specific field is not mature yet, there is not adequate knowledge in material design. Thus, there is a need in discovering the materials that will lead to photomultiplication enabling the construction of more efficient devices in the future. In order to achieve all the accomplishments that will be discussed in this thesis, there was a category of molecules that was the heart of all studies. These molecules, often called as colors of life, due to their importance in many processes occurring in nature were porphyrins. Porphyrins are highly versatile motifs and were the tools that led both into production of deep NIR light but also into improving the detection of weak light.

Keywords: optoelectronics, light emitting electrochemical cell, photomultiplication, porphyrins, near-infrared, aggregation

LIST OF PUBLICATIONS

This thesis is based on the work contained in the following papers, referred to by their Roman numerals in the text. The papers are appended at the end of the thesis.

Paper I. Star-Shaped Diketopyrrolopyrrole–Zinc Porphyrin that Delivers 900 nm Emission in Light-Emitting Electrochemical Cells
Mariza Mone, Shi Tang, Petri Murto, Birhan A Abdulahi, Christian Larsen, Jia Wang, Wendimagegn Mammo, Ludvig Edman, Ergang Wang
Chemistry of Materials 2019, 31, 9721–9728

Paper II. Low-Gap Zinc Porphyrin as an Efficient Dopant for Photomultiplication Type Photodetectors
Mariza Mone, Kaixuan Yang, Petri Murto, Fujun Zhang, and Ergang Wang
Chem. Commun., 2020, 56, 12769-12772

Paper III. Near-Infrared Emission by Tuned Aggregation of a Porphyrin Compound in A Host-Guest Light-Emitting Electrochemical Cell
Mariza Mone, Shi Tang, Zewdneh Genene, Petri Murto, Martyn Jevric, Joan Ràfols-Ribé, Birhan A. Abdulahi, Jia Wang, Wendimagegn Mammo, Mats R. Andersson, Ludvig Edman, and Ergang Wang,
Submitted

CONTRIBUTION REPORT

Paper I. M.M Designed the porphyrin emitter and performed the synthesis and characterization: NMR, MALDI-TOF, TGA, and CV. Performed part of the optical characterization at Chalmers. B.A. synthesized the host PBDTSi-BDD polymer. P.M. performed the DFT calculations and S.T. fabricated the LEC devices. First author wrote the first draft of the manuscript and revised it with all coauthors.

Paper II. M.M. Designed the porphyrin dopant and performed the synthesis and characterization: NMR, MALDI-TOF and CV. Performed part of the optical characterization at Chalmers. P.M performed the DFT calculations and K.Y fabricated the PM type OPDs. First author wrote the first draft of the manuscript and revised it with all coauthors.

Paper III. M.M. Designed the porphyrin emitter and performed the synthesis and characterization: NMR,TGA, DSC and CV. Performed part of the optical characterization at Chalmers. Designed the PBDTSi-BDD-Py host and Z.G. synthesized it. M.J. synthesized the NT-Br_2 monomer. P.M performed the DFT calculations and S.T fabricated the LEC devices First author wrote the first draft of the manuscript and revised it with all coauthors.

PUBLICATIONS NOT INCLUDED IN THE THESIS

Paper

Structural engineering of pyrrolo[3,4-f]benzotriazole-5,7(2H,6H)-dione-based polymers for non-fullerene organic solar cells with an efficiency over 12%

Birhan A Abdulahi, Xiaoming Li, Mariza Mone, Bisrat Kiros, Zewdneh Genene, Shanlin Qiao, Renqiang Yang, Ergang Wang, Wendimagegn Mammo

Journal of Materials Chemistry A, 2019, 7, 19522–19530

TABLE OF CONTENTS

CHAPTER 1

1 INTRODUCTION

Optoelectronic devices, which can convert light-to-energy and vice versa, are without a doubt an integral component in a modernized world. We very much so use optoelectronic devices daily and they exist as functional components in many kinds of areas including (i) communication, where they can be used as optical transmitters or receivers,[1] (ii) medicine, in fields like photodynamic therapy and bioimaging,[2,3] (iii) entertainment, and many more. Optoelectronic devices based on organic semiconductors have attracted considerable attention arising from their intrinsic properties. Three of the most noteworthy advantages when comparing these to their inorganic counterparts include (i) the tuning of their optical, electrochemical and thermal properties due to their easy of chemical modification [4,5] (ii) their easy processability which is enabled by their improved solubility in organic solvents and (iii) and the possibility of their fabrication onto flexible substrates.

1.1 ORGANIC OPTOELECTRONICS IN A NUTSHELL

So how does the story of organic electronics start? Everything dates back to the 1950s, where Hideo Akamatu and Hiroo Inokuchi,[6] inspired by the electrical conductivity of carbon black and graphite, studied the electrical resistance of organic dyes violanthrone, iso-violanthrone, and pyranthrone after pressing them between two electrodes. Interestingly, they realized that when these dyes had been assembled in such a device, they had semiconducting properties similar to that seen in inorganic semiconductors. It was not until 1963, however, that electroluminescence, the phenomenon of the emission of light after the application of an external electric field, was observed by M. Pope *et al*. in organic small molecules.[7] Although reports describing semiconducting polymers have existed since the 1960s,[8] a revolution into the research of organic semiconductors was initiated in 1977, when Nobel awardees Hideki Shirakawa, Alan MacDiarmid, and Alan Heeger[9] introduced polymers to the world of organic semiconductors after exposing *trans*-polyacetylene to chlorine, bromine, and iodine vapors, to acquire the respective halogen doped materials. This led to materials with increased conductivity, even some seven orders of magnitude in the case of iodine. The first successful implementation of organic materials into electroluminescent devices was achieved in 1987. As mentioned earlier, electroluminescence in organic materials had been previously observed, however, the emission of light required the application of voltages in excess of 100 V. Tang and VanSlyke demonstrated a new revolutionary device configuration, later known as the light-emitting diode (OLED).[10] What differentiated their device to earlier constructs was the use of a double organic layer instead of only one, in this case using 8-hydroxyquinoline aluminum (Alq_3) and an aromatic diamine. They incorporated the diamine to serve to act as an electron blocking layer, therefore the recombination process of charges

to produce light was more controlled. With that design, they managed to obtain an external quantum efficiency (EQE) in the order of 1% at 550 nm with the application of a voltage <10 V. Here, the organic molecules incorporated in the emissive layer were vacuum deposited on top of one another. Unfortunately, this technique is not conducive to simple device fabrication on a large scale. This changed in 1990, when J. H. Burroughes *et al*. fabricated the first solution-processed polymer OLEDs that incorporated the yellow emissive conductive polymer poly(p-phenylene vinylene) (PPV) in a single layer device paving the way for more convenient processability.[11] In 1995, the addition of an electrolyte to this architecture lead to changes in the working principle of the current utilization for light-emitting devices.[12] That new device construct was itself named light-emitting electrochemical cell (LEC).

Since this thesis focuses mainly on LECs, it would be prudent to dedicate additional attention to the working principles of LECs and differentiating this technology from OLEDs, the current leading light-emitting technology. This discussion will include why LEC warrants further scientific attention, despite the fact they tend to be less efficient than OLED.

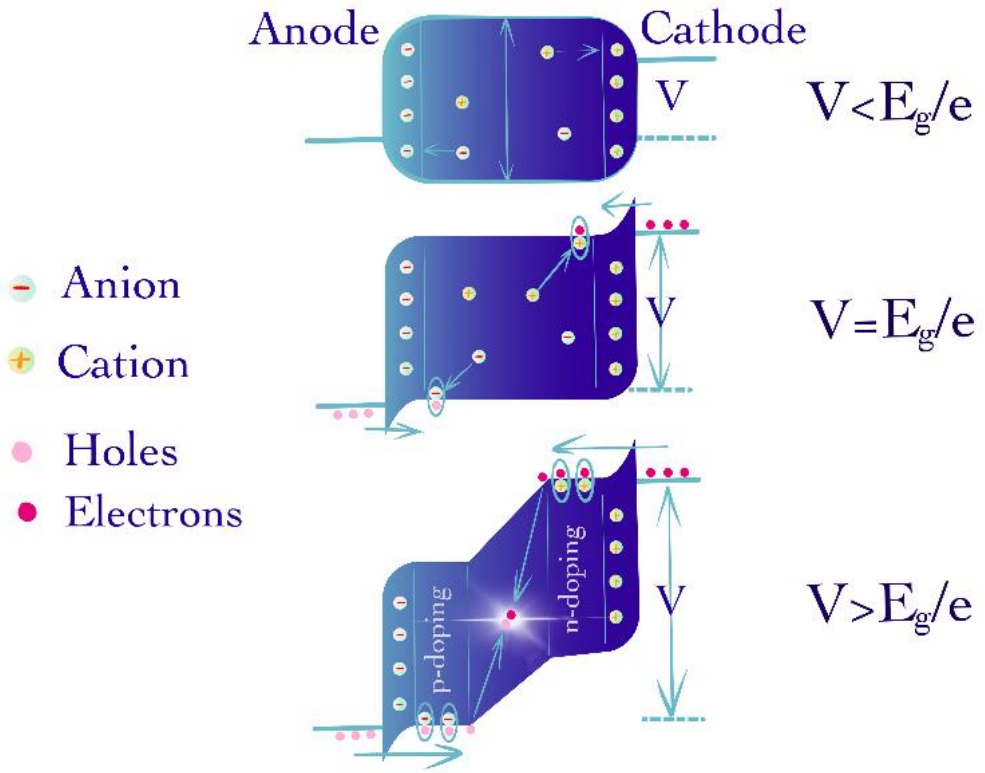

Figure 1.1. Working principle of an LEC; (top) the formation of electric double layers with the application of an external voltage (middle)bending of the energy levels and injection of holes and electrons; (bottom) formation of a p-n junction and recombination to form excitons.

The main steps involved in the operation of an OLED consist of (i) the injection of electrons and holes at the electrodes through the application of an external electric field, (ii) the migration of the electrons and holes toward one another, and (iii) the formation of excitons through the

combination of electrons and holes, which will in an ideal scenario recombine radiatively resulting in the production of a photon (light).[13] H**ow does an LEC device operate?** In order to explain that, it is easier if we look at **Figure 1.1**. An LEC device contains an electrolyte in the main emissive layer, and upon exposure to an external electric field charge separation of the electrolyte occurs as they migrate towards the respective electrodes. The ion drifting will result in the formation of thin films at the electrode interfaces, which are known as electric double layers (EDLs).[14] These extremely thin layers are endowed with a very high electric field, which are able to cause bending of the energy levels at the interfaces between the electrode and the active layer. When the applied voltage overcomes the energy gap potential of the semiconducting material, then injection of electrons and holes from the respective electrodes can occur. The injected electrons and holes will be compensated by the ions stemming from the electrolyte forming n- and p-type doped regions, respectively. The two initially small doped regions will gradually increase in size until they meet each other to form a p-n junction, a process that leads to increase of the cell´s conductivity and hereafter decreasing the voltage across the junction.[14,15] Finally, the injected charges will flow to the depletion region through the stabilized n- and p- doped region, where they will recombine forming excitons and subsequently decay, radiatively emitting photons.

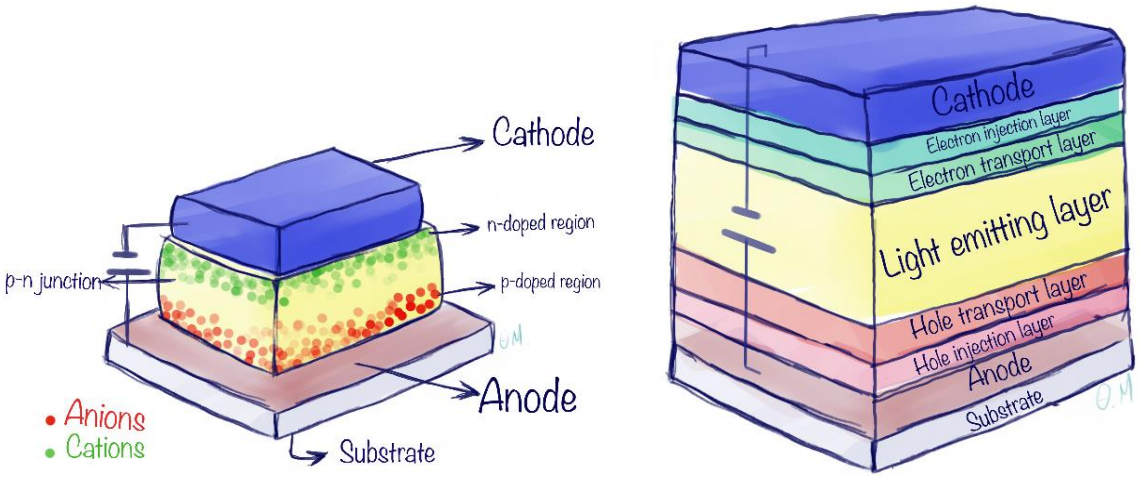

Figure 1.2. (left) Device architecture of an LEC and (right) a state-of-the-art OLED.

A striking difference between OLEDs and LECs can be found in their device architecture. **Figure 1.2** represents the configuration of a state-of-the-art LEC and OLED. The most obvious difference that one notices when looking at the illustration is the complexity of an OLED. An OLED contains, apart from the main emissive layer and the electrodes, a stack of extra layers of differing thicknesses, which include electron/hole injection layers and electron/hole charge transport layers, in addition to the active light emitting layer. In contrast, an LEC consists of a main emissive layer which is composed of a mixture of the photoactive species and an electrolyte, in conjunction with the electrodes. We should also mention the difference in the fabrication processes for both

technologies. Both LECs and OLEDs can be produced via solution roll-to-roll processing, however, when constructing a cutting-edge OLED, due to the number of layers, the preferred method of choice is vacuum deposition. Vacuum deposition allows for a controlled film thickness and fabrication of multilayer devices by successive deposition of the layers[16], however it comes with the drawbacks of both high energy consumption and a slower production speed.[17] On the other hand, solution processing is comparably faster and in combination with the simplicity of an LEC assembly has paved the way for the fabrication of light-weight,[18] flexible,[19-22] stretchable,[23,24] and large-area LEC devices,[25,26] at low-cost[27] with the possibility of scalable printing and coating methods[20-22,25,28-30].

Conversely, optoelectronic devices that can sense light, in contrast with LECs that are designed to produce light, yet also makes use of organic semiconducting materials are referred to as organic photodetectors (OPDs). A small part of this thesis focuses on OPDs and more specifically photomultiplication (PM) type OPDs. Photodetectors are very important devices, since they are able to convert an optical input to an electronic response, finding application in industrial production, military affairs, biochemical detection, optical communication and many more. The main OPD technology studied nowadays are those photodetectors that operate based on the internal photoelectric effect with their operational mechanism being responsible for EQE values that do not overcome unity.[31] However, Hiramoto *et al*.[32] in 1994 constructed an OPD device that could photo-multiply the received signal leading to an EQE exceeding unity on PM type OPDs. The driving force for that study aimed at understanding the mechanism of photomultiplication in organic materials,[33] developing more efficient devices[34,35] and making devices with a specific spectral response [36,37].

Photomultiplication type OPDs, as mentioned earlier, are a part of a much newer concept, with such devices operating under a different working principle. When fabricating a PM type OPD, the device architecture looks very similar to that of any other photodetector, consisting of an electron donating and an electron accepting material which are blended and then sandwiched between two electrodes. However, what makes a huge impact on their operation is the ratio of the organic components used in the photoactive layer. More specifically, one of the materials is used as the main component in the active layer, serving as a matrix for the other, which is used in a very small quantity, typically 1% in the bulk heterojunction. [37-39]

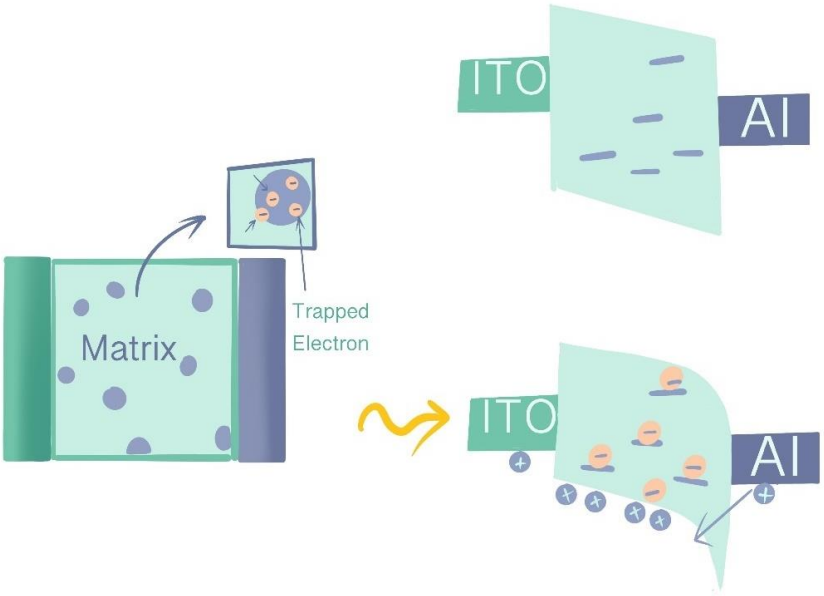

Figure 1.3. (left) Device architecture of a PM type OPD. The main conjugated material is denoted as matrix while the purple circles represent the electron traps and (right) PM type OPD in the dark (above) and under light illumination (below).

So how do PM type OPDs operate? Let´s take an example, where the matrix is an electron donating material and is doped with a small amount of a suitable electron acceptor. After photon absorption from the photoactive layer, excitons are generated. These excitons are bound electron-hole pairs with a very high binding energy, which in order to separate need to reach the donor-acceptor interface. Thus, they need to effectively diffuse through the medium to reach that interface. When the charge transfer excitons reach the donor-acceptor interface, the electrons will be collected by the acceptor. However, since the acceptor is in minute quantities (1-15 %), there are no continuous paths for the electrons to travel to the respective electrode, but they are instead trapped by the acceptor seen in **Figure 1.3** (left). The trapped electrons will build up a Coulombic field which will lead to interfacial bending of the energy levels, especially by those trapped close to the Al cathode (see **Figure 1.3** (right)). This interfacial energy level bending will narrow the hole injection barrier from the Al electrode onto the HOMO of the donor material and as a result hole tunneling will take place through the continuous channels of the donor matrix.[34] The tunneling injection of charge carriers under light illumination may lead to a PM phenomenon with EQE of higher than 100%, which is an advantage of this particular OPD technology.

1.2 Aim and Outline of The Thesis

Firstly, this thesis deals with LECs and more specifically on the design of near infrared (NIR) LECs. When we talk about NIR LECs we refer to active components that emit light covering the electromagnetic spectrum from 700 nm to 1400 nm. Although not visible by the naked eye, devices that emit NIR light are highly important due to the range of applications in which they can be employed. These fields include medicine, where it can be used in photodynamic therapy and

bioimaging of biological tissues (semitransparency window), or optical communications where information can be stored and transferred at very high speeds, and even security applications like fingerprint recognition.[40-42] However, when compared to visible emitters, NIR emitters in LEC constructs suffer from significantly lower efficiencies. To date, highly efficient NIR based LECs remain evasive. The materials that have been most successfully employed in NIR LECs are mainly complexes based on expensive, rare metals that are not always suitable for large scale applications. In addition, promising results have also been obtained using polymers, however, their emission bands typically do not exceed 800 nm. Therefore, in this work we aimed on developing new organic deep NIR emitting compounds for LECs. One such possibility includes porphyrins. Porphyrins also been referred to as the colors of life, because nature uses them for many of the processes happening in nature and have always fascinated researchers and will continue doing so. Their optical properties are tunable by chemical modification, and strategies like extension of the π-conjugation out from the core yielding highly planar structures using a combination of electron donating with electron withdrawing groups are some of the means that usually lead to red-shifting of both absorbance and emission, and will be discussed in the thesis. It was hoped that these factors could be exploited in the pursuit of new emitters for LECs.

Nevertheless, NIR emitters such as highly conjugated porphyrins are subject to aggregation, which is undesirable for LEC performance. In order to overcome this phenomenon, NIR emitters are typically incorporated in host-guest systems, where the host acts as a matrix for the guest, which itself, is used in lower concentrations. The role of the matrix is not just to disperse the emitter, in fact, there are some general considerations when combining a guest with a host to obtain the best device characteristics. This does not just involve addressing solubility, but also includes energy level and optical spectra matching, which will be discussed later. However, every system is unique and there is no universal host material that can perform well with every emitter and each combination should be studied independently. Thus, another aspect of this work was to find the most appropriate porphyrin/polymer combinations in order to achieve the best possible performing NIR emitting devices.

Regarding PM, OPD devices with ultra-high efficiencies have already been demonstrated. However, the number of organic materials that have been measured in PM type OPDs are somewhat limited, and in order to get a better understanding of this technology, more organic molecules need to be studied. Moreover, the voltages that are often required to operate such devices are quite high, sometimes surpassing 20 V, which can be harmful for their long-term stability. In this regard, one of the aims of the thesis was to chemically functionalize the porphyrin core in such a way to prove whether or not such derivatives can efficiently act as a trap for electrons and lead to devices that can exhibit efficiencies surpassing unity.

Before going into the discussions of the results achieved in this work, an introduction to the material properties (Chapter 2) and figures of merits of the LEC and PM type OPD devices (Chapter 3) will be given. The work conducted on porphyrin based NIR LECs is presented in Chapter 4 which focuses on covering papers (I) and (III), in addition to some new unpublished results. While the results achieved on PM type OPDs based on a porphyrin dopant are reviewed in Chapter 5 which covers paper (II). Finally, the conclusions and outlook are drawn in Chapter 6.

CHAPTER 2

2 CONJUGATED MATERIALS, OPTOELECTRONIC PROPERTIES AND PORPHYRINS

What are the properties that make conjugated organic compounds interesting for organic optoelectronic devices? In turn, how can we determine their properties to gauge suitability for use in devices? What are the characteristics of porphyrins that make them ideal emitters for NIR LECs? These are some of the questions that will be answered in this chapter.

2.1 π-CONJUGATED MATERIALS

When we talk about organic optoelectronics, then we refer to those electronic devices that make use of organic materials which are in turn photo-responsive. The characteristic feature of organic chemical compounds that is exploited in optoelectronics, and therefore responsible for their electrical conductivity, is the degree of π-conjugation. **But what are π-conjugated materials?** This chapter will start by briefly explaining what π-conjugation is, and how the electronic properties reflect conjugation pathways.

The electronic configuration of carbon in its most stable state, the ground state, is $1s^2\ 2s^2\ 2p_x^1\ 2p_y^1$, and according to Valence Bond Theory (VBT), carbon should form only two bonds (due to its two half-filled orbitals) however, that does not happen in reality since carbon is able to form four bonds. **How can carbon form four bonds though?** The explanation for this question came in the 1930s by the American chemist Linus Pauling.[43]

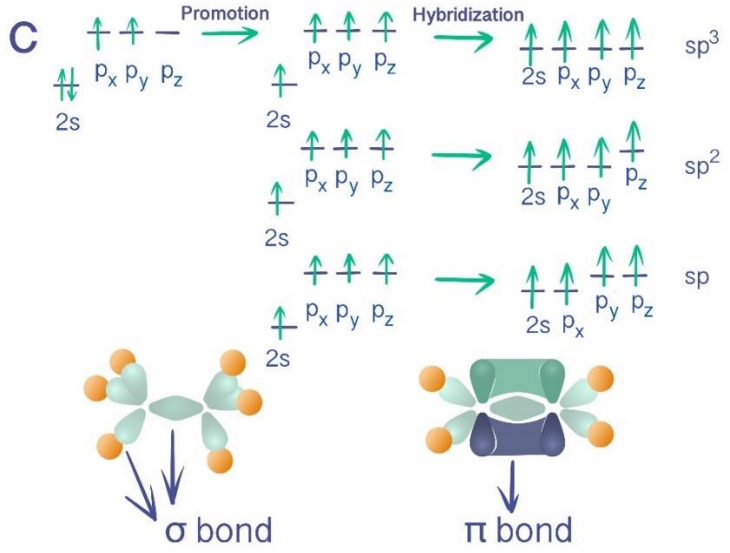

Figure 2.1. (top) Orbital hybridization in carbon and the energetic degeneracies as a saturated hydrocarbon (sp^3), alkene (sp^2) and alkyne (sp) and (bottom) the electron density clouds in σ and π bonding in ethane and ethene.

Linus Pauling introduced the concept of hybridization, in which by mixing s and p orbitals as shown in **Figure 2.1** (top) new hybrid orbitals could be formed, explaining the geometry in carbon-based compounds. In saturated organic compounds, the molecular orbitals (MOs) result from the overlap of two atomic orbitals of neighboring C atoms for example with their electron density projected along the bond axis, referred to σ (sigma) orbitals which form a σ bond (**Figure 2.1** (bottom)). However, organic compounds that only have single bonds (saturated compounds), are not interesting for optoelectronics, as the electron pairs are held fixed between the two atoms. What holds more interest are organic compounds that consist of alternating single and multiple bonds. By looking at **Figure 2.1**, we observe that sp^2 hybridization for example, will leave behind one half-filled $2p_z$ orbital. When this carbon forms a bond with another carbon the axis of their half-filled $2p_z$ orbitals will be perpendicular to the σ bonds and overlap in a side-by-side fashion. This side-by-side overlap of the non-hybridized $2p_z$ orbitals leads to the formation of what is called a π (pi) bond with the electrons occupying these orbitals called π electrons. The presence of the π orbitals leads to a more planar geometry with the π electron density being equally distributed above and below the plane between the atoms (**Figure 2.1**). When we have an extended structure of alternating single and multiple bonds in an organic chemical compound, either in the form of a small molecule or a polymer, the π electrons can delocalize (diffuse) between neighboring π orbitals, since they are less tightly held into the π bonds, and that is known as a conjugated system.

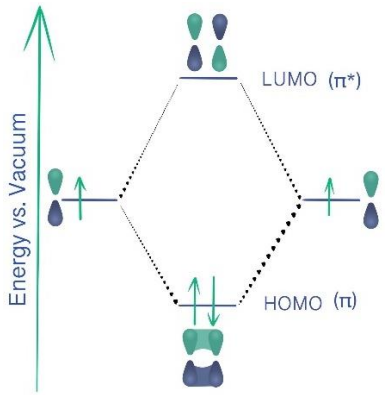

Figure 2.2. Molecular orbital diagram indicating the formation of the π bond in ethene. The bonding and antibonding MOs are shown.

For the sake of simplicity, let´s take the simplest example of ethene, where the π bond results from the combination of the $2p_z$ atomic orbitals, which can be combined in two ways, as it is shown in **Figure 2.2**, either in-phase (they add to each other) or out-of-phase (they cancel each other out). The in-phase combination, where the signs of the atomic orbitals are the same, will create a bonding (π) MO while the out-of-phase, with opposite atomic orbital signs will create an antibonding (π*) MO, the latter being higher in energy. Extension of the π system affects the energy difference between the π and π*, typically reducing the energy of the electronic transition The highest in energy bonding molecular orbital is known as the highest occupied molecular orbital (HOMO),

while the lowest in energy antibonding molecular orbital is known as the lowest unoccupied molecular orbital (LUMO). For organic optoelectronics, the relative positioning of the HOMO and LUMO levels are important as their position defines the energy needed to excite an electron in a molecule.

The energy difference between the HOMO and LUMO energy levels is known as the band gap (E_g) and is a very important parameter since it expresses many of the properties of organic materials. The HOMO and LUMO in organic electronics are analogous terms to the valence and conduction bands defined in semiconductors physics. In a conductor no band gaps exist, and electrons can move freely. On the other hand, an insulator possesses such a large gap between the valence and the conduction band that no electrons can be promoted to the conduction band and will always remain empty. In semiconductors, this energy difference is small enough that with an appropriate stimulus, electrons can move from the valence to the conduction band (i.e. A HOMO to LUMO transition). This energy difference is relatively small in organic conjugated materials, in the order of 1-3 eV, and that is why they can be classified and employed as semiconductors.

2.2 Absorption and Emission of Light from Organic Conjugated Materials

Optoelectronic devices can transform light into energy and vice versa via the use of semiconductors. Thus, it is worth highlighting some of the fundamental processes that occur when light interacts with these types of conjugated materials.

In photochemistry and photophysics, the term light is referred to the electromagnetic radiation and is capable of electronically exciting a molecule under ideal circumstances. In organic unsaturated compounds by "electronically excite", this refers to the transitions that can be facilitated between the HOMO-LUMO energy levels by electromagnetic radiation of an energetically matched wavelength. These transitions are very much dependent on the π arrangement of the semiconductor. In any case, light does not only include the visible (400-700 nm) part of the electromagnetic spectrum, but also can include the near-UV and NIR. A beam of such electromagnetic radiation is considered as a stream of photons (quanta) of specific energy, where the energy of a photon is defined by the Equation (2.1).

$$E = h\nu \tag{2.1}$$

where h is Planck´s constant (6.63×10^{-34} J s) and ν the frequency of the radiation. The frequency is related to the wavelength of the radiation by the Equation (2.2).

$$\nu = \frac{c}{\lambda} \tag{2.2}$$

where c is the speed of light ($2.997\ 10^8$ m s^{-1}). Upon combination of equations (2.1) and (2.2), we see that the longer the wavelength, the lower the energy the photon will have and vice versa.

When all electrons in an organic semiconductor occupy the lowest energy orbitals, the molecule is said to be in the ground state. The ground state is denoted as S_0, where S stands for singlet since all electrons are spin paired (opposite) through bonding spin. When a conjugated molecule is exposed to light of an appropriate energy, there is a chance that a photon will be absorbed. In that case, the molecule ceases residing in the ground state but now is in the excited state (Sn, n=1, 2…).

What happens after light has been efficiently absorbed by the molecule and been excited to an excited state S_n? After light has been absorbed by the molecule, a number of processes can occur which can be summarized for a hypothetical molecule using a Jablonski diagram (**Figure 2.3**).

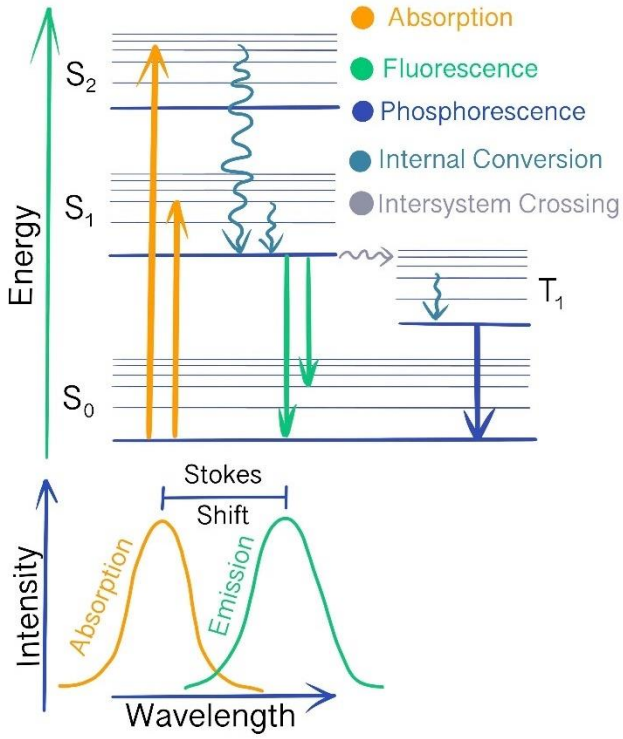

Figure 2.3. Jablonski diagram for a hypothetic molecule describing some of the processes that can occur after the absorption of light.

Depending on the energy input of the incoming photon, transitions can occur from the ground state to any singlet excited state S_n (n=1,2,3…). However, as stated by Kasha´s rule when the electron finally returns to the S_0, this can only take place from the lowest excited states (either from S_1 or T_1). In the case that a molecule resides at a higher excited state than these, it quickly relaxes to its vibrationally relaxed S_1 via internal conversion (IC) and radiationless vibrational relaxation. This excess energy from this process is given off as heat. However, decay from S_1 back to S_0 can itself occur in a number of ways. Return from the S_1 to the S_0 with a subsequent emission of a photon is known as fluorescence. There is also the possibility that no photon will be emitted after the electron

returns to the ground state from the first excited state. This process is denoted as a loss mechanism, as the excess energy is given off as heat and it is similar to IC. In addition, there is also the possibility in some instances, that the S_n will be subjected to intersystem crossing (ISC), forming the triplet excited state (T_n). Conversion of an excited triplet state back to the ground singlet state with the subsequent emission of a photon is known as phosphorescence.

Typical absorption and accompanying emission features can be viewed in the spectrum depicted in **Figure 2.3**. The emission spectrum, whether it arises from either fluorescence or phosphorescence, appears at longer wavelengths than the absorption due to energy loss of the excited state through vibrational relaxation. Generally, the differences in energy between vibrational levels are similar for both ground and excited states, and as the emission occurs from the lowest vibrational levels, this feature appears as a mirror image of the absorption band. The peak-to-peak distance between the lower energy absorption peak and the emission peak is called Stokes shift. Molecules that undergo a notable geometric reorganization from their excited state compared to the corresponding ground state tend to exhibit a bigger Stokes shift.[44,45] Conversely, in organic NIR emitters a small Stokes shift is often observed, which is not ideal for the fabrication of devices with high efficiency.[46] The reason behind that is that a small Stokes shift is accompanied with a greater degree of overlap between the absorption and emission peaks. As a result, the emission intensity is decreased due to self-absorption, through inner filtering effects.[47]

In practice characterization of the optical transitions occurring in a conjugated molecule can be identified by absorption and emission spectroscopy. The absorption of light by a conjugated molecule which is in solution is described by the Beer-Lambert law.

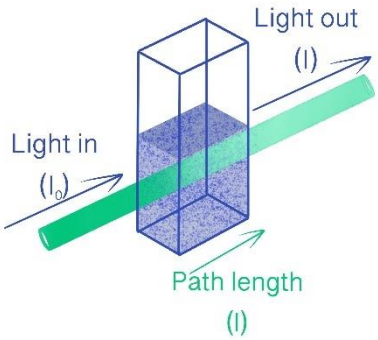

Figure 2.4. Light absorbed by an imaginary sample in solution in a cuvette.

Figure 2.4 illustrates the absorption of a photon source from a sample that is in solution placed in a cuvette of known dimensions. When light of an initial intensity I_0 passes through a solution , the intensity of the light, I, that will be transmitted will depend on the pathlength of the solution (l) , the concentration of the photo-responsive compound in the solution (c) and the ability of the molecule to absorb light which is given by the absorption coefficient (ε).[48] Thus the intensity of light that will be finally transmitted can be given by the equation (2.3)

$$I = I_0\, 10^{-\varepsilon l c} \qquad \textbf{(2.3)}$$

However, what we normally measure in practice is the amount of light absorbed by the sample (in solution) and not that which is transmitted through the sample. This is known as absorbance (A) and is equal to the logarithm of the ratio of incident to transmitted light as shown in the equation (2.4).

$$A = \log\left({}^{I_0}/_{I}\right) = \varepsilon\, l\, c \qquad \textbf{(2.4)}$$

The obtained absorption spectrum of a conjugated organic molecule enables the determination of its optical band gap (E_g^{opt}).[49] The E_g^{opt} is related to the excitation from S_0 to the S_1.

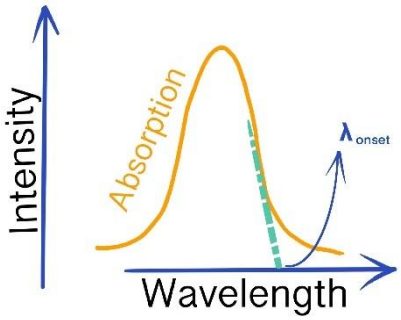

Figure 2.5. Schematic representation of an absorption spectrum and the respective E_g^{opt} estimation.

The E_g^{opt} is calculated from the onset of the low-lying electronic absorption band as it is shown in **Figure 2.5** and by the use of the Equation (2.5).

$$E_g^{opt} = h\,\frac{c}{\lambda_{onset}} = \frac{1240}{\lambda_{onset}} \qquad (2.5)$$

Finally, it should be noted the E_g^{opt} corresponds to the formation of an exciton which is a bound electron-hole pair and in order to separate the exciton into free charges, additional energy is required. This extra energy is known as the exciton binding energy (E_B).[50]

2.3 Electrochemical Characterization

When applying organic semiconducting materials into devices, several layers need to be assembled. In order to achieve a flow of charges through the different layers, we need to be aware of the energy offsets between them. In the case of host–guest systems in LECs, the excitons generated at the host site can be transferred to the guest if there is a proper energy level alignment. Therefore, for efficient

LEC devices, the HOMO and LUMO energy levels of host and guest materials should be carefully estimated and matched.[51]

How can we measure the HOMO and LUMO levels in practice? The HOMO and LUMO levels can be determined directly through photoelectron spectroscopy techniques or indirectly via electrochemistry. The direct methods include ultraviolet photoelectron spectroscopy (UPS) and inverse photoelectron spectroscopy (IPES), which can determine the ionization potential (E_{IP}) and electron affinity (E_{EA}) of a molecule. Parameters E_{IP} and E_{EA} correspond to the HOMO and LUMO energy levels, respectively.[52] However both of those techniques are very complicated, expensive and time consuming, and thereby indirect electrochemical methods are commonly used. The most widely applicable electrochemical method is cyclic voltammetry (CV).

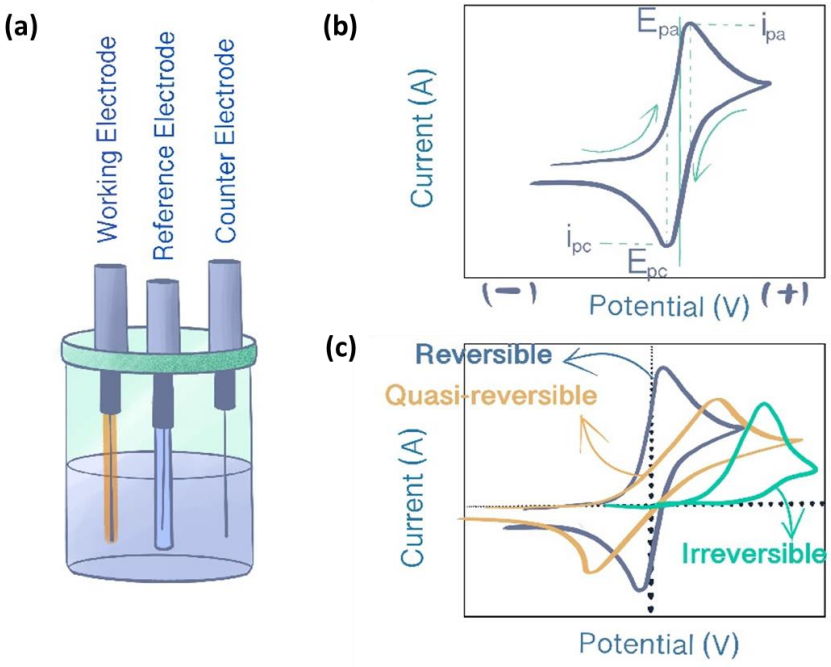

Figure 2.6.(a) A three electrode CV setup (b) Cyclovoltammogram for a reversible redox event, where the anodic peak potential (E_{pa}), cathodic peak potential (E_{pc}), anodic peak current (i_{pa}) and cathodic peak current (i_{pc}) are indicated. The arrows show the scan direction. (c) examples of reversible, quasi reversible and irreversible CV traces

So how is the experiment conducted and how can we extract the frontier energy levels values from the CV? In practice, a three-electrode system is used, which contains (i) a working electrode (composed of a redox inert material), (ii) a reference electrode (which has a well-defined and stable equilibrium potential) and (iii) a counter electrode. The experimental set up is illustrated in **Figure 2.6** (a) The material being studied, a polymer, or a small molecule for instance, is deposited as a thin film onto the surface of the working electrode and immersed in an electrolyte solution. The solvent used should be stable within the applied outer limits of oxidation and reduction potentials

in the experiment, should not dissolve the materials under testing so they do not diffuse from the working electrode and should not react with the analyte. A solvent commonly used for this purpose is acetonitrile (ACN). ACN is a very polar solvent with a broad operating window for the necessary electrochemical analysis, and generally is a poor solvent for π conjugated carbon rich compounds. The electrolyte of choice is typically tetrabutylammonium hexafluorophosphate ($TBAPF_6$), which is of suitable solubility in ACN and is electrochemically inert. The concentration of the electrolyte, typically $TBAPF_6$, is kept at 0.1 M in order to render the solution highly conductive and balance the charges via migration. Prior to commencing the experiment, the electrolyte solution is deaerated with nitrogen in order to remove oxygen. The latter is electrochemically active and if its reduction occurs within in the same potential window as the material under investigation and may interfere with the data values.[53]

A cyclic voltammogram is obtained by measuring the current at the working electrode during the progressive application of a forward and reverse potential sweep.[54] The HOMO and LUMO energy levels of a chemical compound are correlated to the oxidation and reduction potentials (E_{ox} and E_{red}), respectively. In the case of organic semiconducting materials however, due to conformational reorganization and variations of the energy levels which arise from the doping and de-doping process, E_{ox} and E_{red}, are taken from the first oxidation peak onset and the first reduction peak onsets, respectively. [55] As E_{ox} and E_{red} values are linearly dependent on the ionization energy and electron affinity in the gas phase and the CV measurements are performed in a solvent medium, the measured potentials can be calibrated against a known standard potential.[56] A common reference redox couple used is the ferrocene/ ferrocenium (Fc/Fc^+) couple, which has a redox potential of 0.63 V, versus the normal hydrogen electrode (NHE) in ACN at 25°C. In turn NHE has a relative electrode potential of −4.5 V under vacuum, leading to equations :

$$\text{HOMO} = -(E_{ox} + 5.13)\ \text{eV} \tag{2.6}$$

$$\text{LUMO} = -(E_{red} + 5.13)\ \text{eV} \tag{2.7}$$

Electrochemistry gives us a convenient way to measure E_g by the difference of the HOMO and LUMO energies. From the absorption spectra, we can estimate the E_g^{opt} of a molecule, which refers to the excited state, where the electron and the hole are electrostatically bound to each other. On the other hand, the E_g refers to the ionized state where the electron and hole are completely separated. Practically this means that the estimated E_g^{opt} will be smaller than the E_g, while subtracting the E_g^{opt} from the E_g will give an estimation of the exciton binding energy (E_B), the energy that holds the electron and the hole together.[57]

Finally, for fully reversible redox couples exhibiting a one electron transfer, the maximum peak currents, i_{pa} and i_{pc}, should be approximately the same, $\left|\frac{i_{pa}}{i_{pc}}\right| = 1$, while the potential difference

between the cathodic and anodic peaks $|E_{pc} - E_{pa}|$ should be 57 mV at 25°C (**Figure 2.6** (b)).[55] However, this is an ideal situation and not often experimentally observable. When the relative E_{pc} and E_{pa} start to shift further apart, these can be categorized as quasi-reversible. There are also cases in which the peaks are so widely separated that no parts of the two peaks overlap on the potential axis at all and are defined as irreversible.[58] Examples of reversible, quasireversible and irreversible redox events can be seen in **Figure 2.6** (c).

2.4 PORPHYRINS

Porphyrin derivatives were the focus of this study and therefore, it is worth giving an introduction into this interesting family of molecules that make them potentially useful candidates in the field of organic electronics.

Porphyrins are a tetrapyrrolic motif possessing 18-π electrons in their conjugation path as shown in **Figure 2.7**, and their metallated forms play a vital role in many processes occurring in nature. Some of these processes include photosynthesis (chlorophyll) and the transport of oxygen in the human body from the lungs to the tissues (haemoglobin).[59,60] **Figure 2.7** shows the core structure of porphine, the simplest non-metallated porphyrin, where the green highlighted area shows the 18-π electron conjugation path of the molecule.

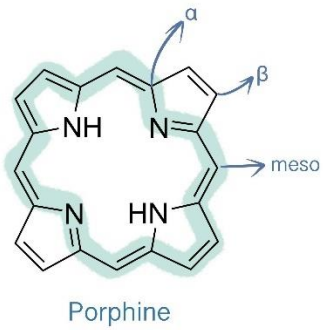

Figure 2.7. Structure of porphine. The α, β and meso positions are indicated. The green line indicates the conjugation path in porphyrins.

Porphyrins with metals nestled in their core are known as metalloporphyrins, while those without metal complexation are otherwise known as free base porphyrins. Based on whether they are coordinated with open or closed shell of valence electron metals, porphyrins can be further classified into regular and irregular, and they differ in their absorption and emission properties.[61] What makes porphyrins interesting for organic optoelectronic applications is their ease of chemical modification leading to a subsequent tuning of their properties. Their chemical modification can be achieved using various methods including substitution at the meso or -β positions and exchanging of the metal center, to name a few (**Figure 2.7**). Interestingly, the metal situated at the porphyrin core can play an influential role in the properties on the final emitter because it can affect the mechanism of emission (fluorescence or phosphorescence).[62] Substitution at the *meso*

position is in general easier to facilitate than the β position, while the impact on the optical properties of the porphyrins can be profound in both cases.[63] With this consideration, the thesis is focused on porphyrin molecules chemically modified at *meso* bridging positions.

For the synthesis of *meso* substituted porphyrins, there are different paths that can be followed, depending on the symmetry we want to give to the final compound. In general, for a 4-fold symmetric tetra-*meso* substituted porphyrin (**Figure 2.8** (left)), a one-step condensation of a pyrrole with a desired aldehyde can be followed.

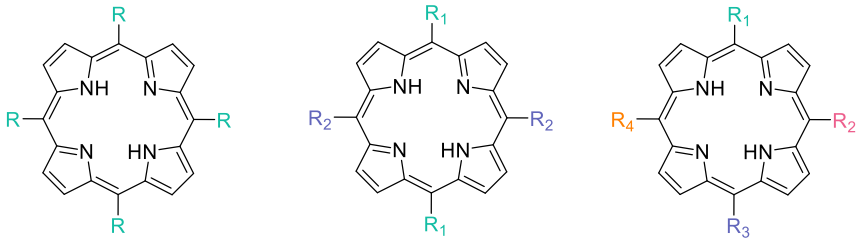

Figure 2.8. (left) 4-fold symmetric porphyrin, (middle) 2-fold symmetric porphyrin, (right) asymmetric porphyrin.

Porphyrins that have a 2-fold symmetry can be constructed by a 2+2 synthesis via the coupling of two dippyrolic intermediates with an aldehyde. Totally asymmetric porphyrins can also be prepared, commencing with the stepwise condensation of individual pyrroles leading to a linear tetrapyrrole and its final cyclization . In this thesis, fully symmetrical porphyrins were studied for application as NIR emitters and so a short description of possible synthetic approaches shall be touched upon.

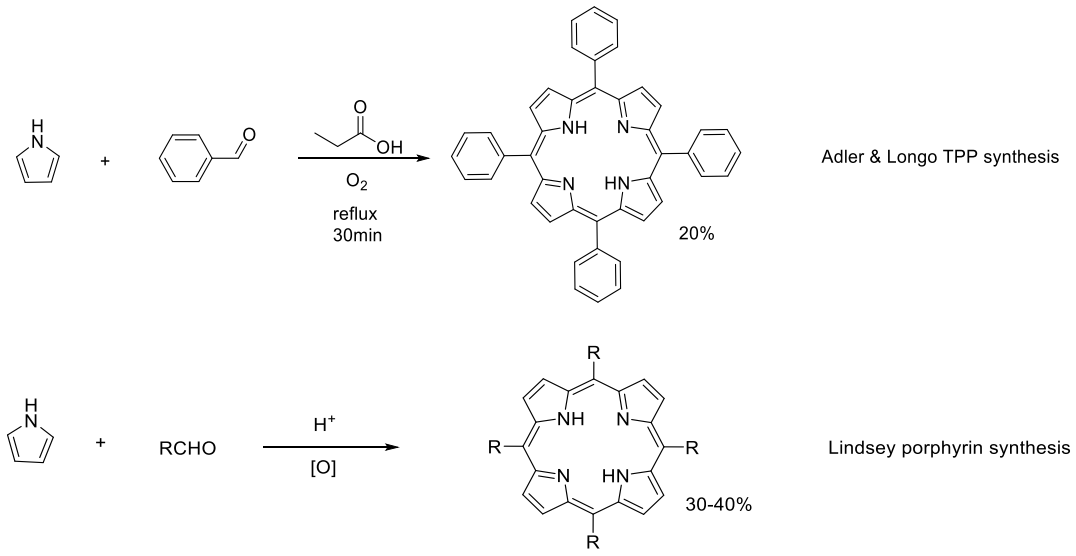

Scheme 2.1. The Adler and Longo (above) and Lindsey (below) porphyrin syntheses.

Two main synthetic protocols are followed for the synthesis of porphyrin with substituents decorating the *meso* positions.[64] These are the Adler and Longo[65], and Lindsey[66] methods. Under

the Adler and Longo conditions, condensation of pyrrole and the aldehyde of choice were facilitated by heating this mixture to reflux point in propionic acid, typically using short reaction times. Moreover, this reaction is exposed to air so that the initially formed porphyrinogen will convert to the desired porphyrin with molecular oxygen acting as the oxidant. This method gives good yields however, it is not suitable for sensitive aldehydes due to the harsh reaction conditions. In the procedure proposed by Lindsey, the condensation of pyrrole and an aldehyde is achieved, however in this case, only catalytic amount of the acid is used, and the reaction is carried out at high dilution. These reaction conditions lead to the formation of a porphyrinogen which then is converted to the final porphyrin by the introduction of an oxidant, commonly 4,5-dichloro-3,6-dioxo-1,4-cyclohexadiene-1,2-dicarbonitrile (DDQ) or *p*-chloranil.

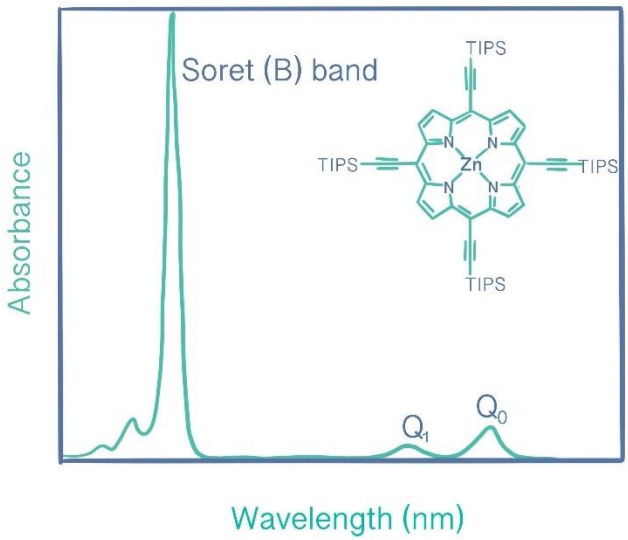

Figure 2.9. Typical absorption spectra of a zinc containing porphyrin. The TIPS group stands for (triisopropylsilyl)acetylene. The Soret (B) band and two Q bands can be observed.

The absorption spectra of porphyrins consist mainly of two active regions. These are the Soret (or B) and the Q bands, which are all attributed to $\pi-\pi^*$ transitions. More specifically, the Soret band can be assigned to a transition to the second excited state ($S_0 \rightarrow S_2$) while the Q bands are assigned to a transition to the first excited state ($S_0 \rightarrow S_1$).[67,68] Free base porphyrins show four Q bands while metalloporphyrins, due to an increased symmetry caused by the metal have only two Q bands. In **Figure 2.9**, the absorption spectrum of a Zn containing porphyrin is shown, clearly evidencing the S and two Q bands.

The absorption bands of porphyrins arise from the transitions between two HOMOs and two LUMOs, and the energies of these transitions are affected by the metal center as well as the substituents directly conjugated to the porphyrin motif. As shown in **Figure 2.10** in a simple metal containing porphyrin, the LUMO is doubly degenerate (the LUMO and LUMO+1 have the same energy) and the HOMO and HOMO-1 are nearly degenerate. [69]

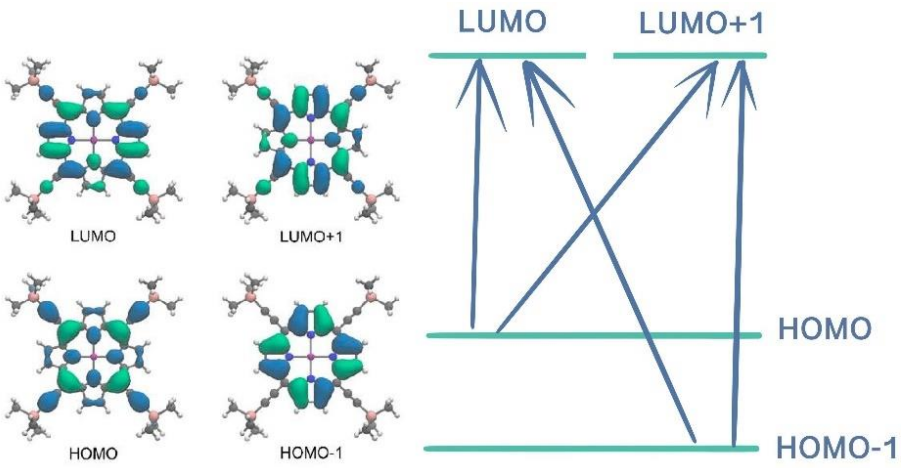

Figure 2.10. Orbital diagram showing the main transitions for the Zn containing ZnP-TIPS$_4$. The energies for the shown transitions have been estimated from DFT and where shown to be L+1: -2.62045772 eV / L: -2.62045772 eV /H: -5.04172801 eV and H-1: -5.41098669 eV .

One of the characteristics that have rendered porphyrins attractive for optoelectronic applications is their narrow emission linewidth, their ease of chemical modification, as well as thermal stability.[70] In general, both fluorescent and phosphorescent NIR porphyrin emitters have been developed, with more efficient being the phosphorescent Pt containing derivatives,[71-73] while in the case of fluorescent emitters, Zn is generally coordinated to the porphyrin. In fact, porphyrin derivatives have been synthesized and employed as emitters into OLED devices. However, reports into porphyrin based LECs are limited and their emissive properties were not concerned with the NIR region.[74-76]

CHAPTER 3

3 ORGANIC OPTOELECTRONIC DEVICES

In chapter 1, a brief overview into the working mechanism of both LECs and PM type OPDs had been given. Not only the design, synthesis and characterization of novel porphyrin derivatives are presented herein, but also their incorporation into functional devices. A short description of the figures of merit often used to characterize the devices is without a doubt necessary. Thus, this chapter is dedicated to introducing the most important figures of merit towards achieving optimal devices.

3.1 ORGANIC LIGHT EMITTING ELECTROCHEMICAL CELLS

A critical measure for evaluating the LEC device performance is external quantum efficiency (EQE or η_{Ext}), which describes the amount of photons that escape from the surface of the device ($N_{ph,out}$) relative to the quantity of electrons injected ($N_{el,in}$) (Equation 3.1).

$$EQE = {}^{N_{ph,out}}\!/_{N_{el,in}} \tag{3.1}$$

It can also be expressed as the product of the internal quantum efficiency (IQE or η_{Int}) of an organic material with the light outcoupling efficiency (η_{out}) and the ideality factor (X_{Ideal}), (Equation 3.2)

$$EQE = IQE \times \eta_{out} \times X_{Ideal} \tag{3.2}$$

The η_{out} denotes the actual light that can be released from the device surface opposed to the light that is trapped in the device and is dependent on the refractive index of the glass substrate as well as the dipole alignment and geometry of the LEC.[77,78] Regarding, the X_{Ideal} that represents the combined additional loss mechanisms due to, e.g., exciton–polaron, exciton–exciton, and exciton–electrode quenching.[79]

The IQE is determined by three parameters, which include; (a) the recombination efficiency (η_{Rec} or γ) that counts for the number of injected carriers (electrons and holes) that recombine into excitons, (b) the fraction of spin allowed excitons (η_{Spin} or η_{ST}), based on spin statistics, the excitons are obtained as 25% singlet and 75 % triplet state , and (c) and the photoluminescence quantum yield (PLQY or Φ_{PL}) describing the probability of an optically excited exciton to emit light.

$$IQE = \eta_{Rec} \times \eta_{ST} \times \Phi_{PL} \tag{3.3}$$

However, the EQE is not the only way to evaluate an LEC device. Another equally important parameter is luminance.[80] Luminance indicates the amount of luminous intensity that can be

detected by the human eye looking at a particular surface from a particular angle of view. Thus, luminance is an indicator of how bright the surface will appear.

The above measures are photometric expressions meaning that they are designed to match the responsivity of the human eye, which is more sensitive to a light source of 555nm. With this being said, it is clear that luminance can be used to describe only visible light but not relevant to light sources such as NIR. For these types of emitting devices, radiance ($W.cm^{-2}$) is used as a measure instead, where the physical properties (energy flow) of light and not its visual perception are characterized.

A very important prerequisite for functional LECs is a fast turn-on time (t_{on}), which is the time taken to achieve the maximum radiance under direct current (dc) bias.[81] Value t_{on} is related to the ionic conductivity of the device and the formation of the p-n-junction double layer, shown in **Figure 1.1**. Since the mobility of ions is typically lower than that of the electronic charge carriers, the LEC turn-on time is slower than that of OLEDs.[82] The addition of ionic liquids into LECs have been proven fruitful in decreasing this parameter due to their high intrinsic ionic conductivities.[83,84]

3.2 Photomultiplication Type Organic Photodetectors

To evaluate the performance of a PM type OPD there are several key parameters that should be considered. Some of the figures of merit for PM type OPDs include the dark current (J_D), parameter EQE which can also be expressed as responsivity (R), specific detectivity (D*), noise equivalent power (NEP) and linear dynamic range (LDR). Those are all important terms which will be given below.

The J_D reflects the current flowing though the device in the absence of illumination and is considered a loss mechanism. The existence of J_D results from the random generation of electrons and holes within the depletion region of the device. In order to decrease the dark current, a common strategy is to incorporate electron or hole blocking layers in the device architecture so that the energy barriers for charge injection from the anode and cathode are increased.[85,86]

One of the most essential parameters of photodetectors that relates to their ability to convert an optical signal to an electric is responsivity (R), and is given from Equation 3.4 :

$$R = \frac{J_L - J_D}{I_{in}} = \frac{J_{Ph}}{I_{in}} \tag{3.4}$$

R is wavelength dependent, so in many cases when emphasis is placed on a spectral region of detection, R is referred to as spectral responsivity. This parameter is directly proportional to the EQE, so they are both a gauge of OPD device efficiency. The EQE value corresponds to the number of charges collected by the respective electrodes relative to the number of incident photons absorbed,[31] meanwhile R is a measure of the electrical output per optical input and can be related to one another by Equation 3.5 :

$$\mathrm{EQE} = \frac{J_{ph} h\,\nu}{I_{in}\,e} = \frac{Rh\nu}{e} = \frac{R\,h\,c}{\lambda\,e} \tag{3.5}$$

where h ($6.626*10^{-34}$ J s) is Planck's constant, ν is the frequency of the photon, e ($1.602*10^{-19}$ C) is the absolute value of electron charge, λ is the incident light wavelength and c ($2.998*10^{8}$ m/s) is the speed of light.

In defining the sensitivity of a photodetector, where sensitivity in this case refers to the ability of the photodetector to detect weak signals, noise current (i_n) is crucial. Term i_n indicates any fluctuations that may mask the received signal. Since i_n is random in nature, it can only be described statistically by the root mean square of these fluctuations, which include (i) shot noise (i_s^2) (ii) thermal noise also known as Johnson noise (i_t^2) and (iii) flicker noise (i_f^2), as presented in Equation 3.6:[87]

$$i_n = \sqrt{i_s^2 + i_t^2 + i_f^2} \tag{3.6}$$

For a weak optical signal, the photocurrent can be indistinguishable from the noise current. Consequently, the relative strength of the photocurrent and noise is of high importance to determine the feasibility of the photodetection. The common metric that is used to describe the minimum optical power that can be distinguished from the noise is the noise equivalent power (NEP), and is described by Equation 3.7:[31,88]

$$NEP = \frac{i_n}{R} \tag{3.7}$$

The noise performance of a photodetector can also be expressed in terms of detectivity (D), which is inversely proportional NEP(Equation 3.8):

$$D = \frac{1}{NEP} \tag{3.8}$$

The higher the detectivity, the more efficient the photodetector is in detecting weak signals through the noise. However, in practice the characteristic that is discussed in literature is not D, but specific detectivity (D^*) because it allows for a direct comparison of photodetectors with different surface areas (A) and operational bandwidths (Δf). The relationship between those characteristics can be seen in Equation 3.9 :

$$D^* = \frac{\sqrt{A\,\Delta f}}{NEP} = \frac{R\sqrt{A\,\Delta f}}{i_n} = \frac{R}{\sqrt{2eJ_D}} \tag{3.9}$$

The last characteristic aspect relevant to photodetectors that needs mentioning is the dynamic range (DR). More specifically, the DR of a photodetector is reflected by the operational light intensity range and is given by the ratio of the maximum and minimum detectable photoresponse. In fact,

photodetectors are evaluated by their linear dynamic range (LDR).This takes into consideration the total dynamic range, which is the range where the photoresponse scales linearly with intensity. A photodetector with a large LDR can be used to measure both strong and weak light signals. LDR is expressed as the number of orders of magnitude of light intensity (or equivalently current) over which the photodetector operates linearly and can be estimated by Equation 3.10:

$$LRD = 20 \log \frac{I_{up}}{I_{low}} \tag{3.10}$$

CHAPTER 4

4 SYNTHESIS AND CHARACTERIZATION OF NIR PORPHYRIN EMITTERS FOR LECS

A variety of structural motifs have been utilized as NIR emitters in LECs, which include polymers, ionic dyes and ionic transition metal complexes (iTMCs) (**Figure 4.1**). When the emissive layer is constituted of polymers and/or small molecules, the addition of a small amount of electrolyte is required to provide mobile ions for *in situ* electrochemical doping.[89] On the other hand, iTMCs, themselves, consist of an ionic pair and therefore do not require the addition of an electrolyte.[90]

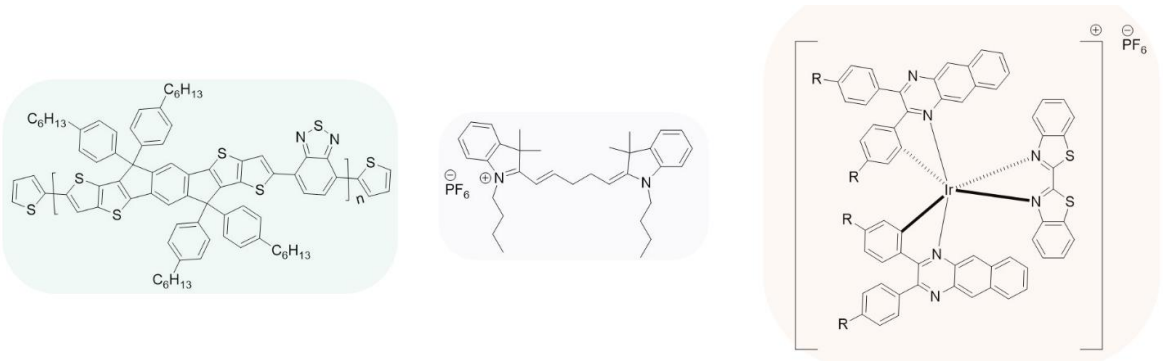

Figure 4.1 examples of (left) a NIR emitting polymer, [79] (middle) a NIR ionic dye , [91] and (right) an iridium based NIR ionic transition metal complex.[92]

For NIR LEC polymers incorporating the [indacenodithieno[3,2-b]thiophene (IDTT) unit, like the one shown in **Figure 4.1** (left), have shown good charge transport properties and broad absorption spectra extending into the NIR region. LEC devices incorporating this polymer in the active layer not only showed fast turn on time of a few seconds, but also exhibited a NIR EL spectrum, which was evidenced by a λ_{max} of 725 nm and a very high radiance of ~1.5 mW/cm^2 at a relatively low drive voltage of ~6 V.[26] IDTT based donor-acceptor polymer analogues, with and without fluorine atoms decorating the backbone have also been reported and compared.[79] Interestingly, from this work, the latter showed the highest radiance of 129 μW/cm^2 with an EL peak at 705 nm and a driving voltage of 3.4 V. On the other hand, the fluorinated analogues exhibited a diminished stability, thought to arise from undesired interactions with the electrolyte in the emissive layer. Regarding small molecules, Pertegás *et al*. adapted a host-guest system to fabricate devices which incorporated two ionic cyanine dyes (**Figure 4.1** (middle)) in the emissive layer.[91] A host-guest strategy was employed to reduce exciton quenching and emission losses and the best performing device gave an EQE of 0.44% at 706 nm.

However, more literature on NIR LECs describes iTMCs, based on Ir and Ru coordination complexes. Ru(II) complexes show low PLQYs and therefore afford low-efficiency devices. Xun and

coworkers reported a series of Ru complexes and some of these demonstrated very deep NIR EL (880-1040 nm), however, this was accompanied with very low radiance values (9-4 mW Sr^{-1} m^{-2}). In addition, some ionic iridium complexes were studied, which showed deep NIR electroluminescence (778-882 nm) with the application of very low voltages (2.3-4 V), and satisfactory efficiencies (0.036% at 882 nm) when used in devices.[92] Very recently, [93] a series of devices consisting of an ionic Ir complex were reported, exhibiting NIR emission based on excimer formation. These devices showed very high radiances (143-303 μW cm^{-2}) and EQEs (0.26-0.57%) values for an EL maxima >800 nm. The last three studies mentioned in this paragraph are some from the few exhibiting NIR emission exceeding 800 nm in LECs.

In essence, all the organometallic complexes aforementioned, demonstrated NIR emissions exceeding 800 nm in LECs, however, it would be prudent to pursue different candidate materials that emit above 800 nm that do not employ costly transition metals. In this chapter, three separate explorations using novel porphyrin derivatives as NIR emitters will be presented. In all instances, synthetic strategies centered on the extension of conjugation from the *meso* positions of the porphyrin core to give derivatives with NIR emitting properties . In addition, research presented in this chapter will address aggregation quenching problems, which is commonly observed when looking at the optical properties of these types of molecules.

4.1 A DPP Containing Porphyrin Emitter

Although metalloporphyrins have been efficiently used as NIR emitters in OLED devices,[71,94-96] they have not been much studied to the same extent in LECs. Costa and co-workers synthesized a series of porphyrins with different metal centers (Zn, Sn, Pt, and Pd) and obtained the best LEC performances from the Zn and Pt metalloporphyrins, which delivered dual EL peaks at 650 and at 650–750 nm with an EQE of 0.016–0.017%, but at a low emission output[75]. The synthesis of Zn containing porphyrin BODIPY dyads[97] has also been reported, which exhibited deep-red EL (630-670 nm) and stabilities of ~1000 h. In any case, we focused upon the synthesis of Zn porphyrins for NIR emitters employed in the active layers of the LECs. Transition metal Zn was used as an alternative to the Ir and Ru metals commonly employed in deep NIR emitting LECs, due to its abundancy and low cost. Strategies like extension of the conjugation, whilst maintaining planarity were employed in order to obtain suitable absorption and emission properties of the desired emitters. The next paragraph will start by listing some of the strategies employed in synthesizing NIR active molecules and then will continue with a discussion relative specifically to the Zn porphyrin derivatives made in this study.

4.1.1 Design Strategy, Synthesis and Characterization

In order to design molecules that will potentially lead to the emission of NIR photons, several parameters should be taken into consideration prior to the synthesis. Extending the conjugation of an organic molecule is a common tactic used to red shift both the absorption and emission.

Moreover, to properly harness this effect, planar and rigid structures should be realized, so that the overlap of the π system is optimal.[98] Some of the strategies that are commonly applied to obtain planar structures are (i) fusing ring systems[41] (that also stabilizes the quinoid form), (ii) linking the substituents of the molecules through acetylenic linkages, where steric interactions between neighboring groups may be an issue [99] and (iii) introducing non-covalent intramolecular interactions which can lock the conformation flat.[100,101]

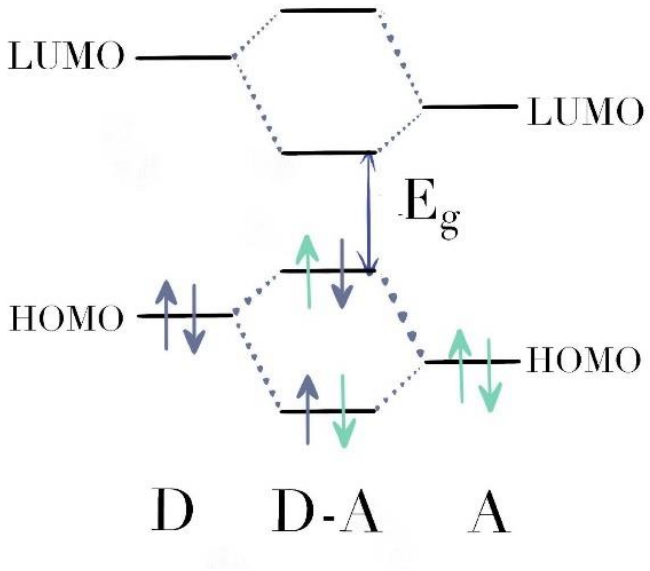

Figure 4.2 Illustration of energy level hybridization in a molecule comprising an electron donating group (D) and electron accepting moiety (A).

Direct conjugation of an electron rich donor moiety, such as the metalloporphyrin core, with an electron deficient acceptor has also been proven as an extremely potent way to influence its optical properties. This arrangement is known as a push–pull system and is very effective in red-shifting the absorbance. After the donor (D) and the acceptor (A) are combined, hybridization of their MOs will lead to the creation of new HOMO and LUMO energy levels as shown in **Figure 4.2.** The new HOMO and LUMO will be shifted upwards and downwards, respectively, resulting in a narrower E_g, and thus a more redshifted absorbance and emission.[98,102,103] The magnitude of the E_g reduction is highly dependent on the strength of both donor and acceptor, i.e.. the degree of polarization through the π network.

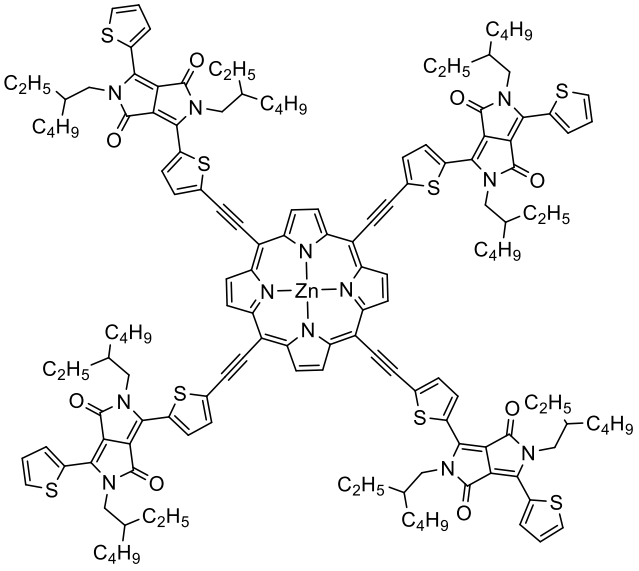

Figure 4.3 . Chemical Structure of ZnP(TDPP)$_4$ emitter.

The structure of a target emitter is presented in **Figure 4.3**, which took into consideration the aforementioned design strategies. Initially, we aimed at extending the conjugation of the porphyrin core from the *meso* positions. For this, four thiophene-diketopyrrolopyrrole (TDPP) units could be connected to the porphyrin core via acetylenic bridges. The latter connection could be possible by using a Sonogashira coupling reaction.

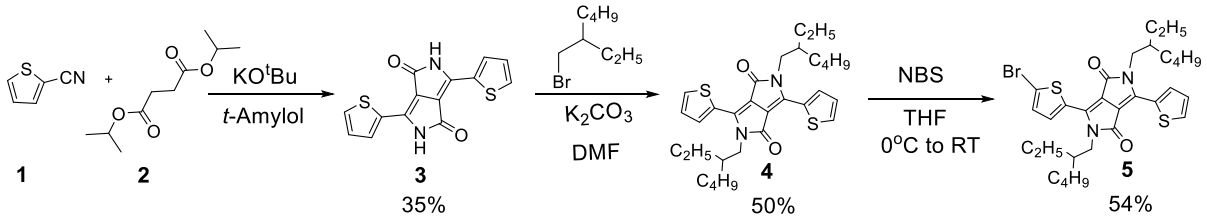

Scheme 4.1. Synthesis of mono-brominated TDPP (**5**).

As TDPP is highly planar,[104] and when these units are connected to the porphyrin using acetylenic bridges, a flat macro structure would be expected. The TDPP motif is often used as a strong electron accepting moiety when synthesizing materials for organic optoelectronics. Therefore, we aimed to produce a molecule with substantial donor-acceptor polarization that would, in turn, result in the reduction of the energy difference between the HOMO-LUMO levels and give rise to optical transitions at more redshifted wavelengths. The synthesis of **5**, seen as a possible coupling partner for a Sonogashira reaction, can be seen in **Scheme 4.1**. Diketopyrrolopyrrole **3** was made possible *via* the succinic ester route, where condensation of 2 equivalents of 2-thiophenenitrile **1** with diisopropyl succinate **2** in the presence of highly basic potassium *tert*-butoxide gave **3** in 35% yield. Compound **3,** a highly planar motif**,** exhibited a low solubility deriving from its solid state arrangement in parallel sheets that exhibit strong two directional hydrogen bonding.[105] In order to overcome the lack of solubility caused by hydrogen bonding, a *N,N´* disubstitution with 2-

ethylhexyl bromide was performed. This alkylation step was carried out in dimethylformamide (DMF) as the solvent and deprotonation was facilitated with base potassium carbonate to give **4**, which could be conveniently purified by column chromatography. These branched chain alkyl substituents have stereogenic centers and the thought is that an element of this character will be adequate to force these mobile solubilizing groups out of the plane when tethered to the porphyrin core. The outcome of this may lend itself to a reduction in the potential of porphyrins to aggregate by π-stacking. The next step involved the monobromination of **4**, which as a result gives a suitable coupling partner ***5*** for the reaction with terminal alkynes using a Sonogashira protocol. As **4** is symmetric, the possibility of bromination of both thiophene units at the *5* position was equal. This was, nevertheless, accomplished by adding 1 equivalent of *N*-bromosuccinimide (NBS) portion-wise to the reaction vessel while maintaining the temperature at 0 °C. Purification, and separation from **4** and dibrominated compound was possible by subjecting the reaction mixture to column chromatography.

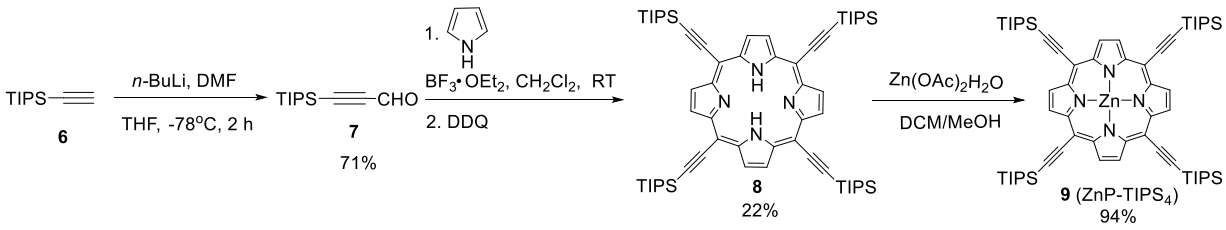

Scheme 4.2. Synthesis of ZnP-TIPS$_4$ (**9**) where TIPS stands for (triisopropylsilyl)acetylene.

As mentioned above, acetylenic linkages were used to connect the TDPP moiety to the porphyrin *meso* positions. The role of the acetylenic bridges was two-fold. Firstly, they contribute to the extension of the conjugation in the overall molecule. Secondly planarity can be maintained as these are buffering groups, where no steric interference between porphyrin and side groups can occur. For the synthesis of the porphyrin core, two main steps were followed. Initially, aldehyde **7** (**Scheme 4.2**) needed to be prepared, prior to proceeding to the construction of the porphyrin core under Lindsey conditions. The choice of this aldehyde was motivated by the fact that the porphyrin forming reaction goes well and the acetylenic TIPS protecting group can withstand these reaction conditions. The reaction forming **7** was facilitated by subjecting triisopropylsilyl acetylene to *n*-BuLi at low temperature and subsequent trapping with electrophile anhydrous DMF. The subsequent reaction of **7** with pyrrole under Lindsey conditions [106] did indeed lead to the formation of the porphyrin **8**. Metal Zn (II) was set into the core of the free base porphyrin **8**, using zinc acetate dihydrate yielding **9**. Compound **9** is a highly versatile building block which, after a deprotection step can be used in a subsequent Sonogashira coupling reaction protocol.

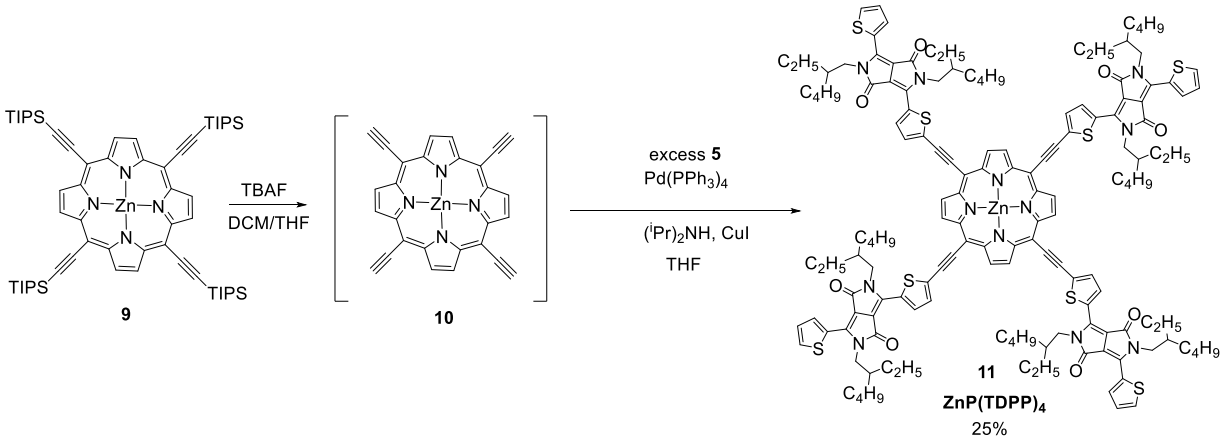

Scheme 4.3. Synthesis of **ZnP(TDPP)$_4$ 11.**

More specifically, the silyl protecting groups on **9** could be conveniently deprotected with the use of tetrabutylammonium fluoride (TBAF). Intermediate **10** was isolated after a fast work up and was directly used in the next step, due to the instability of the terminal alkynes. The deprotected intermediate was coupled via Sonogashira cross coupling employing an excess of ***5*** to furnish ZnP(TDPP)$_4$ in 25% yield, for a total of 8 reaction steps.

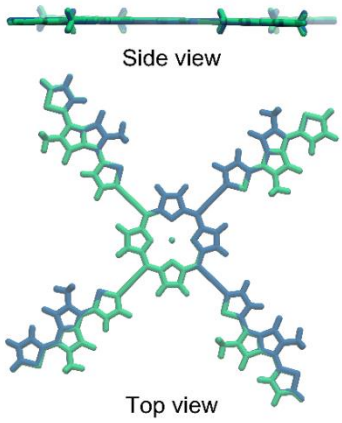

Figure 4.4. Side and top view of the superimposed geometry-optimized ground state (S_0, green structure) and lowest-energy excited state (S_1, blue structure).

DFT calculations were performed on ZnP(TDPP)$_4$ to gain further insight into the geometric conformation of this tetra-substituted porphyrin. **Figure 4.4** shows both side and top views of the superimposed geometry optimized ground and lowest energy excited states. It is quite clear that ZnP(TDPP)$_4$ adopts a coplanar ground state conformation (green structure), which is maintained upon achieving the lowest excited state (blue structure). The observation is more clear from the side on view, where one can see the overlap between these two conformations. In essence, DFT thus corroborated our design strategy in obtaining a very flat structure and thus the potential for good overall π overlap, which was important for pushing the optical properties into the NIR domain.

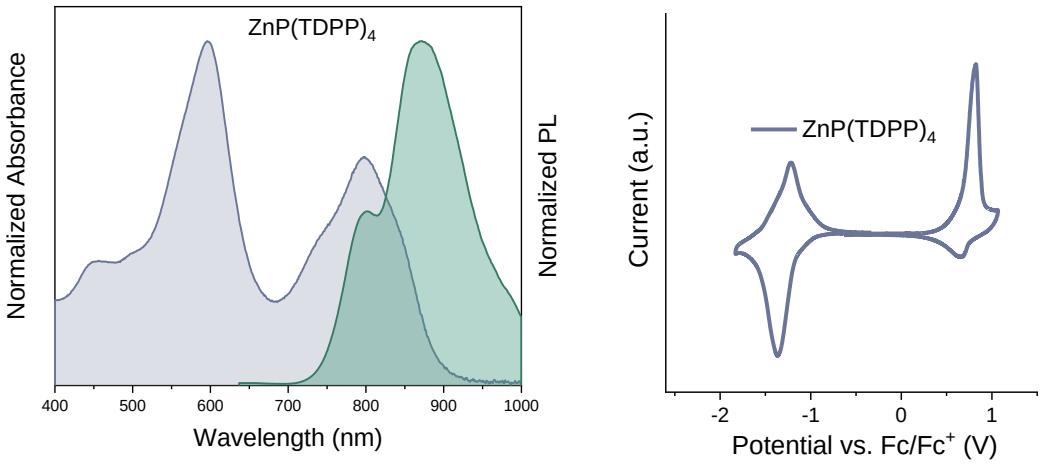

Figure 4.5. (a) Normalized Absorption (purple) and PL (green) spectra of the $ZnP(TDPP)_4$ emitter in a toluene/pyridine 99:1 and concentration 10^{-6} M. (b) CV trace of $ZnP(TDPP)_4$.

To confirm that $ZnP(TDPP)_4$ indeed showed the desired optical transitions in the NIR region, we recorded the absorption and PL spectra. In order to prepare solutions of $ZnP(TDPP)_4$, it was necessary to add a small amount of pyridine (1%) to the toluene solution. This addition of the co-solvent was necessary to dissolve the porphyrin derivative, as its solubility was hindered by a tendency to undergo π–π stacked aggregation. Interestingly, pyridine can axially coordinate to the Zn center thus interfering with this π-π stacking effect.[107] From **Figure 4.5** (a), two absorption peaks were observed at λ_{max} 596 nm and 797 nm, which could be attributed to the S and Q bands of the porphyrin, respectively. It was seen from the PL spectrum that $ZnP(TDPP)_4$ exhibited two features in its emission at 800 nm and 872 nm, thus indeed realizing the synthesis of a novel deep NIR emitter, which did not involve the use of precious metals. Moreover, the lowest energy peak in the absorption (797 nm) spectrum and the high energy PL peak (800 nm) of the porphyrin overlapped to a large extent, showing an extremely small Stokes shift of only 3 nm. This small Stokes Shift was in agreement with the DFT calculations which supported that the ground and excited states both should exhibit similar and robust conformations.[69] The E_g^{opt} was determined to be 1.38 eV by taking the absorption onset and thereafter subjecting this value to Equation 2.5.

Information about the energy levels of $ZnP(TDPP)_4$ was also collected using electrochemistry. These redox potentials were vital for the fabrication of efficient devices, as the energy levels needed to be matched with a suitable host polymer. From the onset of the oxidation and reduction potentials, and by making use of the equations discussed in chapter 2, the HOMO and LUMO levels were calculated to be –5.77 eV and –3.97 eV, respectively. The HOMO/LUMO levels translated to an E_g of 1.80 eV, being 0.42 eV wider than the E_g^{opt}, which was expected as E_g also takes into consideration the exciton binding energy, E_B. From **Figure 4.5** (b), it could also be seen

that both the electrochemical oxidation and reduction processes of the material were quasi-reversible.

4.1.2 Host-Guest system Properties

Porphyrins typically π stack into aggregates which suppresses their emissive properties and so the next step was to attempt to disperse this compound in such a way so as to maximize the emissive properties of $Zn(TDPP)_4$. Usually, the efficiency of organic emitters in the solid state declines dramatically when compared to solution measurements through self-quenching[79] although exceptions do exist, such as molecules showing aggregation induced emission.[108] In order to alleviate the quenching, doping of the material into a host matrix, in a so called 'host-guest' system, is one way in overcoming this technical obstacle. Apart from suppressing this quenching, the charge transport properties of the emitter can also be improved by using a suitable host.[109] **What are the required characteristics of a host material?**

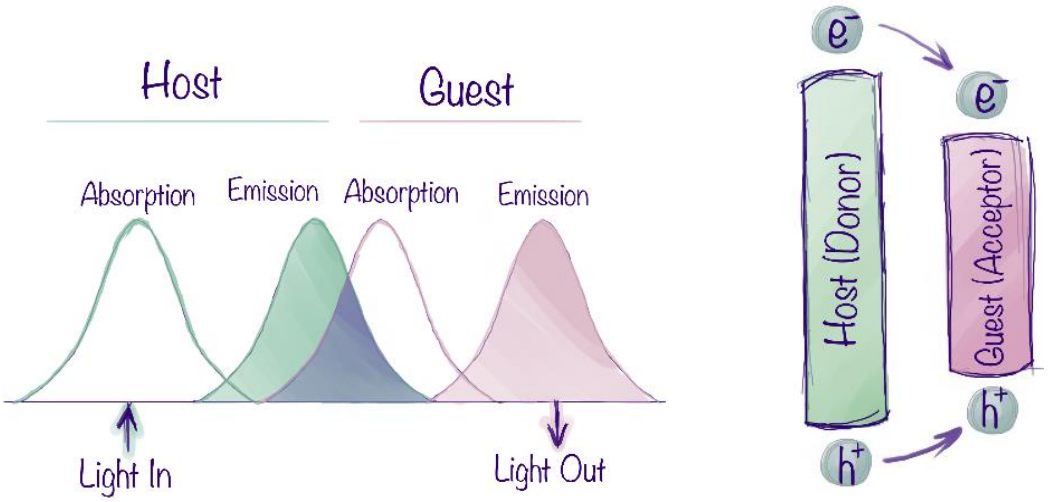

Figure 4.6. (left) The necessary relationship between the absorption/emission characteristics of the donor and those of the acceptor for a Förster energy transfer process and (right) Schematic energy profile of a host guest system with type I band alignment.

The choice of host also includes gauging compatibility of the optical properties with the emissive guest such that they have a spectral overlap. This can be explained in more detail if we look at **Figure 4.6** (left). After light is absorbed by the host molecule, its excited state is formed. The excited state energy can be transferred to a nearby guest molecule. However, for this energy transfer to occur, the emission of the host molecule needs to have an overlap with the absorption of the guest molecule. This energy transfer process occurring between a donor (D) molecule in the excited state and an acceptor (A) molecule in the ground state is known as Förster resonance energy transfer (FRET).

In addition, apart from the matched optical properties of the system, the electrochemical, and more specifically the HOMO and LUMO levels of both components have to be considered. It should be mentioned that these electrochemical properties are highly important for the device construction. Usually the HOMO and LUMO energy levels of the guest are selected so that they are inside the energy levels of the host as shown in **Figure 4.6** (right). In that type of alignment, usually referred to as type I band alignment, the HOMO sites of the guest will likely act as traps for holes, while the LUMO sites will act as traps for electrons in the system. Subsequently, upon charge injection these trapped holes and electrons at the guest molecule will provide sites for electron-hole recombination and finally exciton formation.[110,111]

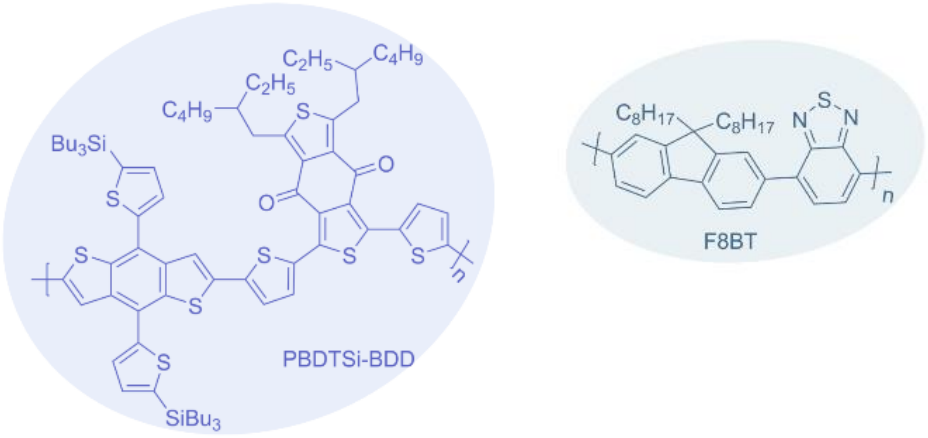

Figure 4.7. The chemical structures of polymer-based hosts PBDTSi-BDD and F8BT.

A number of host polymers were tested in conjunction with ZnP(TDPP)$_4$, however, the results for most of these were not encouraging and the discussion will focus upon only two of them, specifically PBDTSi-BDD and F8BT (**Figure 4.7**). PBDTSi-BDD was the host that showed the most promising device characteristics when combined with ZnP(TDPP)$_4$, out of all tested polymers so we optimized that system. The second host F8BT is an archetypal host material that is typically employed in technologies like light emitting diodes and field-effect transistors due to its good luminescent properties and charge mobilities, and so we used it as a benchmark for our study.[112-115]

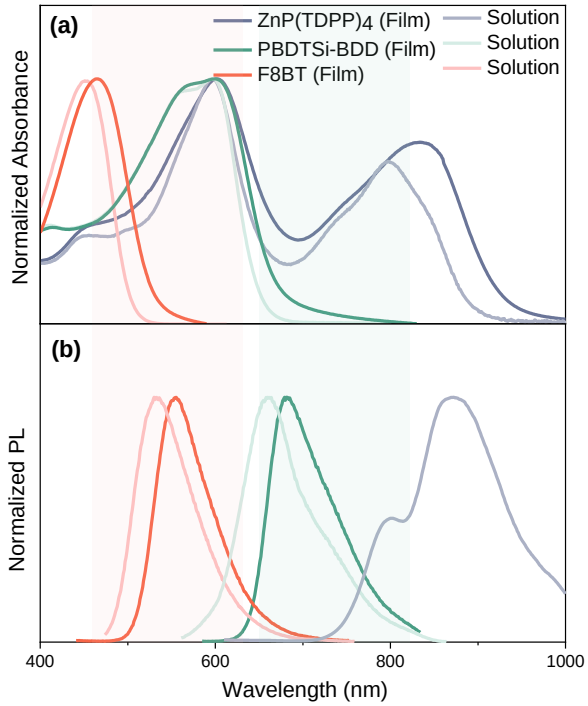

Figure 4.8. (a) Absorption and (b) PL spectra of ZnP(TDPP)$_4$, PBDTSi-BDD, and F8BT as thin films and solutions. The solution spectra were measured in toluene/pyridine 99:1 for ZnP(TDPP)$_4$ or toluene for PBDTSi-BDD and F8BT. The red and green highlights in the graph are used in order to show the spectral overlap between the hosts and the guest material.

The optical properties of the selected host and guest materials are shown in **Figure 4.8**. It is clear that both host polymers have a suitable spectral overlap with ZnP(TDPP)$_4$ as indicated by the red and green highlights. More specifically, the emission of the F8BT host overlaps with the S band of the porphyrin absorption, while the emission of the PBDTSi-BDD overlaps with the Q band. This observation indicated that a FRET is possible for both of these combinations.

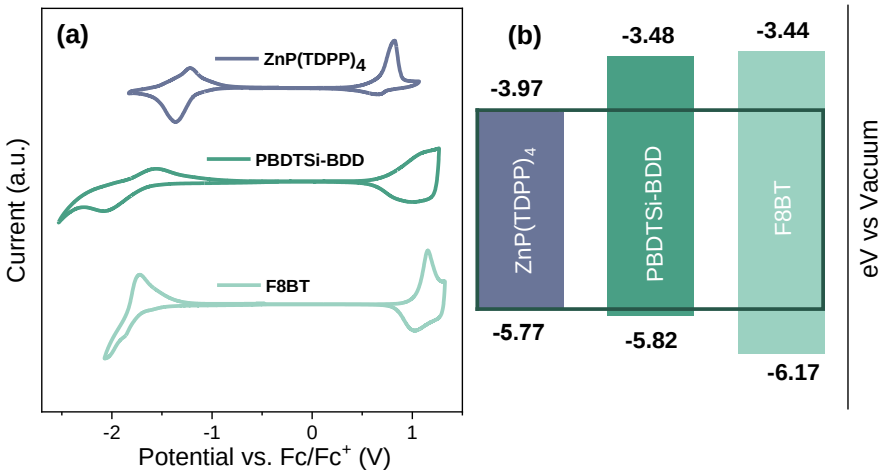

Figure 4.9. (a) CV traces of PBDTSi-BDD and F8BT hosts alongside guest Zn(TDPP)$_4$, in thin film (b) The energy levels determined from the CV data.

The CV traces of host polymer films can be seen in **Figure 4.9** (a), while their energy levels were estimated from the first oxidation onset potential (E_{ox}) and the first reduction onset potential (E_{red}), relative to the Fc/Fc^{+} redox couple. For PBDTSi-BDD and F8BT, the HOMO/LUMO levels were found to be –5.82/–3.48 and –6.17/–3.44 eV, respectively. The energy level diagram of all active materials can be seen in **Figure 4.9** (b). The porphyrin guest does indeed form a type I band alignment with both of these hosts, as its energy levels are included between the energy levels of the polymers. This indicated that charge injection from the host to the guest was plausible for both of these systems.

4.1.3. NIR-LECs Performance

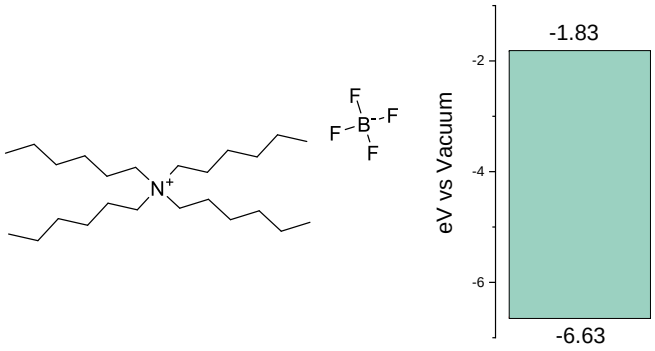

Figure 4.10. (left) The chemical structure of $THABF_4$ and (right) the electrochemical stability window of $THABF_4$.[116]

For the fabrication of the NIR-LECs, the active layer was spin-coated on top of an ITO/PEDOT:PSS anode. The emissive layer was composed of a blend of the F8BT or PBDTSi-BDD hosting $ZnP(TDPP)_4$ in conjunction with the ionic liquid tetrahexylammonium tetrafluoroborate ($THABF_4$) (**Figure 4.10**). This electrolyte was used as it was endowed with a wide electrochemically stability window, thus it will remain inert during the doping process during device operation.[116] The mass ratio of the electrolyte was held consistently at 5%, while the guest ratio was varied in order to optimize device performance. Finally, an Al cathode was deposited on top of the emissive layer.

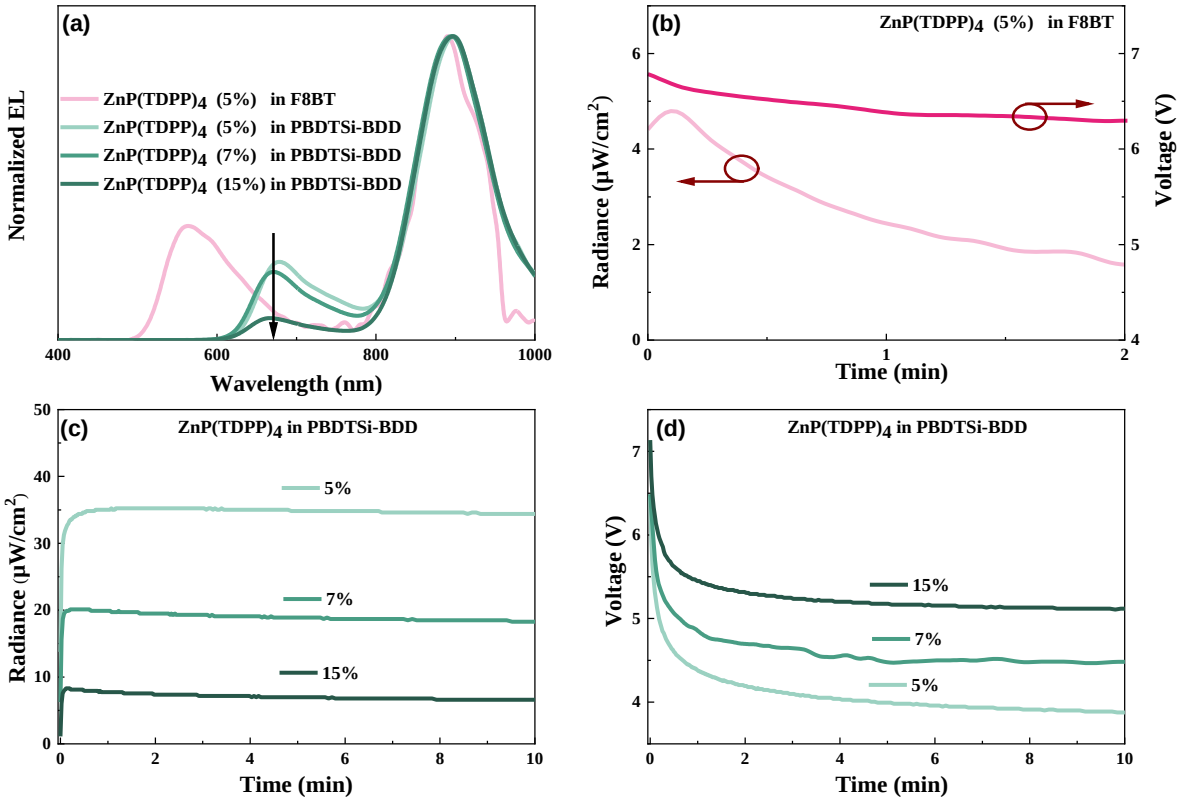

Figure 4.11 (a) Steady-state EL spectra as a function of host polymer with variable ZnP(TDPP)$_4$ concentrations. (b–d) Temporal evolution of the voltage and radiance as a function of host selection and ZnP(TDPP)$_4$ concentration, as identified in the legends.

Only a 5 mass% loading of ZnP(TDPP)$_4$ was used for the devices fabricated with F8BT, while on the other hand, PBDTSi-BDD hosted devices with 5, 7 and 15 mass% emitter loadings. From the EL spectra (**Figure 4.11** (a)), two emission peaks were present for all device constructs. When F8BT was used as the host, emission peaks were observed at 565 nm and 890 nm, which were assigned to F8BT and ZnP(TDPP)$_4$, respectively. Meanwhile, these features in PBDTSi-BDD based devices, were observed at 675 nm and 900 nm, corresponding to host and guest accordingly. The presence of remnant host peaks revealed that the host-to-guest energy transfer was indeed incomplete for all systems, however, it was less evident using polymer host PBDTSi-BDD. In fact, this could be quantified as 28% remnant host emission from F8BT and 19% from PBDTSi-BDD when ZnP(TDPP)$_4$ guest was used at 5 mass%. This could be attributed to a better spectral overlap between the emission of PBDTSi-BDD with the Q band of the emitter.

The temporal evolution of radiance and voltage during constant-current driving can be seen in **Figure 4.11** (b–d). When F8BT was used as the host (**Figure 4.11** (b)), the recorded peak radiance was very low at ~5 μW cm^{-2}, with an EQE value of 0.003%. Typically, during constant current operation, the formation of the p-n junction as described in chapter 1 balances the injection of holes and electrons , so that they recombine more efficiently into excitons, which in turn improves

the radiance of the LEC. However, this transient characteristic was not observed for F8BT (**Figure 4.11**(b)). The use of PBDTSi-BDD as the host resulted in improved device performances. In this instance, three different guest concentrations were used, namely 5, 7 and 15 mass% guest, and the concentration dependent device characteristics are illustrated in **Figure 4.11** (c-d) The best performing NIR LEC was achieved when the guest was introduced in only 5 mass% concentration, giving a peak radiance of 36 $\mu W\ cm^{-2}$, corresponding to an EQE of 0.028%. This radiant output was obtained with the application of a voltage as low as 3.8 V, and ~93% of the emission was located in the deep NIR regime, that being above 800 nm.

Generally speaking, NIR emitters in LECs tend to result in lower efficiencies than LECs that emit in the visible spectrum. In essence, this can be explained by the energy gap law for radiationless transitions. [117] The energy gap law is an intrinsic quenching mechanism, implying that at longer wavelengths (i.e. decreased energy gap), overlap between the lowest vibrational levels of the S_1 or the T_1 with the higher vibrational levels of S_0 and can lead to increased radiationless transitions and thus decreased photoluminescence efficiencies.[118-120] This statement thus reveals that is extremely difficult to produce NIR emitting molecules that can show exceptionally high performances.

Finally, to summarize, with proper molecular design, the synthesis of an emitter with a deep NIR EL was achieved. Although the efficiency of the devices using $ZnP(TDPP)_4$ was not overly impressive, this was not surprising because according to the energy gap law, the excited state of $ZnP(TDPP)_4$ has a higher propensity to undergo radiationless decay back to the ground state. Nevertheless, this work highlights potential for the use of Zn porphyrins being used as functional components in LECs, when NIR emission is required

4.2 An NT Containing Porphyrin Emitter

A problem commonly encountered with NIR emitters, and very much so for porphyrins, is their tendency to form aggregates. Aggregates however cannot easily be avoided if one considers their molecular design. They are normally very flat, coplanar, conjugated structures which are very prone to π-π stacking.[121] In this section, we tried to exploit from the observed high aggregation seen in the PL of a novel porphyrin emitter. By using an appropriate host polymer, aggregation was mitigated and, in fact, controlled aggregate formation could be achieved, where the EL was redshifted and the efficiency of fabricated NIR LECs were increased.

4.2.1 Design Strategy

In the previous section, a diketopyrrolopyrrole derivative was used as the acceptor component to decorate the periphery of the porphyrin core, which was itself considered as having donor character. This push-pull electronic arrangement found in $ZnP(TDPP)_4$ in conjunction with an extended π conjugation and highly planar structure led to a molecule, which was optically active

in the NIR region. Here, a similar design strategy was followed, however in this case, we chose a relatively unstudied weaker electronic acceptor to tether to the porphyrin core.

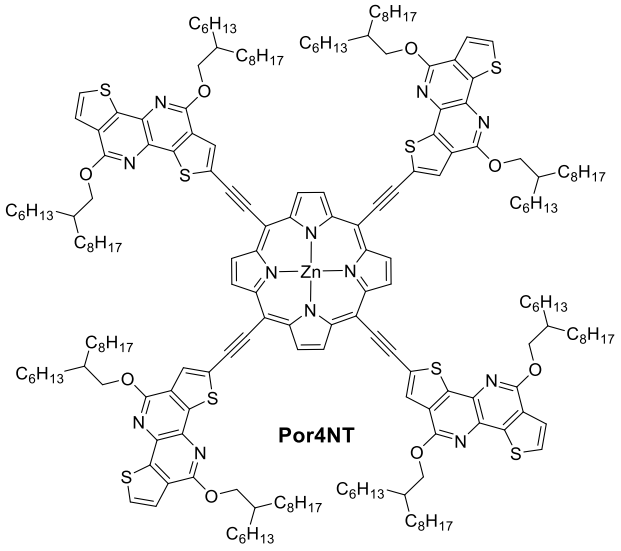

Figure 4.12. The chemical structure of the Por4NT emitter.

The acceptor we chose was 5,10-bis((2-hexyldecyl)oxy)dithieno[3,2-*c*:3',2'-*h*][1,5]naphthyridine (NT). Four NT units were connected to the *meso* positions of the porphyrin via acetylenic linkers and for the sake of convenience was named as Por4NT (**Figure 4.12**). In addition, we chose to accessorize the peripheral acceptors with longer branched side chains. So, the 2-ethylhexyl side chains found in ZnP(TDPP)$_4$ were replaced by (2-hexyldecyl)oxy branched side chains, of which two were connected to each NT unit. The purpose of this was to further increase the solubility and proccesibility of the emitter, so there will be no need to employ pyridine for any solution based measurements or manipulations.

4.2.2 Material Synthesis and Characterization

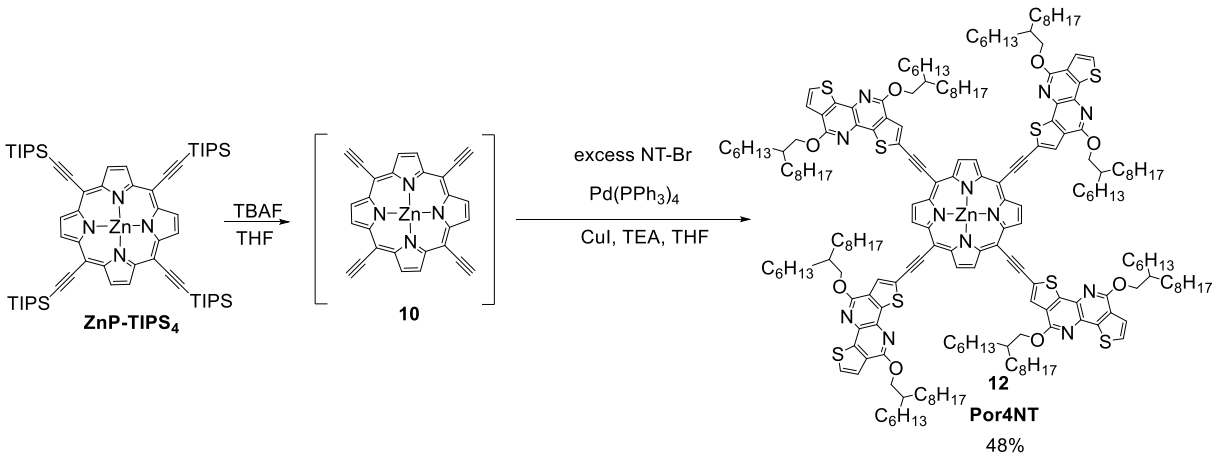

Scheme 4.4. Synthesis of **Por4NT**.

The synthesis of Por4NT followed similar conditions to that of $ZnP(TDPP)_4$ (**Scheme 4.4**). It should be mentioned that the NT-Br monomer was kindly provided by Mats Andersson's laboratory at Flinders University. Initially, $ZnP\text{-}TIPS_4$ was desilylated with TBAF, and after a rapid work up, was followed by a Sonogashira coupling of the reactive intermediate with NT-Br affording Por4NT as a dark green paste with a metallic luster in 48% yield. Indeed, Por4NT possessed an exceptional solubility in common organic solvents, and therefore the use of pyridine could be avoided during the purification steps. Thermogravimetric analysis (TGA) and differential scannic calorimetry (DSC) of solid Por4NT revealed a high decomposition temperature of 300 °C under an inert atmosphere, and no thermal transitions occurred between -50 and 250 °C (see SI of Paper III at the end of the thesis for more information).

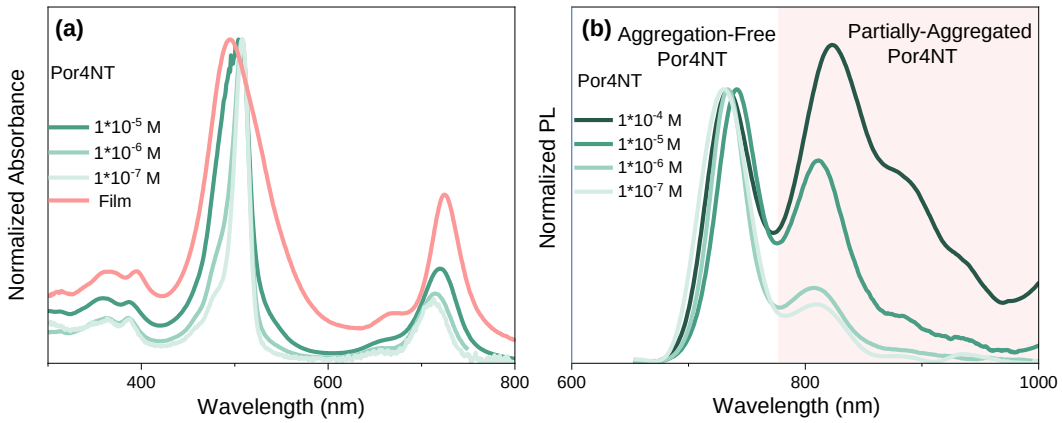

Figure 4.13. (a) The normalized absorption spectra of Por4NT as toluene solutions at three concentrations and as a thin film. and (b) the normalized emission spectra of Por4NT at differing concentrations in toluene. The concentrations are indicated in the legend.

The absorption and emission spectra of Por4NT were studied in order to evaluate the optical properties of this new derivative and are presented in **Figure 4.13** (a) and (b). Absorption spectra of this porphyrin emitter were measured at varying concentrations in toluene and in solid state as a spin coated neat film. Two main expected absorption bands were observed, namely the S and Q bands,[122] for which in solution were located at ~515 nm and ~705 nm, respectively. It should be mentioned that unlike for what was observed with $ZnP(TDPP)_4$, both Q bands in Por4NT were distinguishable, which we attributed to the choice of the different acceptor. A possible explanation for this observation can be found in the electron density of the frontier orbitals (Figures A2 and A3 Appendix) that were related to the Q absorption band as estimated by DFT calculations. For $ZnP(TDPP)_4$, the electron density was delocalized over the entire structure, while for Por4NT, it was more localized at the porphyrin core leading to a smaller effect on the Q absorption band. Meanwhile, absorption measurements at increased concentrations lead to a blue-shifting of the S band, in addition to red-shifting of the Q bands. This observation was in fact more apparent in the

thin film measurement. The optical energy gap of Por4NT was also determined from the absorption onset and found to be 1.61 eV.

From Figure 4.13 (b), it was immediately obvious that the emissive properties of Por4NT were highly concentration dependent. Two main peaks were observed at ~730-740 nm and ~810-820 nm, with the lower energy feature showing an increase of relative intensity when compared to the higher energy peak, as the concentration of the porphyrin was increased. Moreover, the longer wavelength peak appeared broader as well as more redshifted at higher concentration. PLQYs of the emitter were measured at varying concentrations with an integrating sphere and their values are presented in **Table 4.1.** It is clear that the PLQYs dramatically dropped with increasing concentration, while no emission at all was observed from the Por4NT film.

Table 4.1. PLQYs of Por4NT at varying concentrations in toluene and as a spin coated film.

Concentration (M)	10^{-7}	10^{-6}	10^{-5}	10^{-4}	Film
PLQY [%]	29.3	25.4	12.8	3.8	N/A

From the data obtained both from the absorption and PL spectra we could draw two conclusions. Firstly, this emitter has a high tendency to aggregate, as shown from PL spectra both in solution and in solid state,[123] and secondly this aggregation was mainly seen in the PL spectra, while the absorption features were concentration invariant. The shorter wavelength PL peak was thought to be an emission from "aggregation-free Por4NT" molecules, and the longer-wavelength PL band was attributed to "partially aggregated Por4NT" molecules. Since no emission was observed from the Por4NT film, we ascribed it to "fully aggregated Por4NT" molecules.

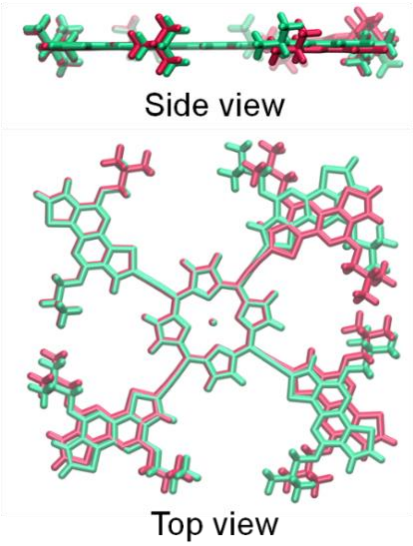

Figure 4.14. Side-view and top-view conformation of Por4NT in the geometry-optimized ground state (S_0, red structure) and the lowest-energy excited state (S_1, green structure).

DFT calculations were also performed to gain an insight into the molecular conformation of this molecule and reinforce the results obtained from the PL spectra. The overlapping S_0 (red structure) and S_1 (green structure), conformations are presented in **Figure 4.14** (a) where we see that both S_0 and S_1 adopted a very similar highly coplanar conformation. This coplanar conformation indeed supported the idea of aggregate formation.

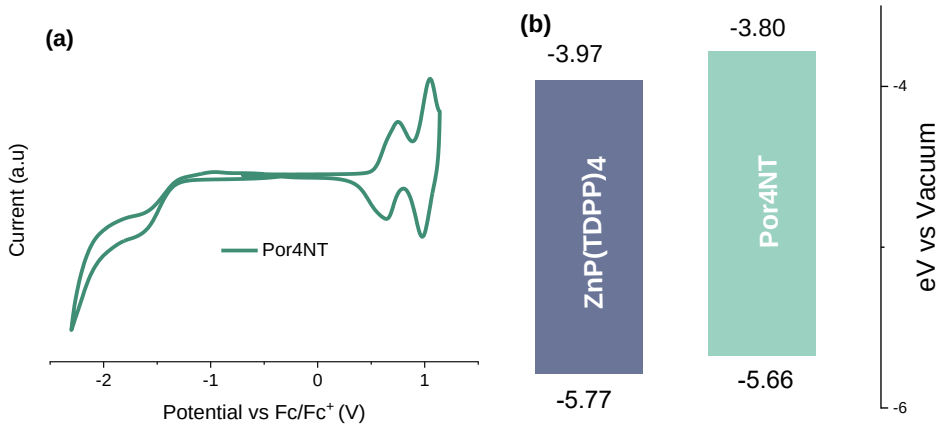

Figure 4.15. (a) CV trace of Por4NT (b) Energy level diagrams comparing ZnP(TDPP)$_4$ with Por4NT.

A CV trace of Por4NT film is shown in **Figure 4.15** (a). The HOMO and LUMO levels were estimated to be -5.66 eV and -3.80 eV, respectively, which give an energy gap of 1.86 eV. Upon comparison of the energy levels for Por4NT with ZnP(TDPP)$_4$, we noticed that the HOMO levels of the latter were more downshifted, by 0.17 eV for the LUMO and 0.11 eV for the HOMO. This observation was indeed in agreement with our hypothesis that the DPP unit possessed stronger electron accepting capabilities. Regarding the reversibility of the electrochemical oxidation and reduction process, we observed that the oxidation process was quasi-reversible, while the reduction event showed a lack of reversibility.

4.2.3 Host-guest System properties

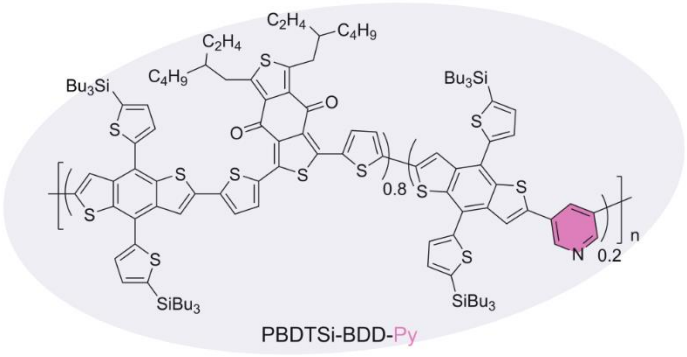

Figure 4.16. Chemical structure of the PBDTSi-BDD-Py host.

The decreased PLQYs with increasing solution concentration and the lack of emission in the solid state led us to the incorporation of Por4NT into a host-guest system for the fabrication of LECs.

For this guest, three polymer hosts were used; F8BT, PBDTSi-BDD, which had been introduced earlier, and the new host polymer PBDTSi-BDD-Py, the structure of which is shown in **Figure 4.16**. PBDTSi-BDD-Py is a terpolymer consisting of the same monomeric units as PBDTSi-BDD, only with the addition of a third component, pyridine (Py), where the connectivity of this heterocycle to the polymer chain occurred at the 3- and 5- positions. The hypothesis in deciding to employ this particular host was that it was thought that by introducing this polar unit to the backbone of PBDTSi-BDD, it would render the polymer chain more flexible and the electrolyte could possibly penetrate easier through this modified medium, enhancing the ion mobility. Moreover, since pyridine can coordinate axially to the zinc metal center of Por4NT, which was assumed to occur, this could counteract the effects associated with aggregation.

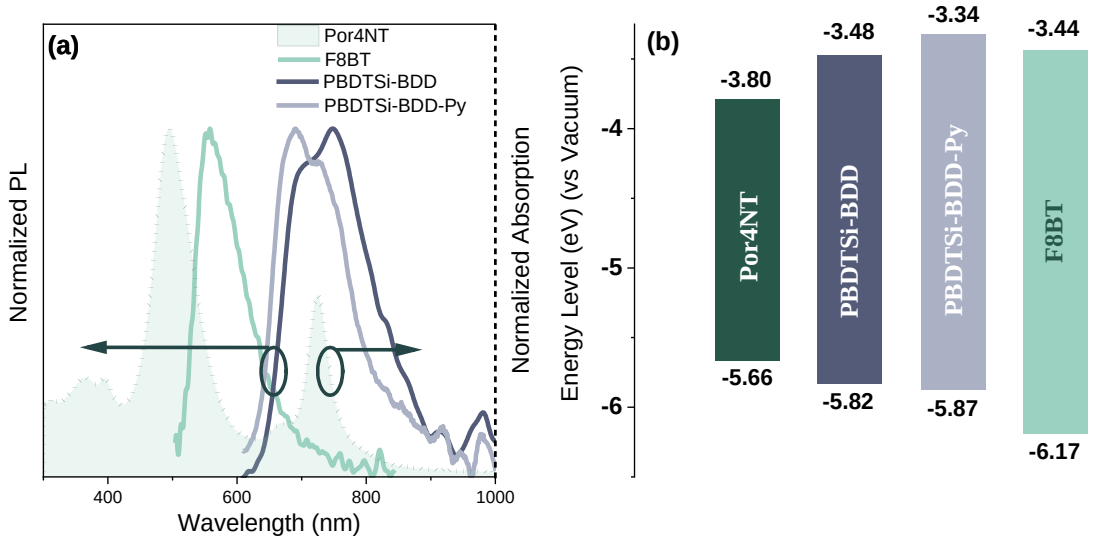

Figure 4.17. (a) Absorption profile of Por4NT emitter and PL of the host polymers (b) Energy level diagram for Por4NT and host polymers used in this study.

Figure 4.17 (a) presents the absorption spectrum of Por4NT overlaid with the PL for all polymeric hosts. In order to have an efficient host-to-guest energy transfer, a spectral overlap between the host emission and the guest's absorption is crucial to obtain an efficient FRET. For polymer hosts PBDTSi-BDD and PBDTSi-BDD-Py, there was a clear overlap between their emission and the low energy Q band of Por4NT, while in the case of host F8BT, the overlap was with the higher energy S band. Those findings indicated that energy transfer was likely for all three scenarios.

The energy levels for all these components are presented in **Figure 4.17** (b). The derived HOMO values of PBDTSi-BDD and PBDTSi-BDD-Py host polymers were -5.82 and -5.87 eV, while their LUMOs were positioned at -3.48 and -3.34 eV, respectively. The LUMO level of F8BT was positioned in between that of the two other host polymers at -3.44 eV, whereas the HOMO was much deeper at -6.17 eV. This implied that both electrons and holes will be trapped on the Por4NT

guest, which could be beneficial for the host-to-guest energy transfer during electrical driving of host-guest blends in devices.

4.2.4. NIR-LECs Performance

The final part of this work was to test our hypothesis by incorporating these components into working LEC devices. For that, NIR LECs were fabricated where the concentration of the emitter in the host-guest blend was adjusted depending on the performance with the respective polymeric host. More specifically, 5 mass% loaded Por4NT guest devices were fabricated for all host-guest combinations, then 7 mass% devices were fabricated for the combinations of the porphyrin derivative with both PBDTSi-BDD and PBDTSi-BDD-Si. While in the case of the most promising combination, PBDTSi-BDD-Py/Por4NT, a device with a 10 mass% loading of emitter was also constructed. Each blend of host/guest/ionic liquid was spin-coated on top of the ITO/PEDOT:PSS anode and Al cathodes were deposited on top of the functional layer.

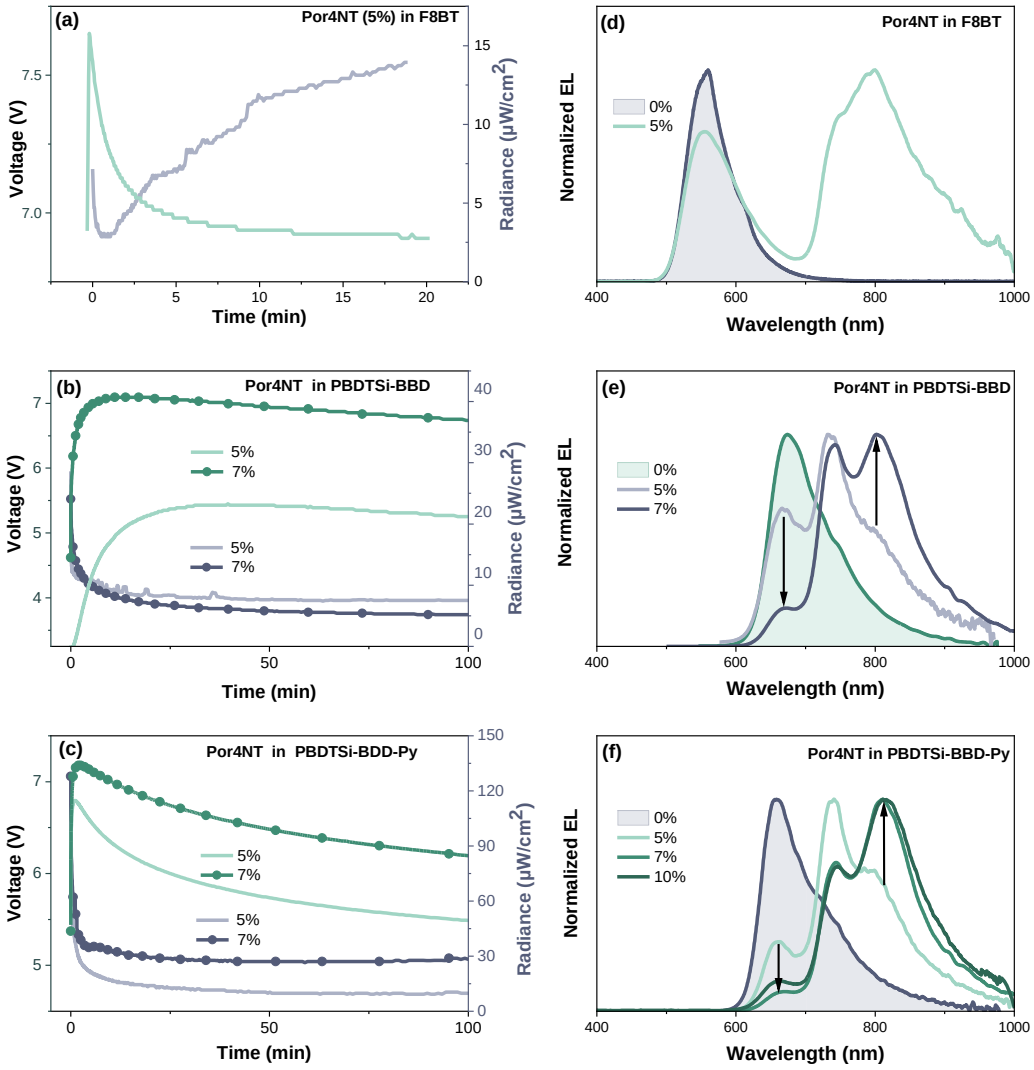

Figure 4.18. (**a-c**) The temporal evolution of the voltage and radiance for the host-guest LECs comprising (a) F8BT, (b) PBDTSi-BDD, and (c) PBDTSi-BDD-Py as the hosts. (**d-f**) The steady-state EL spectra of host-only

and host-guest LECs, with the host being (d) F8BT, (e) PBDTSi-BDD and (f) PBDTSi-BDD-Py. The arrows indicate improved host-to-guest energy transfer. The devices were driven by a current density of 75 mA/cm^2.

The parameters that characterize a functional LEC during constant-current operation is the decrease of the applied voltage necessary for device operation and an increase of observed radiance with time. The electrochemical doping during device operation will render the active material more conductive and in addition to the formation of a p/n-double layer, which will balance the charge injection and transport, the applied voltage will be reduced. At the same time, the more balanced electron and hole injection should lead to faster recombination into excitons and radiance will be improved. [124] By looking at **Figures 4.18** (**a-c**), we observed that all devices featured a decreasing voltage and an increasing radiance at a constant current density of 75 mA/cm^2 and we can conclude from this that all three polymer hosts used with Por4NT give functional LEC composites. When comparing all the devices at 5% Por4NT loading, we observed that the driving voltage using the PBDTSi-BDD host was the lowest at 3.9 V, while the highest was observed for F8BT with a value of 6.9 V. That observation agrees with the calculated energy levels, seen in **Figure 4.17** (b) as the electron/hole trap depths were the deepest in the case of the F8BT polymer host.

Table 4.2. LEC performances as a function of host selection and Por4NT guest concentration.

Host	Guest conc.	EL peaks [nm]	Peak radiance [μW/cm^2]	Lowest voltage [V]	EQE [%]
F8BT	5%	550, 800	16	6.9	0.013
PBDTSi-BDD	5%	670, 735	23.1	3.9	0.019
PBDTSi-BDD-Py	5%	660, 740, 800	115	4.6	0.095
PBDTSi-BDD	7%	745, 802	40.7	3.6	0.037
PBDTSi-BDD-Py	7%	745, 810	134	5.0	0.121
PBDTSi-BDD-Py	10%	745, 810	33.5	7.9	0.03

Figure 4.18 (d-f) includes the EL spectra from the host only devices as well as the host-guest systems using selected concentrations. It was clear that for all devices, the EL spectra featured a peak originating from the polymer host, indicating incomplete host-to-guest energy transfer. Further characteristic information on the host peaks can be found in **Table 4.2.** Indeed, an increase of the guest concentration lead to a decreased host emission, and Por4NT in a 7mass% blend with PBDTSi-BDD-Py showed the best overall device performance. Upon looking into this blend in more detail, we note that it delivered a strong radiance, peaking at 134 μW/cm^2 with an EQE of

0.121 % and a drive voltage of 5.0 V. Notably, the vast majority of this radiance (~96%) was delivered into the NIR range above 700 nm (80% of which was above 750 nm) and the emission maximum, itself, lay at 810 nm. These promising results obtained from the 7% blend with PBDTSi-BDD-Py, prompted us to the fabricate a third device, this time using a 10 mass% loading of Por4NT. However, all device characteristics were found to be inferior at this higher level (compared to the 7%).

By combining the EL results for the optimized PBDTSi-BDD-Py/Por4NT (7%) host-guest device with the PL data from **Figure 4.13** (b) we could conclude that the NIR emission stemmed primarily from "partially aggregated Por4NT" molecules. Finally, because the radiance and efficiency in the 10% device showed a decrease in performance compared to 7% Por4NT, we believed that the "partial aggregation"-"complete aggregation" threshold for good device performance is positioned at a guest concentration of 7%.

To summarize, aggregation is a phenomenon commonly seen in NIR emitters. The formation of aggregates typically results in the creation of two excited states with different energies, with the probability of radiative transition from the lower-energy state being very low.[125,126] Porphyrin derivative Por4NT, due to the fact that it was fully aggregated in the solid state, did not exhibit any emissive properties, however upon use of an appropriate host changed the outcome. The polymeric host, in particular PBDTSi-BDD-Py, not only gave rise to functional devices when used in a host-guest blend with the emitter but with systematic study we also fine-tuned the concentration of the blend so that we could benefit from the emission of the "partially aggregated Por4NT" and obtain more redshifted NIR-LECs with an increased efficiency.

4.3 Porphyrin Emitters with aldehyde and rhodanine end groups

In this body of work, the synthesis of two new porphyrin emitters and their performance in NIR LECs is described. This work constitutes a comparative study between two porphyrin variants, both of which are substituted with modified benzothiadiazole (BT) acceptors, the structures of which can be seen in **Figure 4.19** coloured pink. In one case, the extremities had aldehyde groups, while for the other porphyrin, the organic dye unit rhodanine (Rh). Aldehyde containing emitters are not typically used for the fabrication of electroluminescent devices, on the account of the inherent instability of this functional group. The question remains, can devices consisting of a functionalised aldehyde emitter operate ? The answer is yes, and the results arising from this hypothesis will be discussed in paragraph 4.3.3. The rhodanine containing emitter is differentiated from the aldehyde, both in the nature of the endcapping acceptor, as well as a longer conjugation length from the porphyrin core. As a comparison, how is this additional degree of conjugation going to affect the

optical properties of the emitter? Will the rhodanine unit positively infuence the emission profile of the porphyrin? The answer to these questions will be explained in this section.

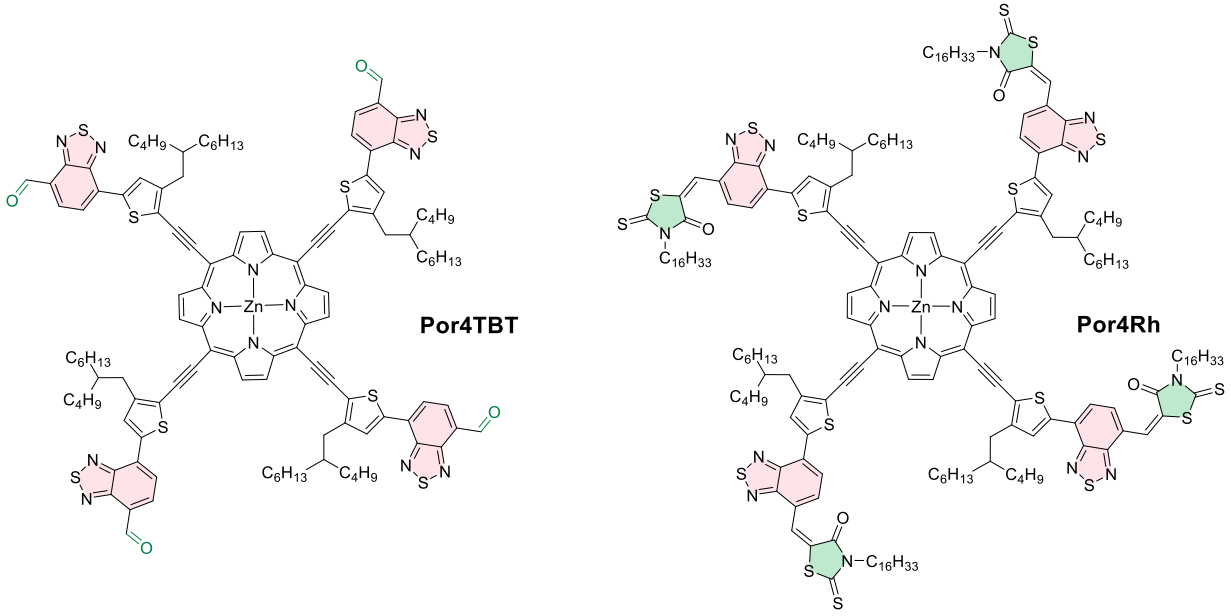

Figure 4.19. Chemical structures of **Por4TBT** and **Por4Rh**.

4.3.1 Design Strategy, Material Synthesis and Characterization

The specific structures of these emitters, named Por4TBT and Por4Rh, are shown in **Figure 4.19**. Intermediate ZnP-TIPS$_4$ (see **Scheme 4.4**) was again the key building block for both these molecules. Before the deprotection and subsequent reaction of this compound, peripheral benzothiadiazole coupling partner **16** needed to be constructed. The BT unit was directly connected to an aldehyde group, boosting its electon accepting properties due to the electron withdrawing nature of the aldehyde. The synthetic strategy involved two synthetic steps, the first of which was a Stille coupling of **13** with a 2-stannyl thiophene (**14**), which featured a branched alkyl chain in the 4-position. These 2-hexylbutyl side chains were considered nessesary in order to improve the solubility of the Por4TBT, as this structure was expected to be highly planar and possibly prone to aggregation. The bromination of **15** could be achieved conveniently using *N*-bromosuccinimide. Using the general procedure, ZnP-TIPS$_4$ was subjected to silyl deprotecting conditions followed by a four-fold Sonogashira reaction with an excess of **16** to produce Por4TBT. For the second porphyrin derivative, Por4Rh, four rhodanine units were adfixed to Por4TBT, taking advantage of the aldehyde functional handles in a subsequent Knoevenagel condensation. Interestingly, rhodanine has often been used in the field of organic solar cells, due to its electron withdrawing nature when constructing D-A arrangements in π-conjugated compounds, and has lead to the production of highly efficient devices in that area.[127] In this work, rhodanine was utilised to study the effect of extending the conjugation further from the porphyrin core, as well as enhancing electron accepting capabilities of the outer units. It should also be mentioned that the

rhodanine unit was endowed with a long 2-hexyldecyl side chain to ensure the formation of a product with satisfactory solubility.

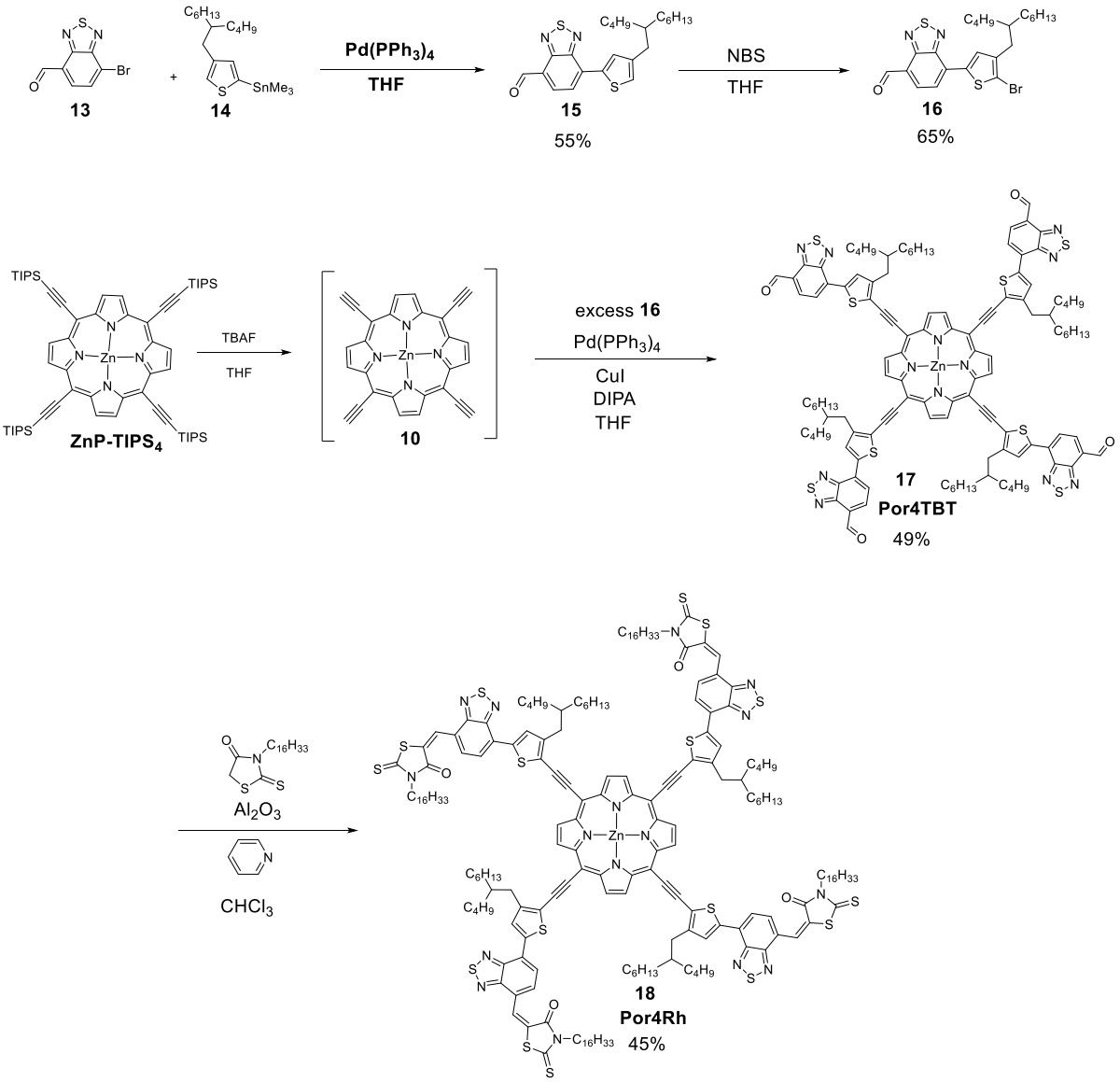

Scheme 4.5. Synthesis of **Por4TBT** and **Por4Rh**.

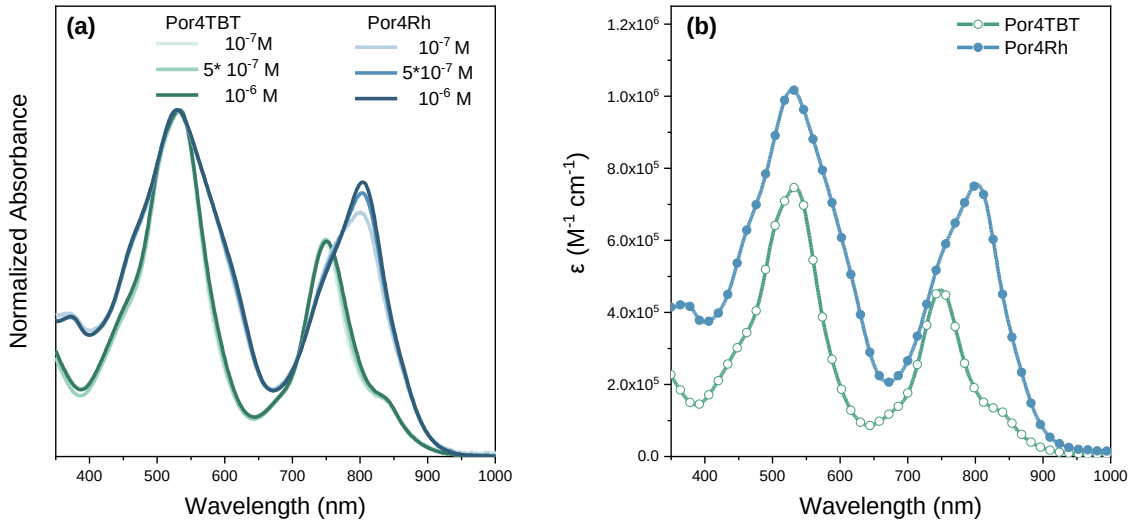

Figure 4.20. (a) Normalized absorption of Por4TBT and Por4Rh in varying concentrations as identified in the legend and (b) molar extinction coefficients as a function of wavelength for Por4TBT and Por4Rh emitters as an average of three different concentrations. The solvent for all measurements was toluene/pyridine 99:1.

The absorption spectra of Por4TBT and Por4Rh were studied at varying concentrations and are presented in **Figure 4.20** (**a**). Por4TBT showed two main absorption maxima at ~530 nm and ~750 nm, while a shoulder appeared at ~830 nm, which could be distinguished as the Q band. Two absorption peaks were observed for Por4Rh and were centered at ~530 and ~800nm. The exact values for the peaks based on their concentration can be seen in **Table 4.3**. Interestingly, the addition of the rhodanine unit did not have any significant effect on the positioning of the S band, however, the Q band was clearly affected, which was intensified and redshifted by ~55 nm depending on the concentration. Overall, both the Q and S bands appeared broader for Por4Rh, which we attributed to the higher degree of conjugation in the molecule. Increasing the concentration did not make any significant change to the absorption profile of Por4TBT, revealing no indication of mass aggregation arising from these measurements. The extinction coefficients of these porphyrin derivatives were also calculated and are presented in **Figure 4.20** (b). Both of the emitters possessed a high extinction coefficient for both S and Q bands, which were in the order of 10^{-5} M^{-1} cm^{-1} for Por4TBT and 10^{-6} M^{-1} cm^{-1} for Por4Rh. It is clear from Figure 4.19 (b) that the incorporation of the rhodanine dye into the structure resulted in an increased absorption coefficient of ~1 order of magnitude. The E_g^{opt} for both chromophores were also estimated from the λ_{onset} of the absorption peaks. Interestingly, both of the molecules possessed identical E_g^{opt} values of 1.38 eV, thus revealing that further extension of the conjugation and use of a different acceptor did not have much effect in decreasing the optical gap. The identical E_g^{opt} values found for both compounds suggested that the energy for the lowest electronic transition accessible via absorption of a single photon ($S_0 \rightarrow S_1$) was the same for both molecules.

Table 4.3. The optical properties of the Por4TBT and Por4Rh emitters as a function of the concentration in toluene/pyridine 99:1 solution.

Concentration [M]	Emitter	S-band Absorption [nm]	Q-band Absorption [nm]	PL [nm]
$1*10^{-6}$	Por4TBT	532	750	772/855
	Por4Rh	528	804	786/890
$5*10^{-7}$	Por4TBT	533	749	771/854
	Por4Rh	529	804	791/883
$1*10^{-7}$	Por4TBT	532	748	770/856
	Por4Rh	531	801	793/882

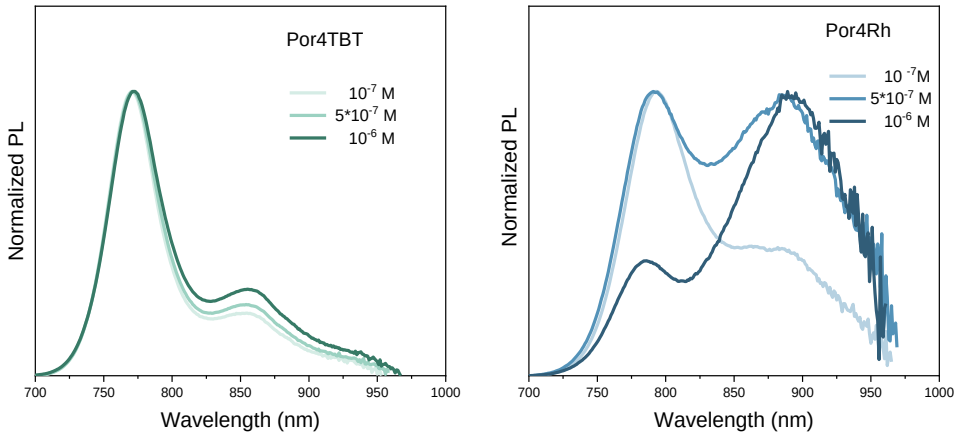

Figure 4.21. Normalized PL spectra of (a) Por4TBT and (b) Por4Rh in varying concentrations as identified in the legend. The solvent employed was toluene/pyridine 99:1.

The PL spectra are presented in **Figure 4.21** (a-b) and also summarized in **Table 4.3**, were recorded at several concentrations. Although the absorption peak maxima did not differ much going from Por4TBT to Por4Rh, the effect of the structural change on the PL was more pronounced. An emission peak for Por4TBT was evidenced at ~750 nm while for Por4Rh this value was ~800 nm, translating to a ~50 nm redshift. Thus, the effect of incorporating rhodanine into the structure led to an emission peak deeper into the NIR regime. Another significant difference between Por4TBT and Por4Rh, was the effect that increased concentration had on the excited state of the emitter. For Por4TBT, an increase of concentration only slightly affected the intensity of the lower energy emissive band in the PL spectra, which can be viewed as a slight increase of its intensity relative to the high energy peak. However, in the case of Por4Rh, the observed trend was different. The intensity of the lower energy emission for Por4Rh increased significantly at higher concentrations. More specifically, at 10^{-6} M concentration, the peak was located deeper in the NIR regime and surpassed the higher energy peak in intensity. Thus, for Por4Rh, emission was evidenced from aggregates and was observed at longer wavelengths.

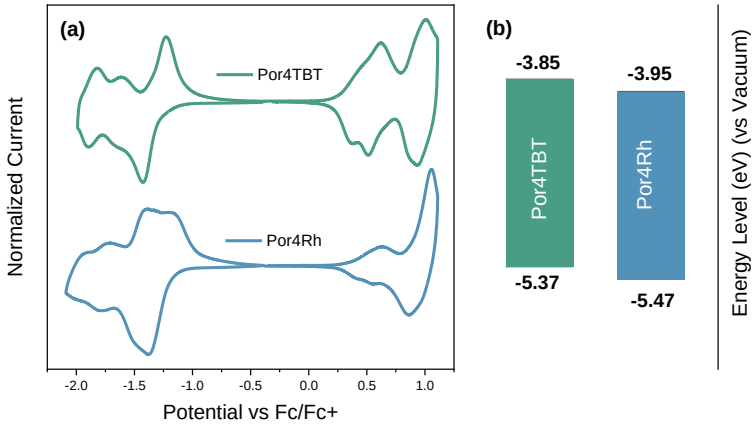

Figure 4.22.(a) CV traces of Por4TBT (upper) and Por4Rh (lower) and (b) energy level diagram of Por4TBT and Por4Rh.

Films of both these porphyrins were subjected to CV, where the cyclovoltammograms can be seen in **Figure 4.22** (a). Both Por4TBT and Por4Rh exhibited quasi-reversible electrochemical p-type doping as well as electrochemical n-type doping. Equations, $E_{HOMO} = -(E_{ox} + 5.13)$ (eV) and $E_{LUMO} = -(E_{red} + 5.13)$ (eV), were used to convert the onset potential for oxidation (E_{ox}) and the onset potential for reduction (E_{red}) to the HOMO and LUMO energy levels, respectively, the results of which are shown in **Figure 4.22** (b). The derived HOMO/LUMO levels have the values of -5.37/-3.85 eV and -5.47/-3.95 eV for Por4TBT and Por4Rh, respectively. The estimated energy levels reveal that indeed the rhodanine had a stronger electron accepting character that led to a downshift of the energy levels. The estimated E_g for both porphyrins were exactly the same, following the trend from the E_g^{opt}, suggesting that the stonger acceptor had no effect in reducing the energy between the frontier orbitals but only shifting them downwards.

4.3.2. Host-guest system and NIR-LECs Performance

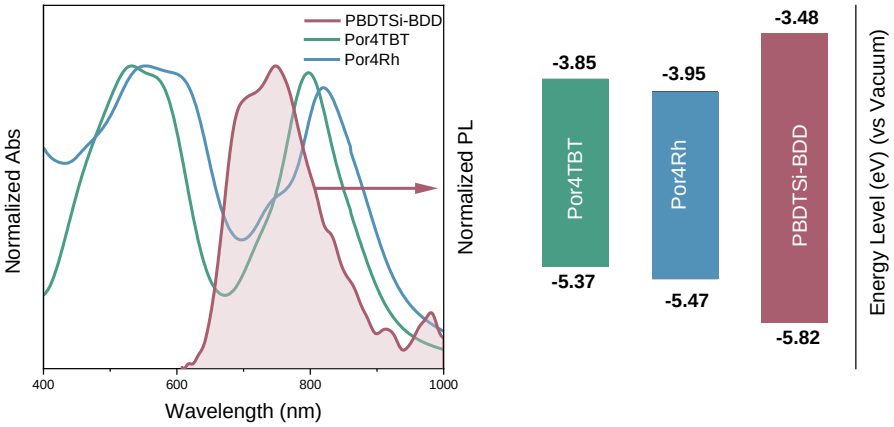

Figure 4.23. (a) Normalized absorption spectra of Por4TBT and Por4Rh and normalized PL spectrum of PBDTSi-BDD obtained in the solid state; (b) Energy level diagram of Por4TBT and polymer host PBDTSi-BDD used as the matrix in this study.

From **Figure 4.23** (a), we can see that there was good spectral match between the emission band of this host and the absorption profiles of the guest materials, since the PL of PBDTSi-BDD overlapped with the Q band of both emitters, thus an energy transfer via Förster mechanism is possible for both scenarios. From **Figure 4.23** (b), we observed that the energy levels of Por4TBT and Por4Rh were both included inside the energy levels of the host, thus the energy transfer from the host to the guest should also be evident in fabricated devices.

NIR LECs were fabricated using blends of either 7% of Por4TBT or Por4Rh along with 5% ionic liquid $THABF_4$ in polymer host PBDTSi-BDD, by spin-coating onto ITO/PEDOT:PSS anodes and capping with an Al cathode.

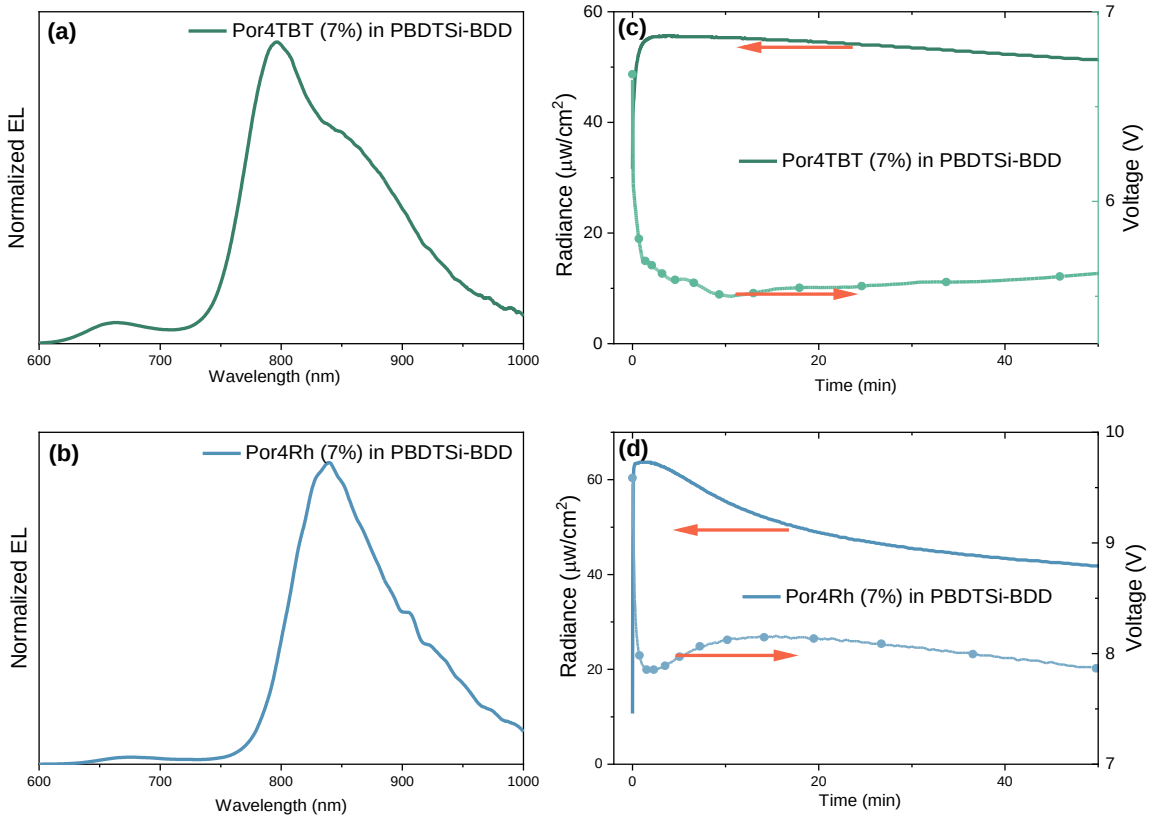

Figure 4.24. (a-b) Steady-state EL spectra for devices containing (a) Por4TBT and (b) Por4Rh in 7 mass% concentration. (c–d) Temporal evolution of the voltage and the radiance as a function of the guest selection, as identified in the legends.

The steady-state EL spectra for devices being driven by a constant current density of J = 74.5 mA cm^{-2} are shown in **Figure 4.24** (a-b). The EL peaks were positioned at 795 nm and 840 nm for Por4TBT and Por4Rh, respectively, following the trend observed from the PL measurements. The energy transfer found in both systems (**Figure 4.24** (a-b)) was highly efficient, translating to a remnant host peak <4% for Por4TBT and <2% for Por4Rh. Thus, by comparing the results from these devices with those previously presented, namely Por4NT and $ZnP(TDPP)_4$, we can conclude

that the porphyrins described in this paragraph were more effective in transferring the emissive energy of the host to the guest porphyrin. Interestingly, a single EL peak was obtained from the blend using Por4Rh, observable beyond 750 nm as opposed to the results from the PL spectra, where two features were seen at higher concentrations, clearly due to aggregation. On the other hand, even though from the PL, the Por4TBT emitter did not exhibit aggregation, in the EL spectrum, a lower energy shoulder could be distinguished next to the main peak. The latter observation, with the presence of a second feature in the EL spectra could be attributed to an incompatibility of Por4TBT, with either the host polymer or the electrolyte leading to phase separation, however, this was not the case for Por4Rh. Needless to say, this speculation needs to experimentally be proven by studying the morphology of the blends of the host, guest and electrolyte.

Table 4.4. Summary of the LEC device performance as a function of guest selection.

Host	Guest (7%)	EL peaks [nm]	Peak radiance [μWcm^{-2}]	Voltage [V]	EQE [%]
PBDTSi-BDD	Por4Rh	840	63.7	7.8	0.059
	Por4TBT	795	55.7	5.5	0.050

Figure 4.24 (c-d) presents the radiance and voltage values of the LECs during the initial turn-on process. In terms of performance, Por4Rh showed the highest radiance of 63.7 μW cm^{-2} and an EQE of 0.059 %, while devices incorporating Por4TBT yielded a radiance of 55.7 μW cm^{-2} at an EQE of 0.05% (the detailed device characteristics can be found in **Table 4.4**). Even though Por4TBT and Por4Rh differ in their emission properties, their E_g and E_g^{opt} were the same, thus a similar performance should be obtained based on the energy gap law. Thus, we attributed the enhanced efficiency of Por4Rh based devices in this case to a better compatibility between the host and the guest. However, more experimental evidence is needed for this conclusion to be absolute. On the downside, the voltage of operation for the Por4Rh based device was as high as 7.8 V, which could be detrimental to the lifetime of this LEC.

Overall, in this work two new emitters were synthesized and studied, both in relation to their optical properties and their performances in LECs. Even though Por4TBT and Por4Rh originated from the same starting materials, where four very electron deficient benzothiadiazole derivatives were connected via acetylenic linkages to the porphyrin core through all four meso positions, their properties had shown some significant differences originating from their connection to an aldehyde (for Por4TBT) and a rhodanine (for Por4Rh) group. More specifically, in the absorption the extended conjugation and the use of the rhodanine end group resulted in an increased extinction coefficient for Por4Rh. Moreover, a notable redshift in the emission of the rhodanine

containing emitter was observed. This redshifting of the PL, in the case of the Por4Rh emitter, could be attributed to the stronger electron accepting character of the rhodanine moiety, which was also confirmed by examining the energy levels of these materials. Finally, fabrication of NIR LECs, revealed that Por4TBT could lead to functional devices, even though the stability of the aldehyde group was a concern in the beginning. The best device characteristics were obtained from the Por4Rh emitter, where a radiance of 63.7 $\mu W\ cm^{-2}$, and an EQE of 0.059 % were obtained at an EL peak located at 840 nm, which were ascribed to a better compatibility between the host and the guest. However, further study is needed to draw a clearer picture of the structure-property relationship, which could be achieved by looking at the morphology of blends of the host/guest and electrolyte.

CHAPTER 5

5 SYNTHESIS AND CHARACTERIZATION OF A PORPHYRIN DOPANT FOR PM TYPE OPDS

The mechanism of photomultiplication, explained in chapter 1, is centered on trapping charges. These charges can be either electrons or holes, however, for this work we will focus on electron trapping. Chemical compounds which can act as traps have been developed and employed either for use in the interfacial layer or in the actual active layer of the devices. The most utilized electron traps have been fullerene based, specifically $PC_{61}BM$ and $PC_{71}BM$, while the charges they trap normally derive from the π conjugated donor polymer poly(3-hexylthiophene) (P3HT) leading to a photomultiplication phenomenon.

5.1. DESIGN STRATEGY

P3HT was chosen as the electron donating component in our study, since it has been previously proven to be effective in demonstrating the photomultiplication effect when combined with acceptor molecules of suitable energy levels. [95, 96] In order for the porphyrin to act as a trap for the electrons photogenerated from the P3HT donor, a sufficient LUMO-LUMO offset should exist between those two entities. This offset is required as it is the driving force for the separation of an exciton into free charges, and hence a necessary condition for electron transfer to occur.[97] Moreover, the offset should be large enough such that after the charge separation occurs, no back transfer of the electron to P3HT can take place, but instead will be trapped on the porphyrin derivative. A few considerations were made into modifying a porphyrin for the purpose of downshifting the LUMO energy level and achieving a large offset against P3HT.

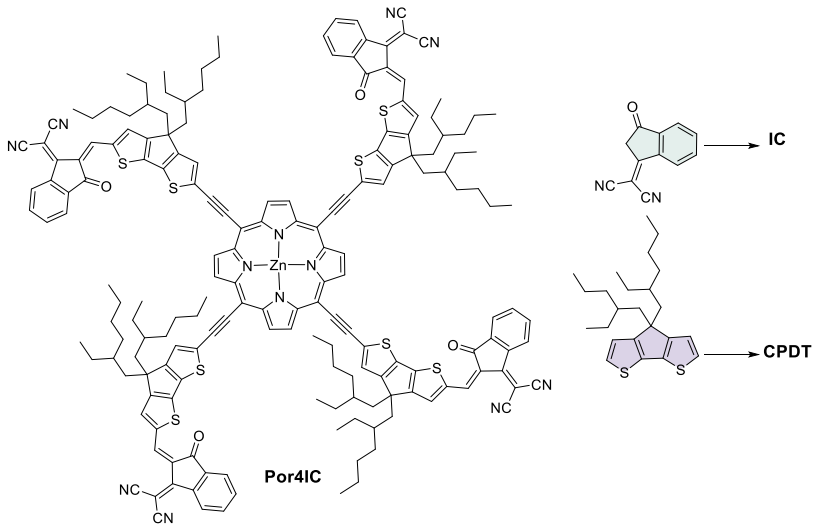

Figure 5.1. Chemical structure of Por4IC. The structures of the IC and CPDT units are represented separately.

Indeed, a common way to influence the energy of the orbitals in organic compounds is to attach conjugated electron donating or withdrawing groups directly to the extended π network of the porphyrin. More specifically, electron donating groups will add electron density to the structure, which will raise the HOMO energy level, whilst the use of electron withdrawing groups will lower electron density resulting in a lower LUMO energy.[78] Taking this into consideration, we envisaged synthesizing and probing the properties of Por4IC (**Figure 5.1**). It was thought that the introduction of highly electron deficient 2-(3-oxo-2,3-dihydro-1*H*-inden-1-ylidene)malononitrile (IC) units to the periphery of the zinc porphyrin would fulfill this requirement The substituted cyclopenta[2,1-*b*:3,4-*b'*]dithiophene (CPDT) groups were incorporated in order to give some degree of solubility to the final molecule as well as a means to extend the conjugation. Indeed, fused-ring derivatives tend to also enhance the planarity and rigidity of structures, while in combination with the acetylenic bridges, it was believed, that the molecule will be highly co-planar. Due to the fact that the porphyrin should be in direct conjugation with four exceptionally powerful electron acceptor units, it was hypothesized that this highly planar arrangement should also give a material with a low band gap.

5.2 Material Synthesis and Characterization

The synthetic procedures employed in obtaining Por4IC are shown in **Schemes 5.1-5.2**.

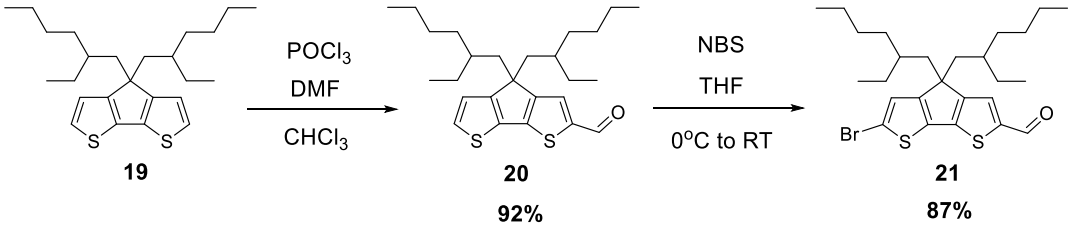

Scheme 5.1. Synthesis of compound **21.**

The synthesis began by a formylation of commercially available compound **19** via a highly regioselective Vilsmeier-Haack reaction to give compound **20** (**Scheme 5.1**). Bromination of **20** with NBS afforded compound **21** which was ready to be coupled to the porphyrin core (**Scheme 5.2**). Compounds **20** and **21** were both synthesized in high yields (92% and 87%, respectively), and were obtained as mixtures of diastereomers, due to stereogenic centers being present on each separate alkyl group.

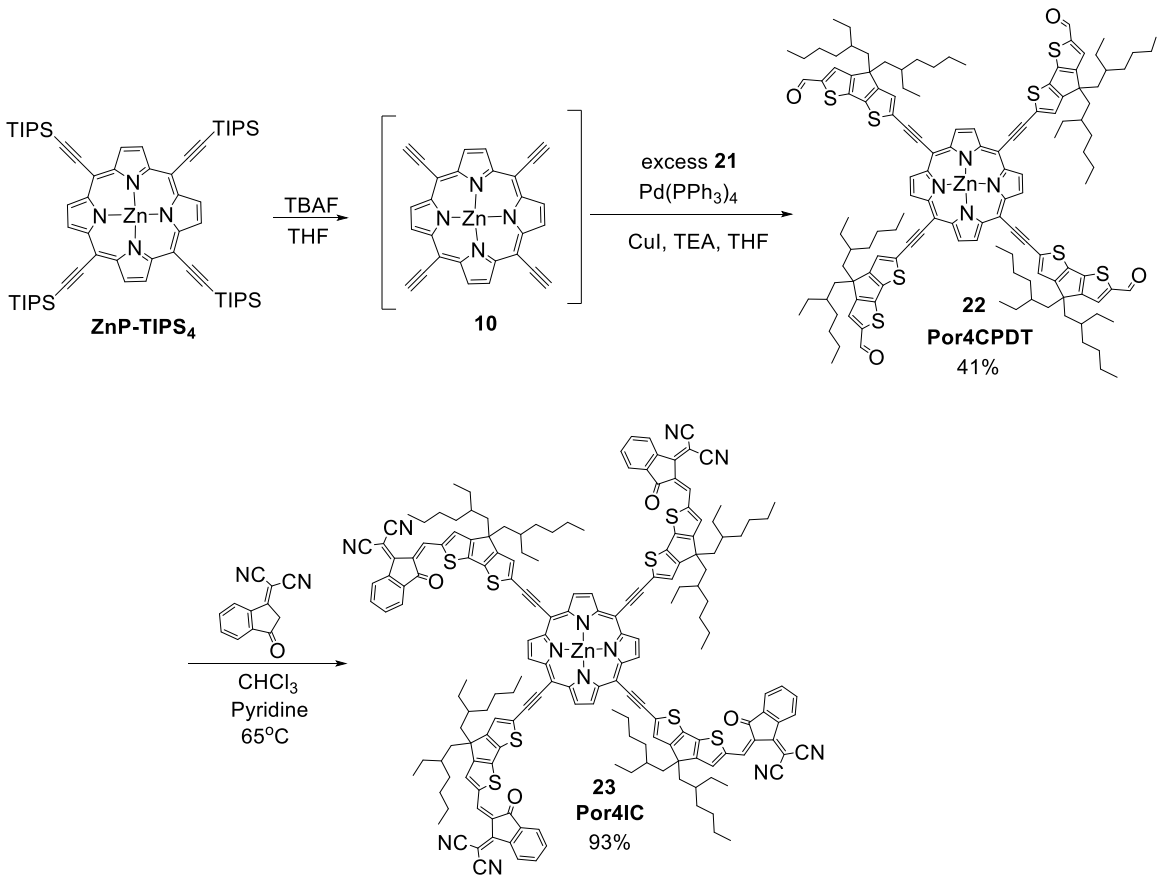

Scheme 5.2. Synthesis of **Por4CPDT** and **Por4IC**.

The preparation of Por4CPDT (**Scheme 5.2**) consisted of the usual protocol involving the desilylation of ZnP-TIPS$_4$. The resulting reactive intermediate was then directly coupled with an excess of **21** to allow for a four-fold Sonogashira reaction affording Por4CPDT in 41% yield. The final stage in the preparation of Por4IC involved a Knoevenagel condensation reaction between IC and Por4CPDT using pyridine as the base (**Scheme 5.2**).

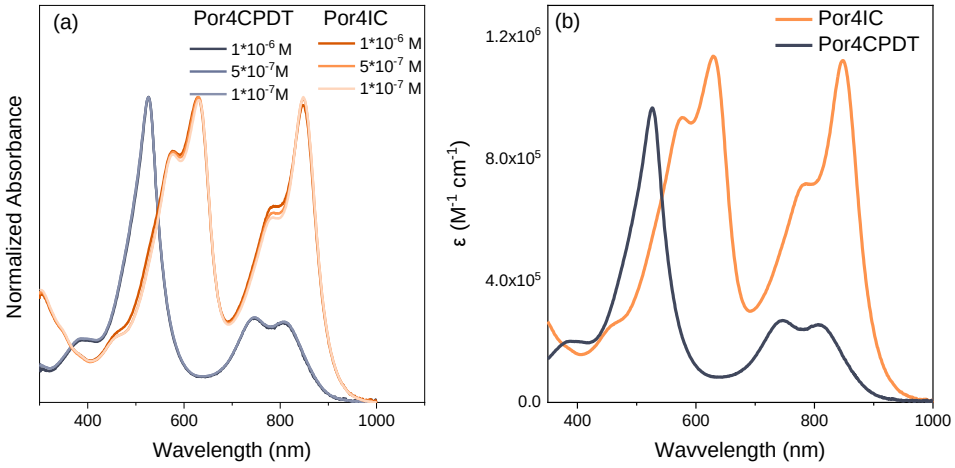

Figure 5.2. (a)Normalized absorption spectra of Por4CPDT and Por4IC at varying concentrations as identified in the legends. The solvent used was a mixture of toluene/pyridine 99:1.

The absorption spectra of Por4CPDT and Por4IC were acquired and are shown in **Figure 5.2**. Compound Por4CPDT exhibited two main absorption maxima. The S band was very sharp and was located at ~525 nm while two Q bands were clearly distinguishable and were located at ~750 and ~810 nm. Extending the conjugation of Por4CPDT further with strong electron accepting IC units, now as Por4IC, did drastically influence the absorption properties. Not surprisingly, this absorption spectrum showed an overall red-shifting of the absorption features towards longer wavelengths. Moreover, the S band was not observed as a very sharp distinct peak, but instead splitting of it occurred, giving rise to two features located at 577 nm and 631 nm. This splitting of the S band has been attributed in the past to coming about from an increased conjugation of the porphyrin.[69] The S band was found at ~630 nm, translating to a redshift of ~105 nm, when compared to the spectral features observed for Por4CPDT. Regarding the Q bands, positioned at ~787 and ~848 nm, the introduction of IC had a very strong effect on their intensities which were almost equal in the intensity to that of the S band. This can be more clearly seen in **Figure 5.2** (b), where the extinction coefficients of these porphyrins have been presented. For Por4CPDT, the extinction coefficient of the Q band was in the order of 10^{-5} M^{-1} cm^{-1}, while for Po4IC this increased by an order of magnitude to 10^{-6} M^{-1} cm^{-1}. The E_g^{opt} was also estimated from the onset of the low-energy band for each compound and was found to be 1.40 eV and 1.35 eV for Por4CPDT and Por4IC, respectively, which were surprisingly similar. Finally, it should be mentioned that increasing the concentrations of these derivatives did not have any remarkable effect on the optical properties of these solutions. Thus, no significant aggregation effects could be distinguished from the absorption spectra for both these new porphyrin derivatives.

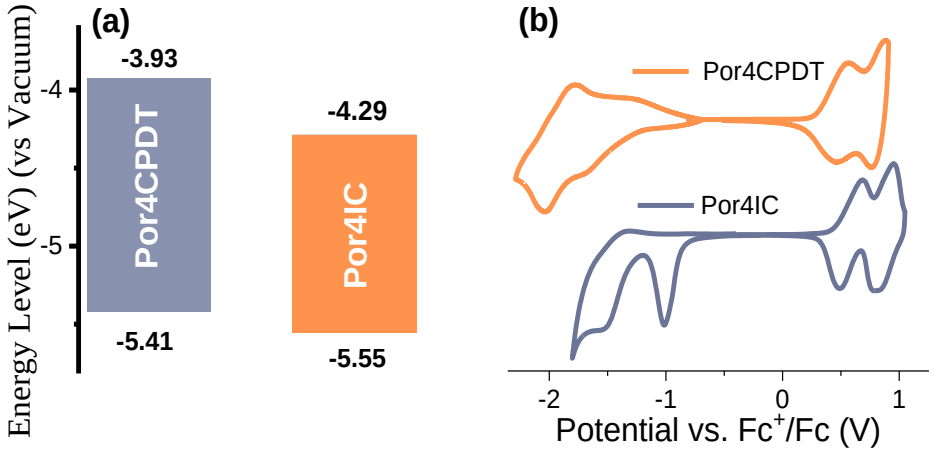

Figure 5.3. (a) Energy level diagram for Por4CPDT and Por4IC (b) the CV traces of Por4CPDT and Por4IC.

As mentioned before, the integration of the IC unit into the porphyrin structure, in the form of Por4IC, led to a very small optical gap. However, the main goal was the downshift of the energy levels and not necessarily decreasing the band gap. Cyclic voltammetry was used to achieve more exact estimates of the frontier molecular orbital energy levels for both Por4CPDT and Por4IC. As

shown in **Figure 5.3**, the HOMO and LUMO energy levels of Por4CPDT, as calculated from the onsets of the oxidation and reduction potentials, were positioned at -5.41 eV and -3.93 eV, respectively. A significant decrease of the E_g had occurred for Por4IC and a downshift of both the HOMO and LUMO levels. More specifically the HOMO/LUMO levels of Por4IC are located at -5.55 eV/-4.29 eV, translating to a relative downshift from Por4CPDT of 0.14 eV/ 0.36 eV, respectively. With this being determined, our goal in producing a molecule with a downshifted LUMO level and thereby a large LUMO–LUMO offset (~1.4 eV) with P3HT was achieved. Porphyrin Por4IC could be considered promising candidate for trapping electrons originating from P3HT.

5.4. PM Type OPDs Design and Performance

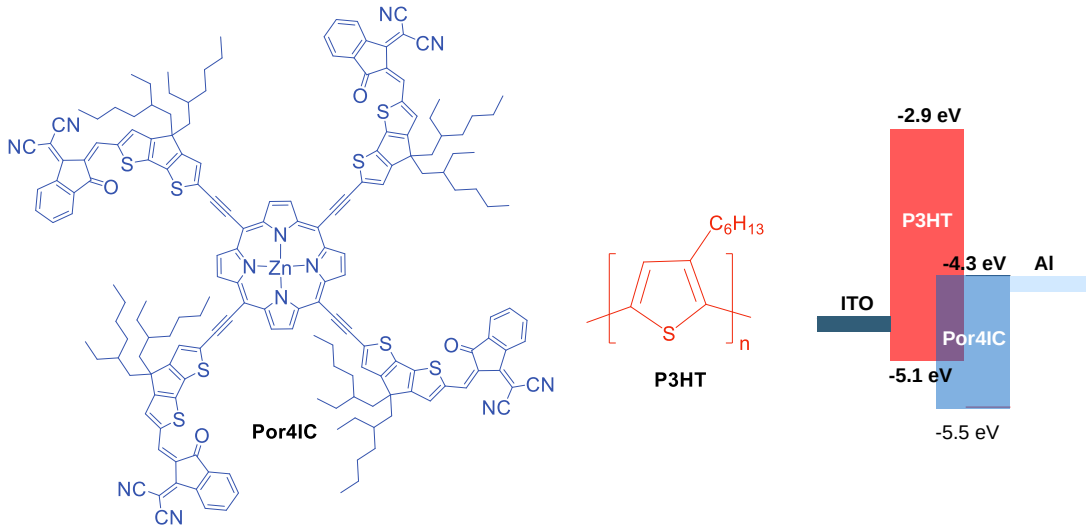

Figure 5.4. (a) Chemical structures of Por4IC and P3HT and (b) Energy level diagram showing the match between Por4IC and P3HT.

In order to test our hypothesis that Por4IC can act as a trap for the electrons photogenerated from P3HT, photomultiplication PM-type OPDs were fabricated and studied. Both the structures of Por4IC and P3HT associated with their relative energy levels can be seen in **Figure 5.4**. As it was mentioned earlier, the LUMO-LUMO offset between P3HT and Por4IC was quite large and is in the order of 1.4 eV, indicating a high probability that the formed excitons will separate at their interface. Moreover, since the LUMO offset was so high, the possibility of the separated electrons to back transferring to P3HT was unlikely, instead they should remain trapped at the porphyrin. Moreover, the energy difference for hole injection from the Al electrode to the HOMO of the P3HT is smaller than that for Por4IC. Thus, due to the smaller barrier, holes will be injected easier to the HOMO of P3HT.

Based on previous literature and the working mechanism of PM-type OPDs, bulk heterojunction devices were fabricated with an active layer consisting of a blend of P3HT/Por4IC in the ratio of 100:1. [30, 93, 95]

What happens when the doping ratio of an electron trap is less than 15%? Let´s start by explaining how the bulk heterojunction will look like, if it was composed of the two materials in equal amounts. In this scenario, an interpenetrating network of acceptor into the donor domains would occur in the active layer, such that it would be possible for the charges to travel to their respective electrodes, after the separation of the exciton. However, if one of the photoactive components was used in very small quantities, for instance Por4IC, the charges generated would be trapped there, since there is no pathway for them to travel. Moreover, the electron mobility will drop dramatically, since the electrons that are created at the donor/acceptor interface will be trapped by Por4IC. Under light illumination conditions at reverse bias, the channels formed by P3HT would assist in hole transportation in the active layers. Those trapped electrons will build up a Coulombic field, leading to interfacial bending of the energy levels, especially by those electrons trapped near the Al cathode. This interfacial energy level bending narrows the hole injection barrier for efficient hole tunneling injection from the Al electrode to the HOMO of P3HT under reverse bias. The injected holes could then be transported efficiently along the continuous channels formed by P3HT and be collected at the ITO electrode.[128]

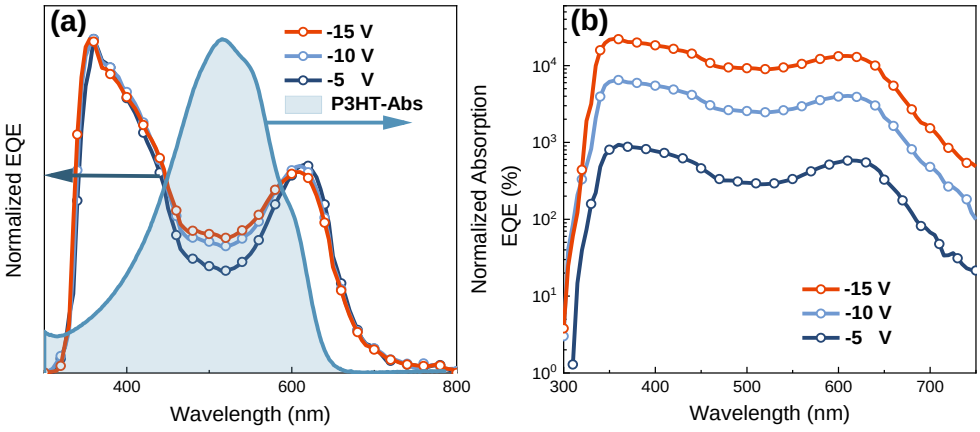

Figure 5.5. (a) Normalized EQE spectra of the OPDs at increasing reverse bias.and absorption spectrum of P3HT thin film[129] and (b) EQE spectra of the OPDs at increasing reverse bias in a logarithmic scale.

The EQE spectra of the devices at different reverse bias values, from -5 V to -15 V were recorded and are presented in **Figure 5.5** (a and b). EQE values exceeding 100% were observed in all cases. Thus, a photomultiplication effect was achieved for all applied voltages. It was evident from **Figure 5.5,** that there were two regions of higher response located at ~350 nm and 610 nm, while a dip was present in the part of the spectrum between them (460-550 nm). If we compare the shape of the absorption spectrum of the P3HT film to the EQE spectra, then we see that there is no match between them. This dip has been previously attributed to a weaker optical field intensity, due to the strong absorption of P3HT in this wavelength region resulting in less trapped electrons in the dopant close to the Al electrode.[34] Moreover, even though Por4IC exhibited a very high absorption coefficient in the order of 10^6 M^{-1} cm^{-1}, we see no contribution at all from the porphyrin in the

spectra, but this could also be attributed to the low amounts of the porphyrin incorporated into the active layer blend (1%). It should also be noted, that increasing the reverse bias resulted in an increase in the EQE, with the maximum EQE being >22 000% (at 355 nm) and >13 000% (at 610 nm) at -15V.

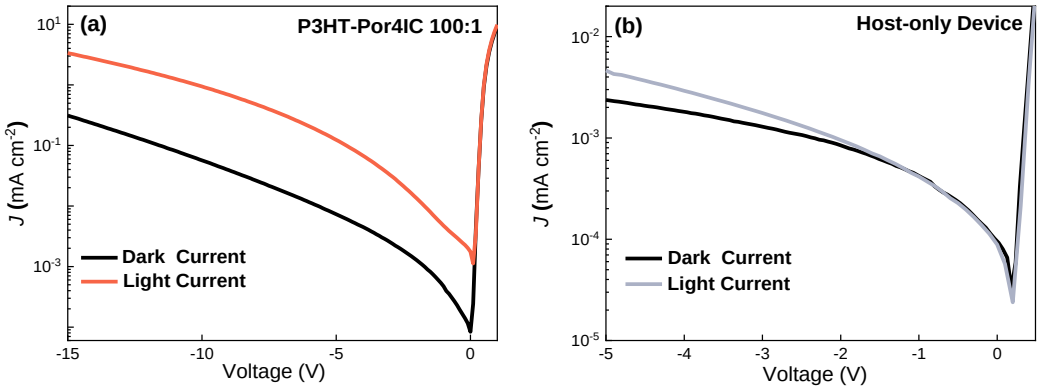

Figure 5.6. J-V curves of the (a) ITO/PEDOT:PSS/P3HT:Por4IC/Al and (b) ITO/PEDOT:PSS/P3HT/Al devices measured in dark and under 2 mW cm^{-2} white light illumination conditions.

Figure 5.6. represents the J-V curves of the (a) P3HT/Por4IC (100:1) and (b) host-only (P3HT) devices in the dark and under light illumination under reverse bias. The J_D for the Por4IC containing devices showed similar values to the J_D of the host only devices. Upon light illumination on the P3HT/Por4IC devices, the current increases indicating functioning devices. However, the same was not observed for the P3HT only devices. As it can be seen in **Figure 5.6** (b), the J_L and J_D curves were almost overlapping with each other, indicating no photoresponse. This confirms that the photocurrent results from hole injection, assisted by the electrons trapped in Por4IC and not by intrinsic traps or defects within the P3HT layer.

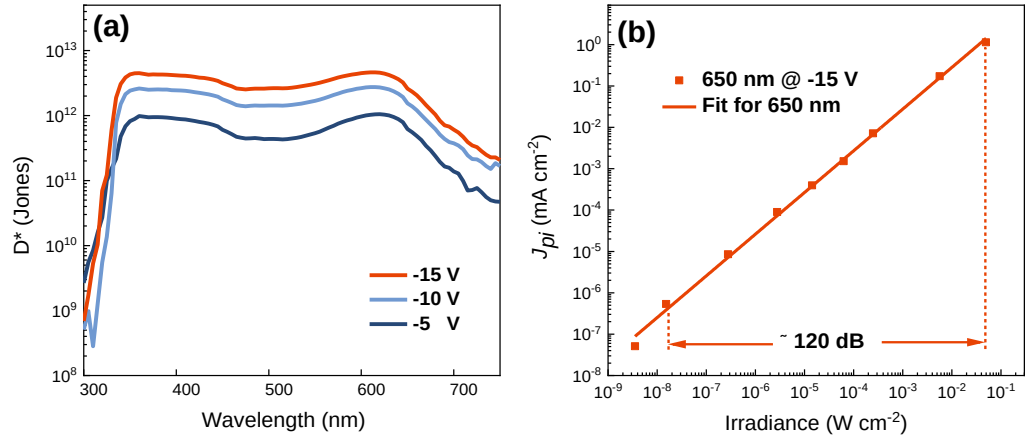

Figure 5.7.(a) Specific detectivity of the PM type OPDs at increasing reverse bias. (b) LDR of the PM type OPDs measured at -15 V bias under 650 nm light illumination, the solid red line is the linear fitting.

The specific detectivity (D*) of the devices was calculated and it is presented in **Figure 5.7** (a). In the region between 460-550 nm, D* was found to be lower following the EQE trend for all PM-

type OPDs. However, very high D* values were obtained for all applied voltages. The detailed values can be seen in **Table 5.1**.

Table 5.1. Specific detectivities of the devices with varying bias in wavelengths specified in the parenthesis.

Bias [V]	D* (355nm) [Jones]	D* (610 nm) [Jones]
-5	8.8×10^{11}	1.0×10^{12}
-10	2.5×10^{12}	2.7×10^{12}
-15	4.4×10^{12}	4.6×10^{12}

Finally, it is worth mentioning that one of the drawbacks of PM-type OPDs is that when they are compared with photodiode-type OPDs, for example, the former tend to have a smaller linear dynamic range (LDR). For the photodetector to have the possibility to be used in a practical manner, the dynamic range should be highly linear. LDR is a crucial parameter for image sensors, because photodetectors need to be able to operate in a broad light intensity range.[101] The LDR of the OPDs was measured by recording the steady-state photocurrent under 650 nm light illumination using different light intensities, varying from 0.05 to 1.52 x 10^8 W cm^{-2} at -15 V as shown in **Figure 5.7** (b). The LDR was estimated to be ~120 dB from Equation 3.10, indicating that this fabricated PM-type OPD has the capability to detect light over a large light intensity range.

In summary, in this work, we synthesized a new porphyrin derivative capable of acting as a trap for electrons generated from P3HT leading to photomultiplication of the signal delivering EQE values exceeding unity. This was attributed to the compatibility of the energy levels between P3HT and Por4IC which led to the enhanced hole tunneling injection from the external circuit due to the energy level tilting and the enhanced hole transport ability under increased reverse bias. These results highlight that modified porphyrin derivatives can indeed be promising dopants for PM-type OPDs.

CHAPTER 6

6 CONCLUSIONS AND OUTLOOK

In this thesis the main effort was devoted to the manipulation of the chemical structure of the porphyrin motif in order to synthesize materials with their optical characteristics located in the NIR regime. Part of the work was devoted to implementing the NIR emitting porphyrins into LEC devices as minority guest in host-guest systems. Moreover, a porphyrin molecule was designed in order to be implemented in PM type OPDs and introduced them as a new promising molecule that can act as a trap, facilitating photomultiplication. The core for all the synthesized emitters was ZnP-$TIPS_4$ motif, which is shown in **Figure 6.1** together with its frontier orbitals.

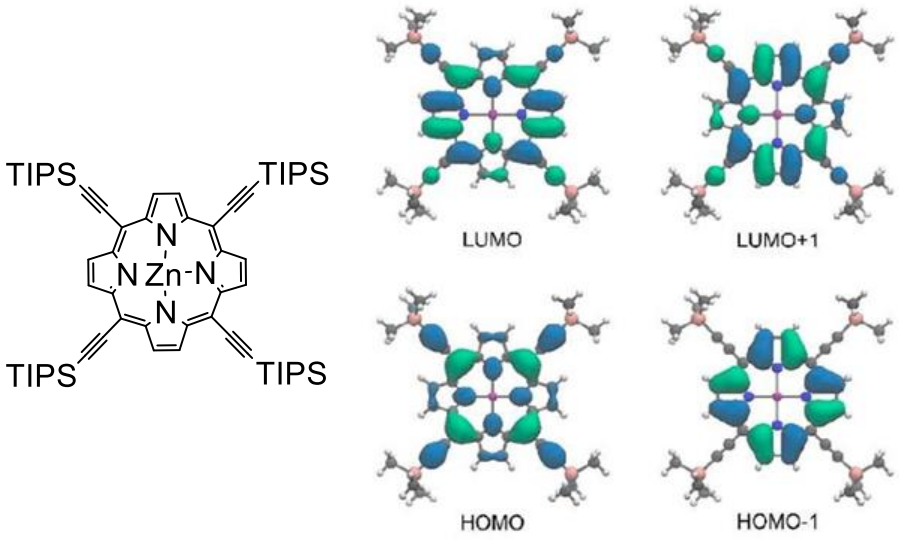

Figure 6.1. (left) Chemical structure of ZnP-TIPS4 (right) Frontier orbitals of ZnP-$TIPS_4$.

All porphyrins that have been presented in this thesis had a few common characteristics. They were very flat structures, which possessed a highly extended π conjugation and were connected to electron accepting moieties via the acetylenic bridges to the *meso* positions. The key characteristic for enhancing the planarity in this work was the insertion of triple bonds in the four *meso* positions. Without the presence of the triple bonds any unit connected to the meso positions would have been forced to twist perpendicular to the porphyrin plane due to unfavorable steric interactions.[130]. In such an instance, delocalization of the π electrons over the structure would not have been possible. The push-pull driving force between the electron donor and the electron acceptor facilitates the delocalization of electrons and had a significant effect in redshifting the PL spectra of these new derivatives, as well as increasing the intensity of the porphyrin Q bands. In fact, in this study, the strength of the acceptor was very important. The strength of the acceptor was quantified from the experimentally calculated energy levels. In general, it was shown that the stronger the

acceptor, as determined by the effect it had on downshifting the HOMO-LUMO levels, the more red-shifted the emission, although exceptions existed. The effect of all these strategies followed to manipulate the porphyrin electronics can be seen in **Figure 6.2,** where the absorption and emission spectra of all synthesized porphyrins in comparison to the ZnP-TIPS$_4$ are presented**.**

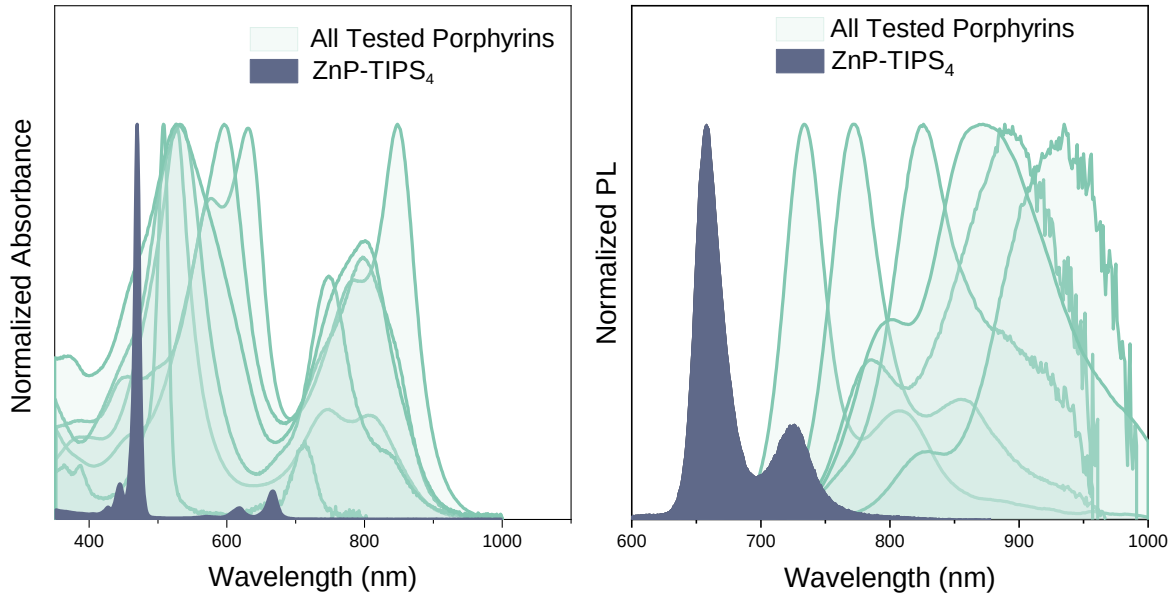

Figure 6.2. Normalized absorption (left) and PL (right) spectra of all porphyrins included in this thesis. The spectra belong to the solutions of the emitters while the concentration is 10^{-6} M. The purpose of the optical spectra in this Figure is to give an impression of the magnitude of the effect that the different strategies had in the spectra of the starting porphyrin core.

As it was early noticed in this work, the new porphyrin molecules showed a very high tendency to aggregate by π-π stacking, while the design of the final compounds into very flat structures was conducive to this behavior. In order to effectively employ the synthesized molecules in LEC devices without the severe effects of aggregation the host-guest strategy was followed and the work on this can be seen in Chapter 4. Polymeric hosts were tested in combination with the porphyrin emitters and as a result functional LECs with deep NIR emission were obtained. Even though the selected hosts had the appropriate characteristics to be combined with emitters, not all of them led to functional devices. In this aspect, more work could be invested in designing better host materials. However, for this to be achieved more studies on the morphology of the hosts-guest blends are necessary. So, the take home message is that optical and electrochemical matching of a host-guest system are not necessarily the only parameters that govern the fabrication of a functional LEC device. Are the materials really compatible with each other? Is any phase separation that can be detrimental to device performance? One proposal for future hosts, when used in combination with porphyrin emitters would be that the host has an ideal quantity of pyridine groups incorporated into the polymer structure. In that way the metal containing porphyrins could coordinate to the pyridine containing polymers leading to a better dispersion of the emitter in the host matrix.

However, due to the bulkiness of the porphyrin derivatives, such as those made in this study, these lone pair donors should not be sterically inaccessible. Another part of the emissive layer in LECs is the electrolyte. The electrolyte is blended with the host and guest species and consequently it will also have an effect on the morphology of the blend. While it has also been shown that lower efficiency, slow turn on times or phase separation have been obtained due to the electrolyte.[131] Thus a morphological study should not be undertaken without taking the electrolyte into consideration.

Another aspect for the designing efficient NIR emitters is the increase of their emission efficiency. As stated, earlier NIR emitters generally show lower EQEs compared to those emitting in the visible region. This is in accordance with the energy gap law, which predicts that with smaller gaps (as it is the case for NIR emitters), an overlap of the wavefunctions of the lower vibrational levels of the first excited state with the higher vibrational levels of the S_0 will lead to an increase in the non-radiative rate.[117,132] Could the efficiency of the emitters presented here be improved by an additional structural modification? This is a hard question to be answered. A potential increase of their efficiency could be made possible by introducing triplet excitons to the excited state, adding to the singlet excitons and thus improving the EQE. In addition, in that scenario a larger Stokes shift could be achieved which would alleviate the observed effects of a self-quenching. However, such a strategy would require the introduction of rare and expensive heavy metals, while the exciton lifetime would be increased making those devices less appealing for real-life applications.

Finalizing, it was shown in chapter 5 that with the proper molecular design porphyrins can act as electron traps facilitating a PM phenomenon leading to devices that can efficiently obtain an EQE over 100%. However, the field of PM type OPDs is relatively new compared to other OPD technologies, and the library of materials small. Though with a small prediction, this will change fast, based on the knowledge that has already been built in relative fields like organic photovoltaics and photodiode type photodetectors. There are many aspects for improvement in the field, one that personally challenges me more is the design of PM type OPDs with a broadband response, ranging from ultraviolet (UV) through to the NIR. How can this be achieved? Probably with design of materials of complementary absorptions. Still, careful consideration should be put upon their combination, since as seen in chapter 5, the optical (absorption) properties of the active layer materials do not necessarily match to their EQE and D* characteristics.

ACKNOWLEDGEMENTS

First, I would like to acknowledge my supervisors Professors Ergang Wang and Mats Andersson for the opportunity they gave me to pursue my PhD and be member of their groups in Chalmers and Flinders University. I also want to thank my third co-supervisor Henrik Sundén for his support whenever things were tough.

I would also like to thank our collaborators from Umeå University, Prof. Ludvig Edman and Shi Tang, for the fabrication and characterization of LEC devices. Without their help a complete work wouldn't have been achieved. I shouldn't forget Professor Fujun Zhang's group in Beijing Jiaotong University, for making my super-efficient OPDs. Thank you.

Special thanks to Petri and Martyn, my mentors. Thank you for helping me with my naïve scientific questions, supporting me and reading my thesis. Petri, I really admire your passion for science, you have been an amazing colleague and a good friend. I am sure you'll be a great Professor in the future. Martyn, you are the best synthetic chemist in the world, I wish I was working with you from the beginning. Thanks for dealing with my moods and thanks for watching my back in Australia. We should go for surfing in Goolwa soon with Fabby and Kingo. You are super nice Martyn, a beast with the heart of a kid. Thank you, GRANMA BEAST!

I also want to thank all my colleagues from Chalmers and GU. Alicja, Xin, Zhihang, Birhan, Anne, Zhaojun, Alex, Clara, Manuel, Sepideh, Emmy, it was great to have you around. Mads you were a great Bro, thanks for helping me and listening to me. I really miss you sometimes. Lotta, how can I forget you. You are the best administrator in the world, the most talented artist on the floor. You made my PhD days more interesting and fun. I cannot imagine a workplace without Lotta. Christian, Kasper, Anette, Hanna, Per, Jerker it was my pleasure to meet you.

I also want to thank my family in Gothenburg, Γιώργο, Charlotte, Δεσποινα, Κώστα, Simon, Celine, Γιώργο. Σας ευχαριστώ για όλη την βοήθεια που μου έχετε δώσει. Όλα θα ήταν πιο δύσκολα για εμένα στη Σουηδία αν δεν είχα εσάς.

Paula, Mohamed, Cedrik, Nestorito. I'm so happy that I know you. You put light in my darkest and toughest times. You are my shining stars.

Finally, θα ήθελα να ευχαριστήσω τους πιο σημαντικούς απ'όλους τους γονείς μου, Σοφία και Θοδωρή, και τα αδέρφια μου, Χρήστο και Πέτρο. Μπορεί να μην ήσασταν μαζί μου τα τελευταία τέσσερα χρόνια αλλά είστε συνέχεια μέσα στην καρδιά μου. Σας ευχαριστώ που συνέχεια με στηρίζεται όσο μακριά κι αν είμαστε. Σας αγαπώ! Μπάμπη εσένα σ'αγαπώ λίγο παραπάνω, ίσως επειδή μου λείπεις πιο πολύ απ'όλους.

BIBLIOGRAPHY

(**1**) Chen, H.; Li, S.; Huang, B.; Xu, Z.; Li, W.; Dong, G.; Xie, J. In *A 1.9Mbps OFDM-based all-organic visible light communication system*, 2016 IEEE International Conference on Communication Systems (ICCS), 14-16 Dec. 2016; 2016; pp 1-6.

(**2**) Chen, Z.; Obaid, S. N.; Lu, L., Recent advances in organic optoelectronic devices for biomedical applications. *Opt. Mater. Express* **2019,** *9* (9), 3843-3856.

(**3**) Bansal, A. K.; Hou, S.; Kulyk, O.; Bowman, E. M.; Samuel, I. D. W., Wearable Organic Optoelectronic Sensors for Medicine. *Advanced Materials* **2015,** *27* (46), 7638-7644.

(**4**) Yoon, M.-H.; Facchetti, A.; Stern, C. E.; Marks, T. J., Fluorocarbon-Modified Organic Semiconductors: Molecular Architecture, Electronic, and Crystal Structure Tuning of Arene- versus Fluoroarene-Thiophene Oligomer Thin-Film Properties. *Journal of the American Chemical Society* **2006,** *128* (17), 5792-5801.

(**5**) Liu, Q.; Surendran, A.; Feron, K.; Manzhos, S.; Jiao, X.; McNeill, C. R.; Bottle, S. E.; Bell, J.; Leong, W. L.; Sonar, P., Diketopyrrolopyrrole based organic semiconductors with different numbers of thiophene units: symmetry tuning effect on electronic devices. *New J Chem* **2018,** *42* (6), 4017-4028.

(**6**) Akamatu, H.; Inokuchi, H., On the Electrical Conductivity of Violanthrone, Iso-Violanthrone, and Pyranthrone. *The Journal of Chemical Physics* **1950,** *18* (6), 810-811.

(**7**) Pope, M.; Kallmann, H. P.; Magnante, P., Electroluminescence in Organic Crystals. *The Journal of Chemical Physics* **1963,** *38* (8), 2042-2043.

(**8**) McNeill, R.; Siudak, R.; Wardlaw, J.; Weiss, D., Electronic Conduction in Polymers. I. The Chemical Structure of Polypyrrole. *Aust J Chem* **1963,** *16* (6), 1056-1075.

(**9**) Shirakawa, H.; Louis, E. J.; MacDiarmid, A. G.; Chiang, C. K.; Heeger, A. J., Synthesis of electrically conducting organic polymers: halogen derivatives of polyacetylene, (CH). *Journal of the Chemical Society, Chemical Communications* **1977,** (16), 578-580.

(**10**) Tang, C. W.; VanSlyke, S. A., Organic electroluminescent diodes. *Applied Physics Letters* **1987,** *51* (12), 913-915.

(**11**) Burroughes, J. H.; Bradley, D. D. C.; Brown, A. R.; Marks, R. N.; Mackay, K.; Friend, R. H.; Burns, P. L.; Holmes, A. B., Light-emitting diodes based on conjugated polymers. *Nat Photonics* **1990,** *347* (6293), 539-541.

(**12**) Pei, Q.; Yu, G.; Zhang, C.; Yang, Y.; Heeger, A. J., Polymer Light-Emitting Electrochemical Cells. *Science* **1995,** *269* (5227), 1086-1088.

(**13**) Giovanella, U.; Pasini, M.; Botta, C., Organic Light-Emitting Diodes (OLEDs): Working Principles and Device Technology. In *Applied Photochemistry: When Light Meets Molecules*, Bergamini, G.; Silvi, S., Eds. Springer International Publishing: Cham, 2016; pp 145-196.

(**14**) Meier, S. B.; Tordera, D.; Pertegás, A.; Roldán-Carmona, C.; Ortí, E.; Bolink, H. J., Light-emitting electrochemical cells: recent progress and future prospects. *Materials Today* **2014,** *17* (5), 217-223.

(**15**) Kanagaraj, S.; Puthanveedu, A.; Choe, Y., Small Molecules in Light-Emitting Electrochemical Cells: Promising Light-Emitting Materials. *Advanced Functional Materials n/a* (n/a), 1907126.

(**16**) Chen, G.; Ling, Z.; Wei, B.; Zhang, J.; Hong, Z.; Sasabe, H.; Kido, J., Comparison of the Solution and Vacuum-Processed Squaraine:Fullerene Small-Molecule Bulk Heterojunction Solar Cells. *Frontiers in Chemistry* **2018,** *6* (412).

(**17**) Kronenberg, N. M.; Steinmann, V.; Bürckstümmer, H.; Hwang, J.; Hertel, D.; Würthner, F.; Meerholz, K., Direct Comparison of Highly Efficient Solution- and Vacuum-Processed Organic Solar Cells Based on Merocyanine Dyes. *Advanced Materials* **2010,** *22* (37), 4193-4197.
(**18**) Asadpoordarvish, A.; Sandström, A.; Larsen, C.; Bollström, R.; Toivakka, M.; Österbacka, R.; Edman, L., Light-Emitting Paper. *Adv. Funct. Mater.* **2015,** *25* (21), 3238-3245.
(**19**) Sandström, A.; Dam, H. F.; Krebs, F. C.; Edman, L., Ambient fabrication of flexible and large-area organic light-emitting devices using slot-die coating. *Nat. Commun.* **2012,** *3*, 1002.
(**20**) Lanz, T.; Sandström, A.; Tang, S.; Chabrecek, P.; Sonderegger, U.; Edman, L., A light–emission textile device: conformal spray-sintering of a woven fabric electrode. *Flexible and Printed Electronics* **2016,** *1* (2), 025004.
(**21**) Zimmermann, J.; Porcarelli, L.; Rödlmeier, T.; Sanchez-Sanchez, A.; Mecerreyes, D.; Hernandez-Sosa, G., Fully Printed Light-Emitting Electrochemical Cells Utilizing Biocompatible Materials. *Advanced Functional Materials* **2018,** *28* (24), 1705795.
(**22**) Zimmermann, J.; Schlisske, S.; Held, M.; Tisserant, J.-N.; Porcarelli, L.; Sanchez-Sanchez, A.; Mecerreyes, D.; Hernandez-Sosa, G., Ultrathin Fully Printed Light-Emitting Electrochemical Cells with Arbitrary Designs on Biocompatible Substrates. *Adv. Mater. Technol.* **2019,** *4* (3), 1800641.
(**23**) Yu, Z.; Niu, X.; Liu, Z.; Pei, Q., Intrinsically Stretchable Polymer Light-Emitting Devices Using Carbon Nanotube-Polymer Composite Electrodes. *Adv. Mater.* **2011,** *23* (34), 3989-3994.
(**24**) Liang, J.; Li, L.; Niu, X.; Yu, Z.; Pei, Q., Elastomeric polymer light-emitting devices and displays. *Nat. Photonics* **2013,** *7* (10), 817-824.
(**25**) Sandström, A.; Asadpoordarvish, A.; Enevold, J.; Edman, L., Spraying Light: Ambient-Air Fabrication of Large-Area Emissive Devices on Complex-Shaped Surfaces. *Adv. Mater.* **2014,** *26* (29), 4975-4980.
(**26**) Murto, P.; Tang, S.; Larsen, C.; Xu, X.; Sandström, A.; Pietarinen, J.; Bagemihl, B.; Abdulahi, B. A.; Mammo, W.; Andersson, M. R.; Wang, E.; Edman, L., Incorporation of Designed Donor–Acceptor–Donor Segments in a Host Polymer for Strong Near-Infrared Emission from a Large-Area Light-Emitting Electrochemical Cell. *ACS Applied Energy Materials* **2018,** *1* (4), 1753-1761.
(**27**) Sandström, A.; Edman, L., Towards High-Throughput Coating and Printing of Light-Emitting Electrochemical Cells: A Review and Cost Analysis of Current and Future Methods. *Energy Technology* **2015,** *3* (4), 329-339.
(**28**) Hernandez-Sosa, G.; Tekoglu, S.; Stolz, S.; Eckstein, R.; Teusch, C.; Trapp, J.; Lemmer, U.; Hamburger, M.; Mechau, N., The Compromises of Printing Organic Electronics: A Case Study of Gravure-Printed Light-Emitting Electrochemical Cells. *Advanced Materials* **2014**, 3235-3240.
(**29**) Mauthner, G.; Landfester, K.; Kock, A.; Bruckl, H.; Kast, M.; Stepper, C.; List, E. J. W., Inkjet printed surface cell light-emitting devices from a water-based polymer dispersion. *Organic Electronics* **2008,** *9* (2), 164-170.
(**30**) Sandström, A.; Dam, H. F.; Krebs, F. C.; Edman, L., Ambient fabrication of flexible and large-area organic light-emitting devices using slot-die coating. *Nature Communications* **2012,** *3*, 1002.
(**31**) Yang, D.; Ma, D., Development of organic semiconductor photodetectors: from mechanism to applications. *Advanced Optical Materials* **2019,** *7* (1), 1800522.

(**32**) Hiramoto, M.; Imahigashi, T.; Yokoyama, M., Photocurrent multiplication in organic pigment films. *Applied Physics Letters* **1994,** *64* (2), 187-189.
(**33**) Huang, J.; Yang, Y., Origin of photomultiplication in C60 based devices. *Applied Physics Letters* **2007,** *91* (20), 203505.
(**34**) Li, L.; Zhang, F.; Wang, J.; An, Q.; Sun, Q.; Wang, W.; Zhang, J.; Teng, F., Achieving EQE of 16,700% in P3HT:PC71BM based photodetectors by trap-assisted photomultiplication. *Scientific Reports* **2015,** *5* (1), 9181.
(**35**) Neethipathi, D. K.; Ryu, H. S.; Jang, M. S.; Yoon, S.; Sim, K. M.; Woo, H. Y.; Chung, D. S., High-Performance Photomultiplication Photodiode with a 70 nm-Thick Active Layer Assisted by IDIC as an Efficient Molecular Sensitizer. *ACS Applied Materials & Interfaces* **2019,** *11* (23), 21211-21217.
(**36**) Wang, W.; Zhang, F.; Du, M.; Li, L.; Zhang, M.; Wang, K.; Wang, Y.; Hu, B.; Fang, Y.; Huang, J., Highly Narrowband Photomultiplication Type Organic Photodetectors. *Nano Letters* **2017,** *17* (3), 1995-2002.
(**37**) Zhao, Z.; Wang, J.; Miao, J.; Zhang, F., Photomultiplication type organic photodetectors with tunable spectral response range. *Organic Electronics* **2019,** *69*, 354-360.
(**38**) Wang, J.; Zheng, Q., Enhancing the performance of photomultiplication-type organic photodetectors using solution-processed ZnO as an interfacial layer. *Journal of Materials Chemistry C* **2019,** *7* (6), 1544-1550.
(**39**) Wu, Y.-L.; Fukuda, K.; Yokota, T.; Someya, T., A Highly Responsive Organic Image Sensor Based on a Two-Terminal Organic Photodetector with Photomultiplication. *Advanced Materials* **2019,** *31* (43), 1903687.
(**40**) Lee, E. C.; Jung, H.; Kim, D., New finger biometric method using near infrared imaging. *Sensors* **2011,** *11* (3), 2319-2333.
(**41**) Minotto, A.; Haigh, P. A.; Łukasiewicz, Ł. G.; Lunedei, E.; Gryko, D. T.; Darwazeh, I.; Cacialli, F., Visible light communication with efficient far-red/near-infrared polymer light-emitting diodes. *Light: Science & Applications* **2020,** *9* (1), 70.
(**42**) Pereira, N. A. M.; Laranjo, M.; Casalta-Lopes, J.; Serra, A. C.; Piñeiro, M.; Pina, J.; Seixas de Melo, J. S.; Senge, M. O.; Botelho, M. F.; Martelo, L.; Burrows, H. D.; Pinho e Melo, T. M. V. D., Platinum(II) Ring-Fused Chlorins as Near-Infrared Emitting Oxygen Sensors and Photodynamic Agents. *ACS Medicinal Chemistry Letters* **2017,** *8* (3), 310-315.
(**43**) Pauling, L., THE NATURE OF THE CHEMICAL BOND. APPLICATION OF RESULTS OBTAINED FROM THE QUANTUM MECHANICS AND FROM A THEORY OF PARAMAGNETIC SUSCEPTIBILITY TO THE STRUCTURE OF MOLECULES. *Journal of the American Chemical Society* **1931,** *53* (4), 1367-1400.
(**44**) Vollmer, F.; Rettig, W.; Birckner, E., Photochemical mechanisms producing large fluorescence stokes shifts. *Journal of Fluorescence* **1994,** *4* (1), 65-69.
(**45**) Chen, Y.; Zhao, J.; Guo, H.; Xie, L., Geometry Relaxation-Induced Large Stokes Shift in Red-Emitting Borondipyrromethenes (BODIPY) and Applications in Fluorescent Thiol Probes. *The Journal of Organic Chemistry* **2012,** *77* (5), 2192-2206.
(**46**) Jiang, J.; Xu, Z.; Zhou, J.; Hanif, M.; Jiang, Q.; Hu, D.; Zhao, R.; Wang, C.; Liu, L.; Ma, D.; Ma, Y.; Cao, Y., Enhanced Pi Conjugation and Donor/Acceptor Interactions in D-A-D Type

Emitter for Highly Efficient Near-Infrared Organic Light-Emitting Diodes with an Emission Peak at 840 nm. *Chemistry of Materials* **2019,** *31* (17), 6499-6505.
(**47**) Lakowicz, J. R., *Principles of fluorescence spectroscopy*. Springer science & business media: 2013.
(**48**) Balzani, V.; Ceroni, P.; Juris, A., *Photochemistry and photophysics: concepts, research, applications*. John Wiley & Sons: 2014.
(**49**) Bredas, J.-L., Mind the gap! *Materials Horizons* **2014,** *1* (1), 17-19.
(**50**) Holze, R., Optical and Electrochemical Band Gaps in Mono-, Oligo-, and Polymeric Systems: A Critical Reassessment1. *Organometallics* **2014,** *33* (18), 5033-5042.
(**51**) Armstrong, N. R.; Wang, W.; Alloway, D. M.; Placencia, D.; Ratcliff, E.; Brumbach, M., Organic/organic′ heterojunctions: organic light emitting diodes and organic photovoltaic devices. *Macromolecular rapid communications* **2009,** *30* (9-10), 717-731.
(**52**) Sworakowski, J.; Lipiński, J.; Janus, K., On the reliability of determination of energies of HOMO and LUMO levels in organic semiconductors from electrochemical measurements. A simple picture based on the electrostatic model. *Organic Electronics* **2016,** *33*, 300-310.
(**53**) Van Benschoten, J. J.; Lewis, J. Y.; Heineman, W. R.; Roston, D. A.; Kissinger, P. T., Cyclic voltammetry experiment. *Journal of Chemical Education* **1983,** *60* (9), 772.
(**54**) Aristov, N.; Habekost, A., Cyclic voltammetry-A versatile electrochemical method investigating electron transfer processes. *World J. Chem. Educ* **2015,** *3* (5), 115-119.
(**55**) Cardona, C. M.; Li, W.; Kaifer, A. E.; Stockdale, D.; Bazan, G. C., Electrochemical Considerations for Determining Absolute Frontier Orbital Energy Levels of Conjugated Polymers for Solar Cell Applications. *Advanced Materials* **2011,** *23* (20), 2367-2371.
(**56**) Djurovich, P. I.; Mayo, E. I.; Forrest, S. R.; Thompson, M. E., Measurement of the lowest unoccupied molecular orbital energies of molecular organic semiconductors. *Organic Electronics* **2009,** *10* (3), 515-520.
(**57**) Krause, S.; Casu, M. B.; Schöll, A.; Umbach, E., Determination of transport levels of organic semiconductors by UPS and IPS. *New Journal of Physics* **2008,** *10* (8), 085001.
(**58**) Elgrishi, N.; Rountree, K. J.; McCarthy, B. D.; Rountree, E. S.; Eisenhart, T. T.; Dempsey, J. L., A Practical Beginner's Guide to Cyclic Voltammetry. *Journal of Chemical Education* **2018,** *95* (2), 197-206.
(**59**) Poulos, T. L., Heme enzyme structure and function. *Chem Rev* **2014,** *114* (7), 3919-3962.
(**60**) G H Krause, a.; Weis, E., Chlorophyll Fluorescence and Photosynthesis: The Basics. *Annual Review of Plant Physiology and Plant Molecular Biology* **1991,** *42* (1), 313-349.
(**61**) Roundhill, D., Photochemistry and Photophysics of Metal Porphyrins, Phthalocyanins, and Metal Ions in Supramolecular Systems. In *Photochemistry and Photophysics of Metal Complexes*, Springer: 1994; pp 321-340.
(**62**) Roundhill, D. M., Photochemistry and Photophysics of Metal Porphyrins, Phthalocyanins, and Metal Ions in Supramolecular Systems. In *Photochemistry and Photophysics of Metal Complexes*, Springer US: Boston, MA, 1994; pp 321-340.
(**63**) Di Carlo, G.; Caramori, S.; Casarin, L.; Orbelli Biroli, A.; Tessore, F.; Argazzi, R.; Oriana, A.; Cerullo, G.; Bignozzi, C. A.; Pizzotti, M., Charge Transfer Dynamics in β- and Meso-Substituted Dithienylethylene Porphyrins. *The Journal of Physical Chemistry C* **2017,** *121* (34), 18385-18400.

(**64**) Barker, C. A.; Zeng, X.; Bettington, S.; Batsanov, A. S.; Bryce, M. R.; Beeby, A., Porphyrin, phthalocyanine and porphyrazine derivatives with multifluorenyl substituents as efficient deep-red emitters. *Chemistry* **2007,** *13* (23), 6710-7.
(**65**) Adler, A. D.; Longo, F. R.; Finarelli, J. D.; Goldmacher, J.; Assour, J.; Korsakoff, L., A simplified synthesis for meso-tetraphenylporphine. *The Journal of Organic Chemistry* **1967,** *32* (2), 476-476.
(**66**) Lindsey, J. S.; Schreiman, I. C.; Hsu, H. C.; Kearney, P. C.; Marguerettaz, A. M., Rothemund and Adler-Longo reactions revisited: synthesis of tetraphenylporphyrins under equilibrium conditions. *The Journal of Organic Chemistry* **1987,** *52* (5), 827-836.
(**67**) Drobizhev, M.; Stepanenko, Y.; Dzenis, Y.; Karotki, A.; Rebane, A.; Taylor, P. N.; Anderson, H. L., Extremely Strong Near-IR Two-Photon Absorption in Conjugated Porphyrin Dimers: Quantitative Description with Three-Essential-States Model. *The Journal of Physical Chemistry B* **2005,** *109* (15), 7223-7236.
(**68**) Gouterman, M., Spectra of porphyrins. *Journal of Molecular Spectroscopy* **1961,** *6*, 138-163.
(**69**) Susumu, K.; Therien, M. J., Design of diethynyl porphyrin derivatives with high near infrared fluorescence quantum yields. *Journal of Porphyrins and Phthalocyanines* **2015,** *19* (01-03), 205-218.
(**70**) Barker, C. A.; Zeng, X.; Bettington, S.; Batsanov, A. S.; Bryce, M. R.; Beeby, A., Porphyrin, Phthalocyanine and Porphyrazine Derivatives with Multifluorenyl Substituents as Efficient Deep-Red Emitters. *Chemistry – A European Journal* **2007,** *13* (23), 6710-6717.
(**71**) Sun, Y.; Borek, C.; Hanson, K.; Djurovich, P. I.; Thompson, M. E.; Brooks, J.; Brown, J. J.; Forrest, S. R., Photophysics of Pt-porphyrin electrophosphorescent devices emitting in the near infrared. *Applied Physics Letters* **2007,** *90* (21), 213503.
(**72**) Borek, C.; Hanson, K.; Djurovich, P. I.; Thompson, M. E.; Aznavour, K.; Bau, R.; Sun, Y.; Forrest, S. R.; Brooks, J.; Michalski, L.; Brown, J., Highly Efficient, Near-Infrared Electrophosphorescence from a Pt–Metalloporphyrin Complex. *Angewandte Chemie International Edition* **2007,** *46* (7), 1109-1112.
(**73**) Huang, L.; Park, C.; Fleetham, T.; Li, J., Platinum (II) azatetrabenzoporphyrins for near-infrared organic light emitting diodes. *Applied Physics Letters* **2016,** *109* (23), 233302.
(**74**) Charisiadis, A.; Bagaki, A.; Fresta, E.; Weber, K. T.; Charalambidis, G.; Stangel, C.; Hatzidimitriou, A. G.; Angaridis, P. A.; Coutsolelos, A. G.; Costa, R. D., Peripheral Substitution of Tetraphenyl Porphyrins: Fine-Tuning Self-Assembly for Enhanced Electroluminescence. *ChemPlusChem* **2018,** *83* (4), 254-265.
(**75**) Weber, K. T.; Karikis, K.; Weber, M. D.; Coto, P. B.; Charisiadis, A.; Charitaki, D.; Charalambidis, G.; Angaridis, P.; Coutsolelos, A. G.; Costa, R. D., Cunning metal core: efficiency/stability dilemma in metallated porphyrin based light-emitting electrochemical cells. *Dalton Transactions* **2016,** *45* (34), 13284-13288.
(**76**) Weber, M. D.; Wittmann, J. E.; Burger, A.; Malcıoğlu, O. B.; Segarra-Martí, J.; Hirsch, A.; Coto, P. B.; Bockstedte, M.; Costa, R. D., From White to Red: Electric-Field Dependent Chromaticity of Light-Emitting Electrochemical Cells based on Archetypal Porphyrins. *Advanced Functional Materials* **2016,** *26* (37), 6737-6750.
(**77**) Saxena, K.; Jain, V. K.; Mehta, D. S., A review on the light extraction techniques in organic electroluminescent devices. *Optical Materials* **2009,** *32* (1), 221-233.

(**78**) Yue, Q.; Li, W.; Kong, F.; Li, K., Enhancing the Out-Coupling Efficiency of Organic Light-Emitting Diodes Using Two-Dimensional Periodic Nanostructures. *Advances in Materials Science and Engineering* **2012,** *2012*, 985762.
(**79**) Tang, S.; Murto, P.; Xu, X.; Larsen, C.; Wang, E.; Edman, L., Intense and Stable Near-Infrared Emission from Light-Emitting Electrochemical Cells Comprising a Metal-Free Indacenodithieno[3,2-b]thiophene-Based Copolymer as the Single Emitter. *Chemistry of Materials* **2017,** *29* (18), 7750-7759.
(**80**) Subeesh, M. S.; Shanmugasundaram, K.; Sunesh, C. D.; Chitumalla, R. K.; Jang, J.; Choe, Y., Host–Dopant System To Generate Bright Electroluminescence from Small Organic Molecule Functionalized Light-Emitting Electrochemical Cells. *The Journal of Physical Chemistry C* **2016,** *120* (22), 12207-12217.
(**81**) Slinker, J. D.; Rivnay, J.; Moskowitz, J. S.; Parker, J. B.; Bernhard, S.; Abruña, H. D.; Malliaras, G. G., Electroluminescent devices from ionic transition metal complexes. *Journal of Materials Chemistry* **2007,** *17* (29), 2976-2988.
(**82**) Shen, Y.; Kuddes, D. D.; Naquin, C. A.; Hesterberg, T. W.; Kusmierz, C.; Holliday, B. J.; Slinker, J. D., Improving light-emitting electrochemical cells with ionic additives. *Applied Physics Letters* **2013,** *102* (20), 203305.
(**83**) Costa, R. D.; Pertegás, A.; Ortí, E.; Bolink, H. J., Improving the Turn-On Time of Light-Emitting Electrochemical Cells without Sacrificing their Stability. *Chemistry of Materials* **2010,** *22* (4), 1288-1290.
(**84**) Costa, R. D.; Ortí, E.; Bolink, H. J.; Graber, S.; Schaffner, S.; Neuburger, M.; Housecroft, C. E.; Constable, E. C., Archetype Cationic Iridium Complexes and Their Use in Solid-State Light-Emitting Electrochemical Cells. *Advanced Functional Materials* **2009,** *19* (21), 3456-3463.
(**85**) Benavides, C. M.; Biele, M.; Schmidt, O.; Brabec, C.; Tedde, S., TIPS Pentacene as a Beneficial Interlayer for Organic Photodetectors in Imaging Applications. *IEEE T Electron Dev* **2018,** *65* (4), 1516-1522.
(**86**) Gong, X.; Tong, M.; Xia, Y.; Cai, W.; Moon, J. S.; Cao, Y.; Yu, G.; Shieh, C.-L.; Nilsson, B.; Heeger, A. J., High-detectivity polymer photodetectors with spectral response from 300 nm to 1450 nm. *Science* **2009,** *325* (5948), 1665-1667.
(**87**) Chow, P. C. Y.; Someya, T., Organic Photodetectors for Next-Generation Wearable Electronics. *Advanced Materials* **2020,** *32* (15), 1902045.
(**88**) Miao, J.; Zhang, F., Recent Progress on Photomultiplication Type Organic Photodetectors. *Laser & Photonics Reviews* **2019,** *13* (2), 1800204.
(**89**) Tang, S.; Edman, L., Quest for an Appropriate Electrolyte for High-Performance Light-Emitting Electrochemical Cells. *The Journal of Physical Chemistry Letters* **2010,** *1* (18), 2727-2732.
(**90**) Matsuki, K.; Pu, J.; Takenobu, T., Recent Progress on Light-Emitting Electrochemical Cells with Nonpolymeric Materials. *Advanced Functional Materials* **2020,** *30* (33), 1908641.
(**91**) Pertegás, A.; Tordera, D.; Serrano-Pérez, J. J.; Ortí, E.; Bolink, H. J., Light-Emitting Electrochemical Cells Using Cyanine Dyes as the Active Components. *Journal of the American Chemical Society* **2013,** *135* (48), 18008-18011.
(**92**) Chen, G.-Y.; Chang, B.-R.; Shih, T.-A.; Lin, C.-H.; Lo, C.-L.; Chen, Y.-Z.; Liu, Y.-X.; Li, Y.-R.; Guo, J.-T.; Lu, C.-W.; Yang, Z.-P.; Su, H.-C., Cationic IrIII Emitters with Near-Infrared

Emission Beyond 800 nm and Their Use in Light-Emitting Electrochemical Cells. *Chemistry – A European Journal* **2019,** *25* (21), 5489-5497.
(**93**) Liu, Y.-X.; Yi, R.-H.; Lin, C.-H.; Yang, Z.-P.; Lu, C.-W.; Su, H.-C., Near-infrared light-emitting electrochemical cells based on the excimer emission of a cationic iridium complex. *Journal of Materials Chemistry C* **2020,** *8* (41), 14378-14385.
(**94**) Sommer, J. R.; Farley, R. T.; Graham, K. R.; Yang, Y.; Reynolds, J. R.; Xue, J.; Schanze, K. S., Efficient Near-Infrared Polymer and Organic Light-Emitting Diodes Based on Electrophosphorescence from (Tetraphenyltetranaphtho[2,3]porphyrin)platinum(II). *ACS Applied Materials & Interfaces* **2009,** *1* (2), 274-278.
(**95**) Ostrowski, J. C.; Susumu, K.; Robinson, M. R.; Therien, M. J.; Bazan, G. C., Near-Infrared Electroluminescent Light-Emitting Devices Based on Ethyne-Bridged Porphyrin Fluorophores. *Advanced Materials* **2003,** *15* (15), 1296-1300.
(**96**) Fenwick, O.; Sprafke, J. K.; Binas, J.; Kondratuk, D. V.; Di Stasio, F.; Anderson, H. L.; Cacialli, F., Linear and Cyclic Porphyrin Hexamers as Near-Infrared Emitters in Organic Light-Emitting Diodes. *Nano Letters* **2011,** *11* (6), 2451-2456.
(**97**) Weber, M. D.; Nikolaou, V.; Wittmann, J. E.; Nikolaou, A.; Angaridis, P. A.; Charalambidis, G.; Stangel, C.; Kahnt, A.; Coutsolelos, A. G.; Costa, R. D., Benefits of using BODIPY–porphyrin dyads for developing deep-red lighting sources. *Chemical Communications* **2016,** *52* (8), 1602-1605.
(**98**) Roncali, J., Molecular Engineering of the Band Gap of π-Conjugated Systems: Facing Technological Applications. *Macromolecular Rapid Communications* **2007,** *28* (17), 1761-1775.
(**99**) Zych, D.; Slodek, A.; Matussek, M.; Filapek, M.; Szafraniec-Gorol, G.; Maślanka, S.; Krompiec, S.; Kotowicz, S.; Schab-Balcerzak, E.; Smolarek, K.; Maćkowski, S.; Olejnik, M.; Danikiewicz, W., 4′-Phenyl-2,2′:6′,2″-terpyridine derivatives-synthesis, potential application and the influence of acetylene linker on their properties. *Dyes and Pigments* **2017,** *146*, 331-343.
(**100**) Liu, Y.; Zhang, Z.; Feng, S.; Li, M.; Wu, L.; Hou, R.; Xu, X.; Chen, X.; Bo, Z., Exploiting noncovalently conformational locking as a design strategy for high performance fused-ring electron acceptor used in polymer solar cells. *Journal of the American Chemical Society* **2017,** *139* (9), 3356-3359.
(**101**) Huang, H.; Yang, L.; Facchetti, A.; Marks, T. J., Organic and Polymeric Semiconductors Enhanced by Noncovalent Conformational Locks. *Chem Rev* **2017,** *117* (15), 10291-10318.
(**102**) Dou, L.; Liu, Y.; Hong, Z.; Li, G.; Yang, Y., Low-Bandgap Near-IR Conjugated Polymers/Molecules for Organic Electronics. *Chem Rev* **2015,** *115* (23), 12633-12665.
(**103**) Cheng, Y.-J.; Yang, S.-H.; Hsu, C.-S., Synthesis of Conjugated Polymers for Organic Solar Cell Applications. *Chem Rev* **2009,** *109* (11), 5868-5923.
(**104**) Li, Y.; Li, H.; Chen, H.; Wan, Y.; Li, N.; Xu, Q.; He, J.; Chen, D.; Wang, L.; Lu, J., Controlling Crystallite Orientation of Diketopyrrolopyrrole-Based Small Molecules in Thin Films for Highly Reproducible Multilevel Memory Device: Role of Furan Substitution. *Advanced Functional Materials* **2015,** *25* (27), 4246-4254.
(**105**) Mizuguchi, J.; Grubenmann, A.; Wooden, G.; Rihs, G., Structures of 3,6-diphenylpyrrolo[3,4-c]pyrrole-1,4-dione and 2,5-dimethyl-3,6-diphenylpyrrolo[3,4-c]pyrrole-1,4-dione. *Acta Crystallographica Section B* **1992,** *48* (5), 696-700.
(**106**) Lindsey, J. S., The synthesis of meso-substituted porphyrins. In *Metalloporphyrins Catalyzed Oxidations*, Springer: 1994; pp 49-86.

(**107**) Favereau, L.; Cnossen, A.; Kelber, J. B.; Gong, J. Q.; Oetterli, R. M.; Cremers, J.; Herz, L. M.; Anderson, H. L., Six-Coordinate Zinc Porphyrins for Template-Directed Synthesis of Spiro-Fused Nanorings. *Journal of the American Chemical Society* **2015,** *137* (45), 14256-14259.
(**108**) Guo, J.; Li, X.-L.; Nie, H.; Luo, W.; Gan, S.; Hu, S.; Hu, R.; Qin, A.; Zhao, Z.; Su, S.-J.; Tang, B. Z., Achieving High-Performance Nondoped OLEDs with Extremely Small Efficiency Roll-Off by Combining Aggregation-Induced Emission and Thermally Activated Delayed Fluorescence. *Advanced Functional Materials* **2017,** *27* (13), 1606458.
(**109**) Stender, B.; Völker, S. F.; Lambert, C.; Pflaum, J., Optoelectronic Processes in Squaraine Dye-Doped OLEDs for Emission in the Near-Infrared. *Advanced Materials* **2013,** *25* (21), 2943-2947.
(**110**) Mäkinen, A.; Hill, I.; Kafafi, Z., Vacuum level alignment in organic guest-host systems. *Journal of applied physics* **2002,** *92* (3), 1598-1603.
(**111**) McNeill, C. R.; Greenham, N. C., Conjugated-Polymer Blends for Optoelectronics. *Advanced Materials* **2009,** *21* (38-39), 3840-3850.
(**112**) Kim, J.-S.; Lu, L.; Sreearunothai, P.; Seeley, A.; Yim, K.-H.; Petrozza, A.; Murphy, C. E.; Beljonne, D.; Cornil, J.; Friend, R. H., Optoelectronic and Charge Transport Properties at Organic–Organic Semiconductor Interfaces: Comparison between Polyfluorene-Based Polymer Blend and Copolymer. *J. Am. Chem. Soc.* **2008,** *130* (39), 13120-13131.
(**113**) Kabra, D.; Lu, L. P.; Song, M. H.; Snaith, H. J.; Friend, R. H., Efficient Single-Layer Polymer Light-Emitting Diodes. *Adv. Mater.* **2010,** *22* (29), 3194-3198.
(**114**) Marcilla, R.; Mecerreyes, D.; Winroth, G.; Brovelli, S.; Yebra, M. d. M. R.; Cacialli, F., Light-emitting electrochemical cells using polymeric ionic liquid/polyfluorene blends as luminescent material. *Appl. Phys. Lett.* **2010,** *96* (4), 043308.
(**115**) Zampetti, A.; Minotto, A.; Squeo, B. M.; Gregoriou, V. G.; Allard, S.; Scherf, U.; Chochos, C. L.; Cacialli, F., Highly Efficient Solid-State Near-infrared Organic Light-Emitting Diodes incorporating A-D-A Dyes based on α,β-unsubstituted "BODIPY" Moieties. *Scientific Reports* **2017,** *7* (1), 1611.
(**116**) Xiong, W.; Tang, S.; Murto, P.; Zhu, W.; Edman, L.; Wang, E., Combining Benzotriazole and Benzodithiophene Host Units in Host–Guest Polymers for Efficient and Stable Near-Infrared Emission from Light-Emitting Electrochemical Cells. *Advanced Optical Materials* **2019,** *7* (15), 1900280.
(**117**) Wei, Y.-C.; Wang, S. F.; Hu, Y.; Liao, L.-S.; Chen, D.-G.; Chang, K.-H.; Wang, C.-W.; Liu, S.-H.; Chan, W.-H.; Liao, J.-L.; Hung, W.-Y.; Wang, T.-H.; Chen, P.-T.; Hsu, H.-F.; Chi, Y.; Chou, P.-T., Overcoming the energy gap law in near-infrared OLEDs by exciton–vibration decoupling. *Nature Photonics* **2020,** *14* (9), 570-577.
(**118**) Tuong Ly, K.; Chen-Cheng, R.-W.; Lin, H.-W.; Shiau, Y.-J.; Liu, S.-H.; Chou, P.-T.; Tsao, C.-S.; Huang, Y.-C.; Chi, Y., Near-infrared organic light-emitting diodes with very high external quantum efficiency and radiance. *Nature Photonics* **2016,** *11*, 63.
(**119**) Thimsen, E.; Sadtler, B.; Berezin Mikhail, Y., Shortwave-infrared (SWIR) emitters for biological imaging: a review of challenges and opportunities. In *Nanophotonics*, 2017; Vol. 6, p 1043.
(**120**) Tuong Ly, K.; Chen-Cheng, R.-W.; Lin, H.-W.; Shiau, Y.-J.; Liu, S.-H.; Chou, P.-T.; Tsao, C.-S.; Huang, Y.-C.; Chi, Y., Near-infrared organic light-emitting diodes with very high external quantum efficiency and radiance. *Nature Photonics* **2017,** *11* (1), 63-68.

(**121**) Chen, W.-C.; Sukpattanacharoen, C.; Chan, W.-H.; Huang, C.-C.; Hsu, H.-F.; Shen, D.; Hung, W.-Y.; Kungwan, N.; Escudero, D.; Lee, C.-S.; Chi, Y., Modulation of Solid-State Aggregation of Square-Planar Pt(II) Based Emitters: Enabling Highly Efficient Deep-Red/Near Infrared Electroluminescence. *Advanced Functional Materials* **2020,** *30* (25), 2002494.
(**122**) Harriman, A., Luminescence of porphyrins and metalloporphyrins. Part 1.—Zinc(II), nickel(II) and manganese(II) porphyrins. *Journal of the Chemical Society, Faraday Transactions 1: Physical Chemistry in Condensed Phases* **1980,** *76* (0), 1978-1985.
(**123**) de Amorim Lima, N. M.; Camargo Avila, H. J.; do Nascimento Marchiori, C. F.; Gondim Sampaio, S.; Ferreira Mota, J. P.; Gomes Pereira Ribeiro, V.; da Silva Clemente, C.; Mele, G.; Cremona, M.; Mazzetto, S. E., Light-emitting porphyrin derivative obtained from a subproduct of the cashew nut shell liquid: a promising material for OLED applications. *Materials* **2019,** *12* (7), 1063.
(**124**) Tang, S.; Buchholz, H. A.; Edman, L., On the selection of a host compound for efficient host-guest light-emitting electrochemical cells. *Journal of Materials Chemistry C* **2015,** *3* (31), 8114-8120.
(**125**) Freeman, D. M. E.; Minotto, A.; Duffy, W.; Fallon, K. J.; McCulloch, I.; Cacialli, F.; Bronstein, H., Highly red-shifted NIR emission from a novel anthracene conjugated polymer backbone containing Pt(ii) porphyrins. *Polymer Chemistry* **2016,** *7* (3), 722-730.
(**126**) Rösch, U.; Yao, S.; Wortmann, R.; Würthner, F., Fluorescent H-Aggregates of Merocyanine Dyes. *Angewandte Chemie International Edition* **2006,** *45* (42), 7026-7030.
(**127**) Holliday, S.; Ashraf, R. S.; Nielsen, C. B.; Kirkus, M.; Röhr, J. A.; Tan, C.-H.; Collado-Fregoso, E.; Knall, A.-C.; Durrant, J. R.; Nelson, J.; McCulloch, I., A Rhodanine Flanked Nonfullerene Acceptor for Solution-Processed Organic Photovoltaics. *Journal of the American Chemical Society* **2015,** *137* (2), 898-904.
(**128**) Li, L.; Zhang, F.; Wang, W.; Fang, Y.; Huang, J., Revealing the working mechanism of polymer photodetectors with ultra-high external quantum efficiency. *Physical Chemistry Chemical Physics* **2015,** *17* (45), 30712-30720.
(**129**) Murto, P.; Genene, Z.; Benavides, C. M.; Xu, X.; Sharma, A.; Pan, X.; Schmidt, O.; Brabec, C. J.; Andersson, M. R.; Tedde, S. F.; Mammo, W.; Wang, E., High Performance All-Polymer Photodetector Comprising a Donor–Acceptor–Acceptor Structured Indacenodithiophene–Bithieno[3,4-c]Pyrroletetrone Copolymer. *ACS Macro Letters* **2018,** *7* (4), 395-400.
(**130**) Huang, Y.; Li, L.; Peng, X.; Peng, J.; Cao, Y., Solution processed small molecule bulk heterojunction organic photovoltaics based on a conjugated donor–acceptor porphyrin. *Journal of Materials Chemistry* **2012,** *22* (41), 21841-21844.
(**131**) Edman, L., Bringing light to solid-state electrolytes: The polymer light-emitting electrochemical cell. *Electrochim Acta* **2005,** *50* (19), 3878-3885.
(**132**) Xue, J.; Li, C.; Xin, L.; Duan, L.; Qiao, J., High-efficiency and low efficiency roll-off near-infrared fluorescent OLEDs through triplet fusion. *Chemical Science* **2016,** *7* (4), 2888-2895.

APPENDIX

SYNTHESIS OF POR4RH

Scheme A1. Synthesis of compound **15**.

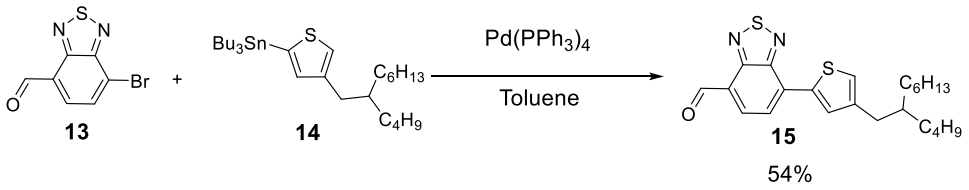

To an argon degassed solution of **13** (1.05 g, 4.32 mmol) and **14** (3.51 g, 6.48 mmol) in dry toluene (50 mL) was added $Pd(PPh_3)_4$ (0.498 g, 0.431 mmol) and the resulting reaction mixture was stirred overnight at 100 °C. The mixture was allowed to cool to room temperature and passed through a pad of silica. Purification of the crude residue by flash column chromatography over silica gel (EtOAc/hexane 5:95) yielded compound **15** (965 mg, 54%) as a yellow solid. ^{1}H NMR (400 MHz, $CDCl_3$) δ = 10.71 (s, 1H), 8.21 (d, J = 7.5 Hz, 1H), 8.13 (s, 1H), 7.97 (d, J = 7.5, 1H), 7.15 (s, 1H), 2.64 (d, J = 6.8 Hz, 2H), 1.73-1.64 (m, 1H), 1.41–1.20 (m, 16H), 0.97–0.80 (m, 6H) ppm. ^{13}C NMR (101 MHz, $CDCl_3$) δ = 188.50, 153.71, 152.31, 143.65, 137.86, 133.34, 132.68, 132.15, 125.52, 125.36, 123.78, 38.90, 34.93, 33.29, 32.98, 31.89, 29.69, 28.85, 26.58, 23.06, 22.68, 14.16, 14.11 ppm.

Scheme A2. Synthesis of compound **16**.

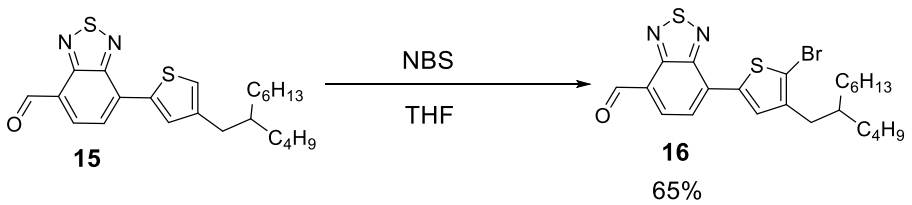

To a stirring solution of **15** (905 mg, 2.18 mmol) in THF (50 mL) was added *N*-bromosuccinimide (427 mg, 2.40 mmol) and the mixture was allowed to react overnight in the dark. The reaction mixture was quenched with saturated aqueous sodium thiosulfate, extracted with ethyl acetate (3 x

150 mL) and the combined organic phase was dried over $MgSO_4$. Purification of the crude residue by flash column chromatography over silica gel (EtOAc/hexane 5:95) yielded **16** (705 mg, 65 %) as a yellow solid. ^{1}H NMR (400 MHz, $CDCl_3$) δ = 10.73 (s, 1H), 8.22 (d, J = 7.7 Hz, 1H), 7.94–7.90 (m, 2H), 2.59 (d, J = 7.2 Hz, 2H), 1.79-1.71 (m, 1H), 1.37–1.23 (m, 16H), 0.93–0.83 (m, 6H) ppm. ^{13}C NMR (101 MHz, $CDCl_3$) δ = 188.44, 153.67, 152.12, 142.88, 137.46, 132.55, 132.26, 131.09, 125.60, 123.33, 115.65, 38.56, 34.21, 33.31, 33.04, 31.88, 29.67, 28.76, 26.49, 23.05, 22.67, 14.13, 14.11 ppm.

Scheme A3. Synthesis of **Por4TBT**.

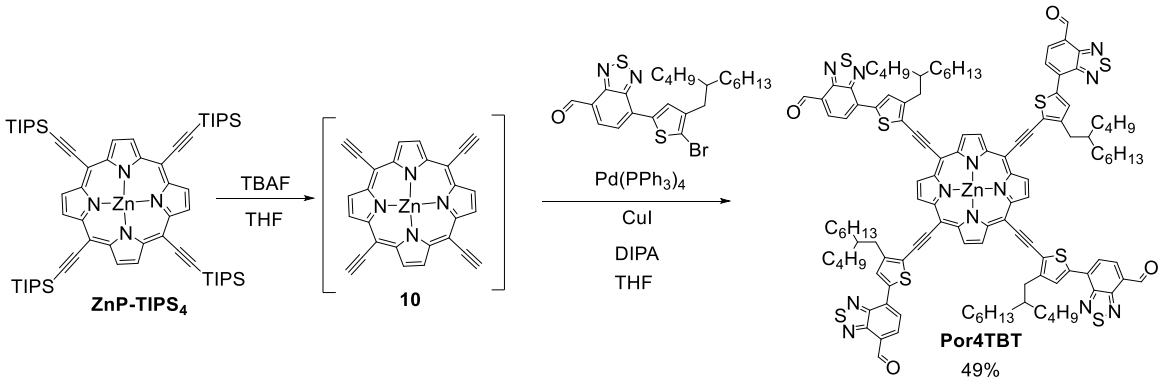

To a stirred solution of **ZnP-TIPS$_4$** (194 mg, 0.177 mmol) in dry THF (40 mL) under nitrogen atmosphere was added slowly a TBAF solution (3.00 mL, 1.0 M in THF, 3.00 mmol). The resulting mixture was allowed to stir at ambient temperature for 30 min, after which time cold 50% aqueous ethanol (100 mL) was introduced to the flask. Concentration of the crude mixture under reduced pressure resulted in the trituration of the desilylated intermediate. The precipitate was carefully collected under a blanket of nitrogen, and washed sequentially with H_2O, ethanol and CH_2Cl_2. Finally, the intermediate was dried under high vacuum for 1 h and was combined with **16** (701 mg, 1.42 mmol), CuI (22.9 mg, 0.120 mmol), DIPA (2 mL) and THF (20 mL). The contents of the flask were purged with argon for 10 min and $Pd(PPh_3)_4$ (45.1 mg, 0.039 mmol) was added and the resulting reaction mixture was stirred overnight at 50 °C. The mixture was allowed to cool to room temperature and passed through a pad of silica. Purification of the resulting crude residue by flash column chromatography over silica gel (toluene/pyridine 99:1) yielded **Por4TBT** (185 mg, 49%) as a purple solid. ^{1}H NMR (600 MHz, pyridine-d_5) δ = 10.94 (s, 4H), 9.74 (s, 8H), 8.53 (s, 4H), 8.21 (d, J = 7.2 Hz, 4H), 8.13 (d, J = 7.2 Hz, 4H), 3.76-3.66 (m,8H), 2.54–2.41 (m, 4H), 2.19–1.65 (m, 30H), 1.63-1.27 (m, 34H), 1.07 (t, J = 7.4 Hz, 12H), 0.97–0.75 (m, 12H) ppm. HRMS (MALDI-TOF) calcd for $C_{120}H_{124}N_{12}O_4S_8Zn$ $[M+H]^+$2116.6920; found: 2116.76523.

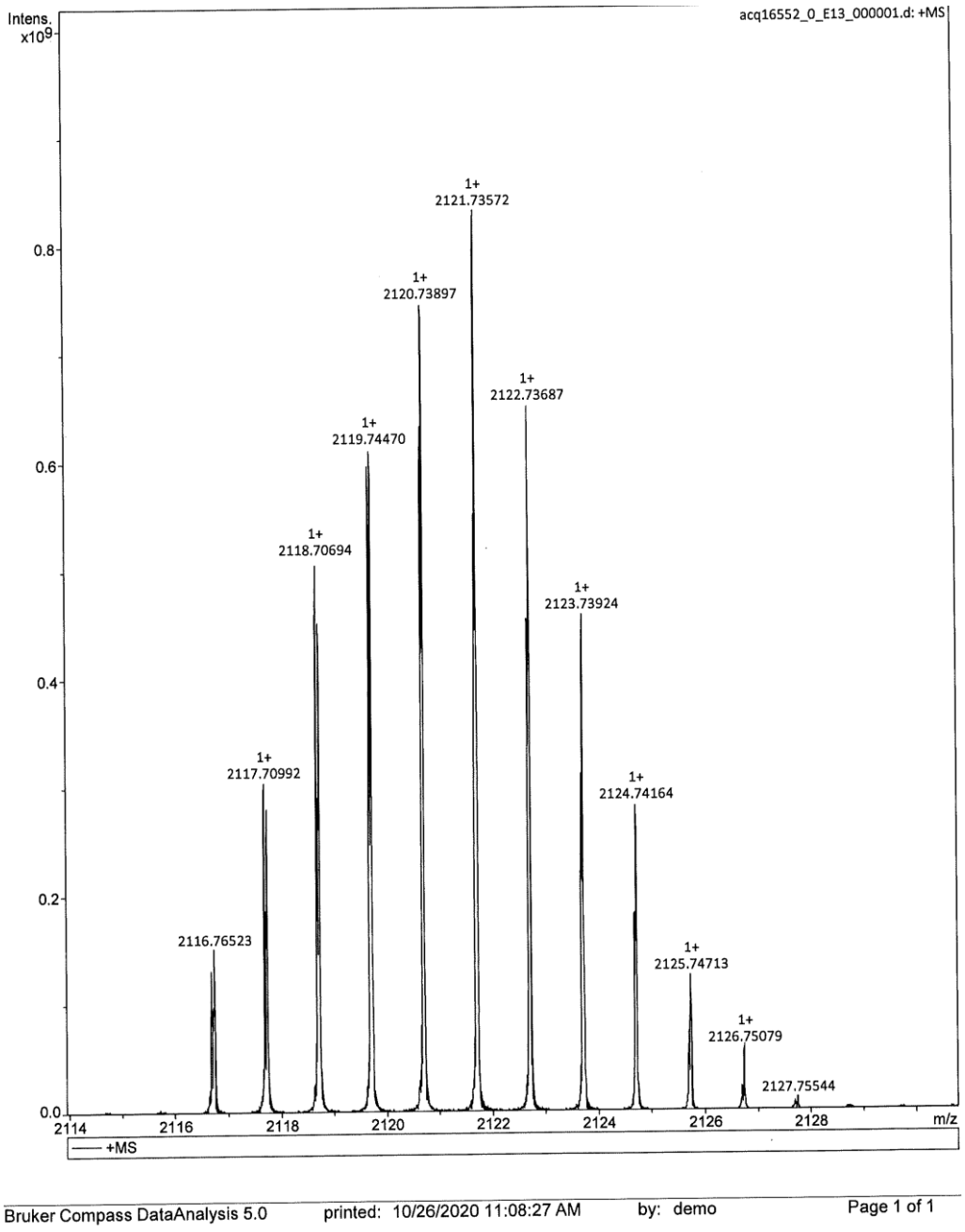

MALDI-TOF of **Por4TBT**

Scheme A4. Synthesis of Por4Rh**.**

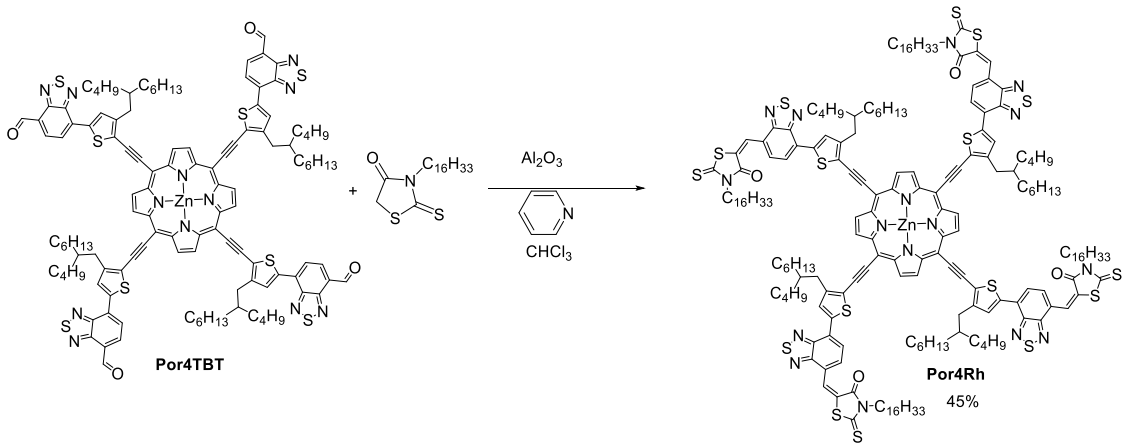

A reaction mixture consisting of Por4TBT (140 mg, 0.066 mmol) alkylated rhodanine (181 mg, 0.506 mmol), Al_2O_3 (277 mg, 2.72 mmol), pyridine (6 mL), and DIPA(4 mL) in $CHCl_3$ (30 mL) was stirred overnight at 50°C. The reaction mixture was allowed to cool to room temperature and passed through a pad of silica. Purification of the crude residue by SEC chromatography (toluene/pyridine, 99:1) yielded Por4Rh (105 mg, 45%) as a dark purple solid. ^{1}H NMR (600 MHz, pyridine-d_5) δ = 9.46 (br s, 8H), 8.47 (br s, 4H), 8.01 (br s, 4H), 7.55 (br s, 4H), 4.40 (m, 4H), 3.76 (br s, 8H), 2.47 (br s, 4H), 2.17-0.84 (m, 220H) ppm. HRMS (MALDI-TOF) calcd for $C_{196}H_{256}N_{16}O_4S_{16}Zn$ $[M+H]^+$ =3473.5138; Found : 3473.5345.

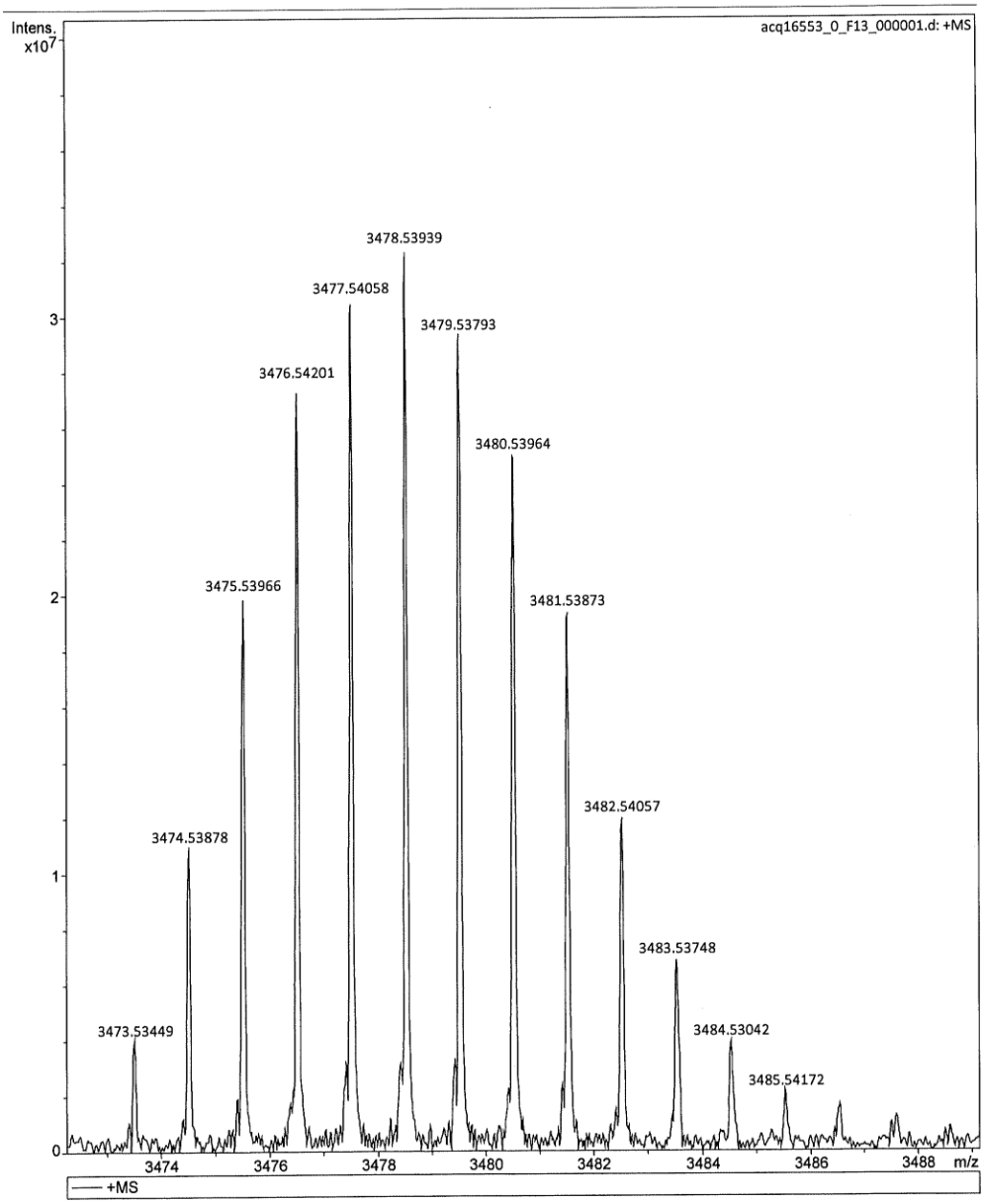

MALDI-TOF of **Por4Rh**.

PL of Por4CPDT and Por4IC

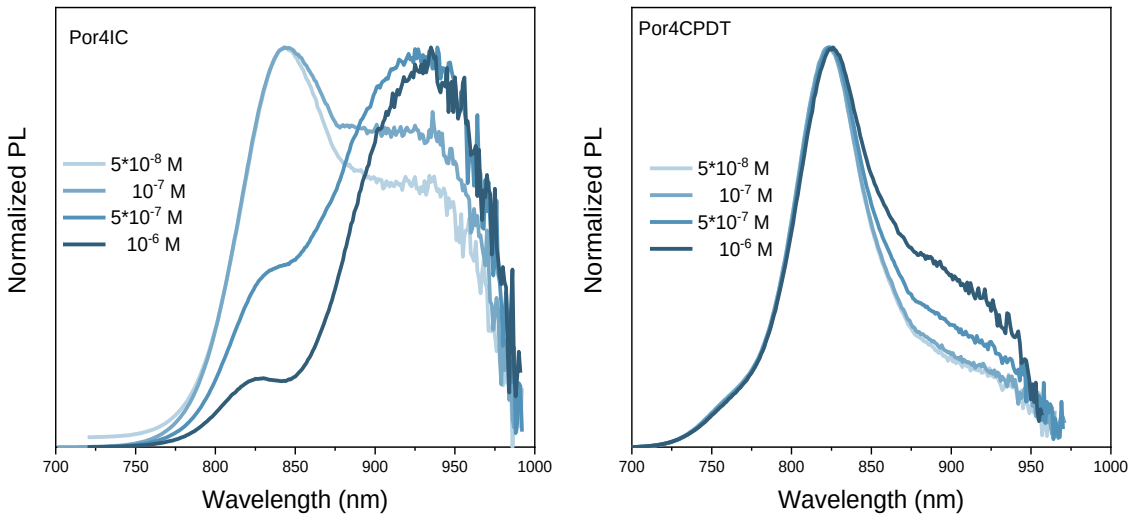

Figure A1. Normalized PL spectra of (a) Por4CPDT and (b) Por4IC in varying concentrations as identified in the legend. The solvent employed was toluene/pyridine 99:1.

DFT Calculated Orbitals Of ZnP(TDPP)$_4$, POR4NT and POR4IC

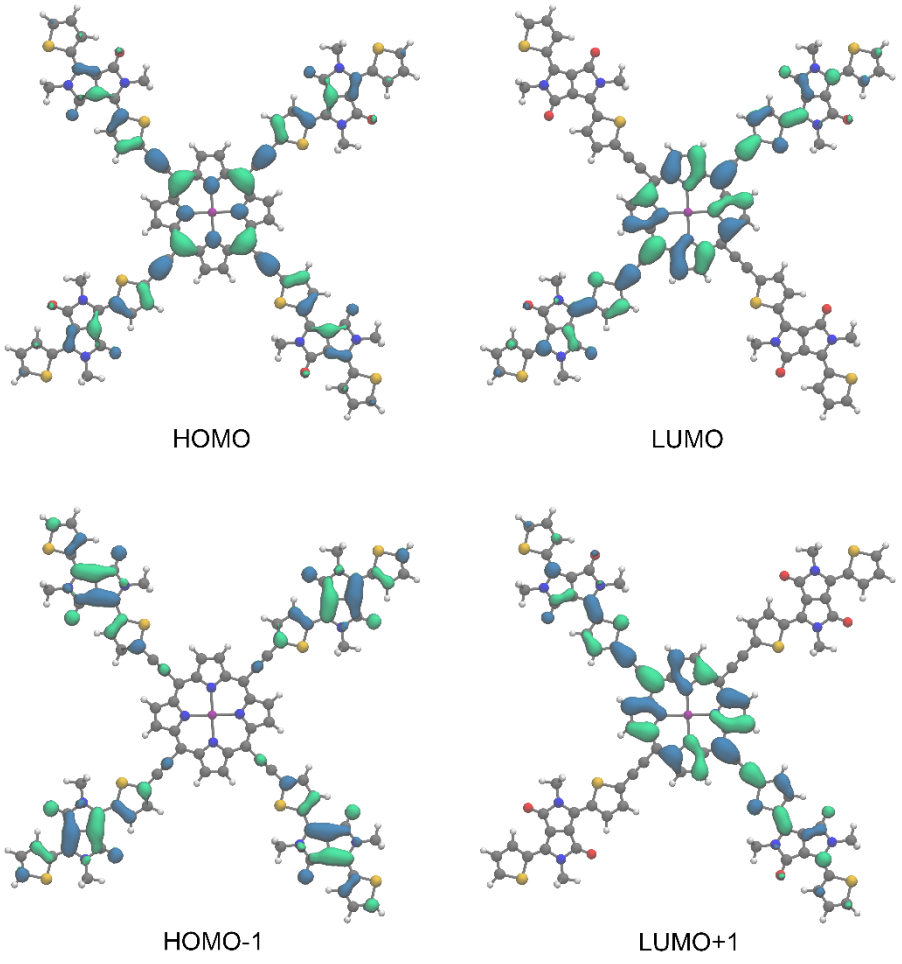

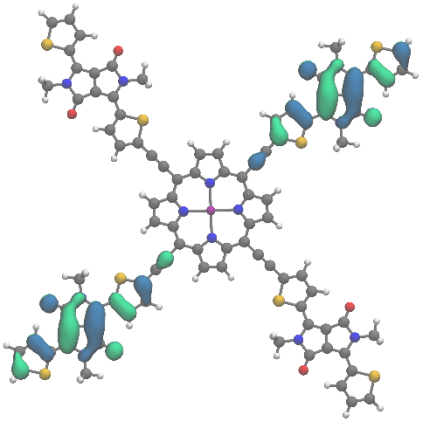

HOMO-2

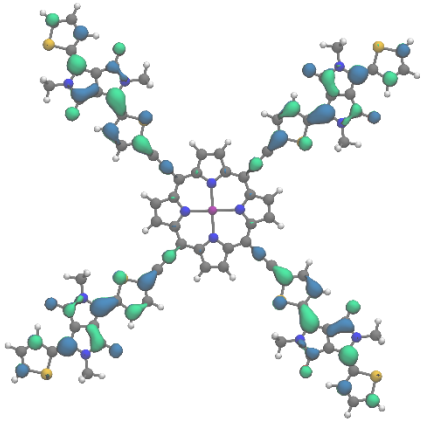

LUMO+2

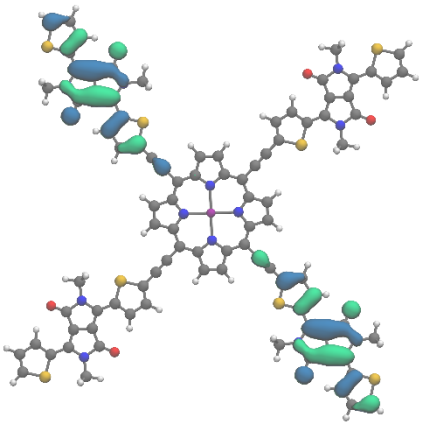

HOMO-3

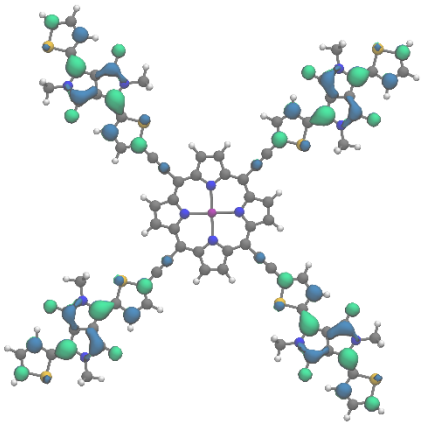

LUMO+3

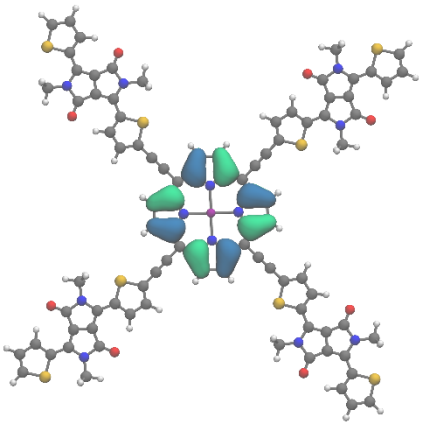

HOMO-4

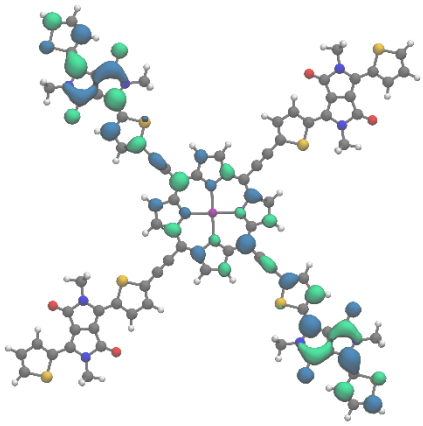

LUMO+4

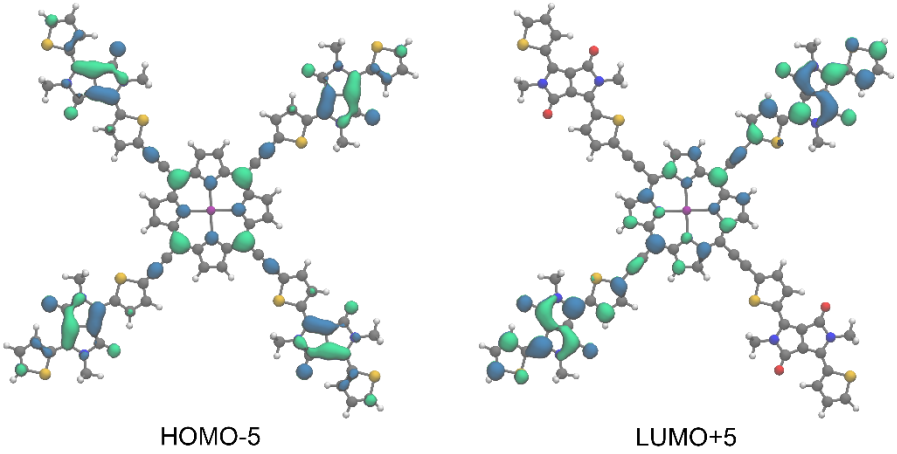

Figure A2. DFT-calculated frontier orbitals describing the electronic ground state of $ZnP(TDPP)_4$, as obtained using CAM-B3LYP functional and PCM with toluene as solvent.

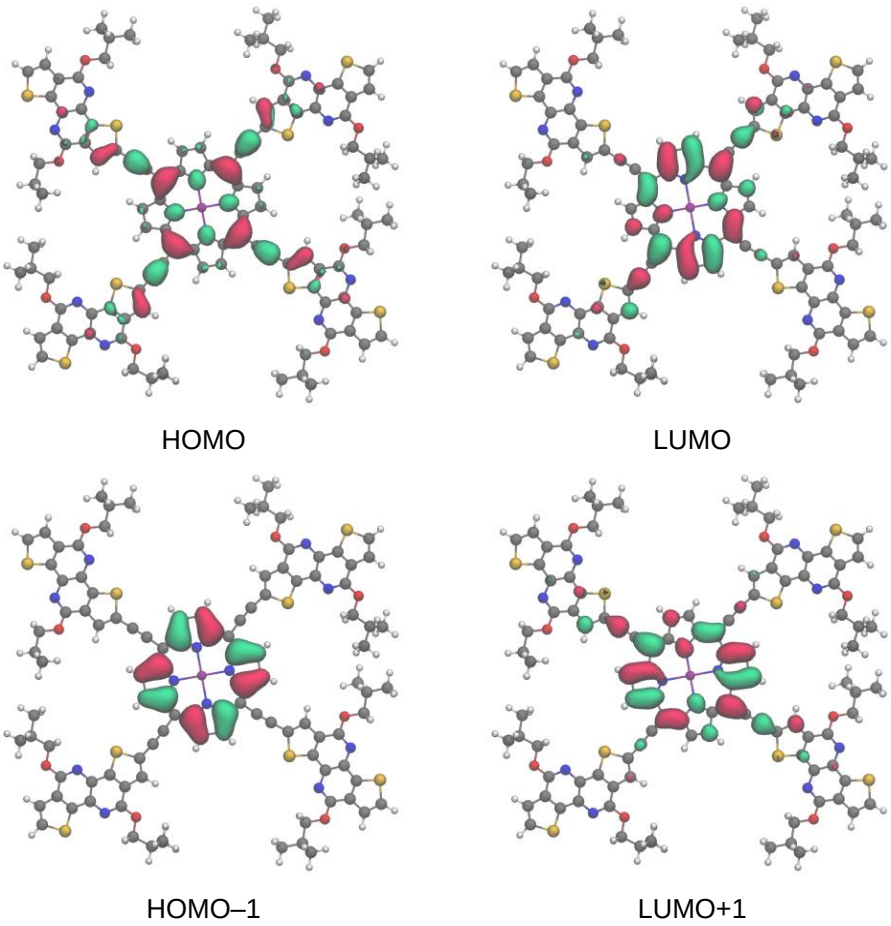

Figure A3. The frontier orbitals of the electronic ground state of the C_{4h} point group conformation of Por4NT with isobutoxy side chains in toluene, as calculated using the CAM-B3LYP functional.

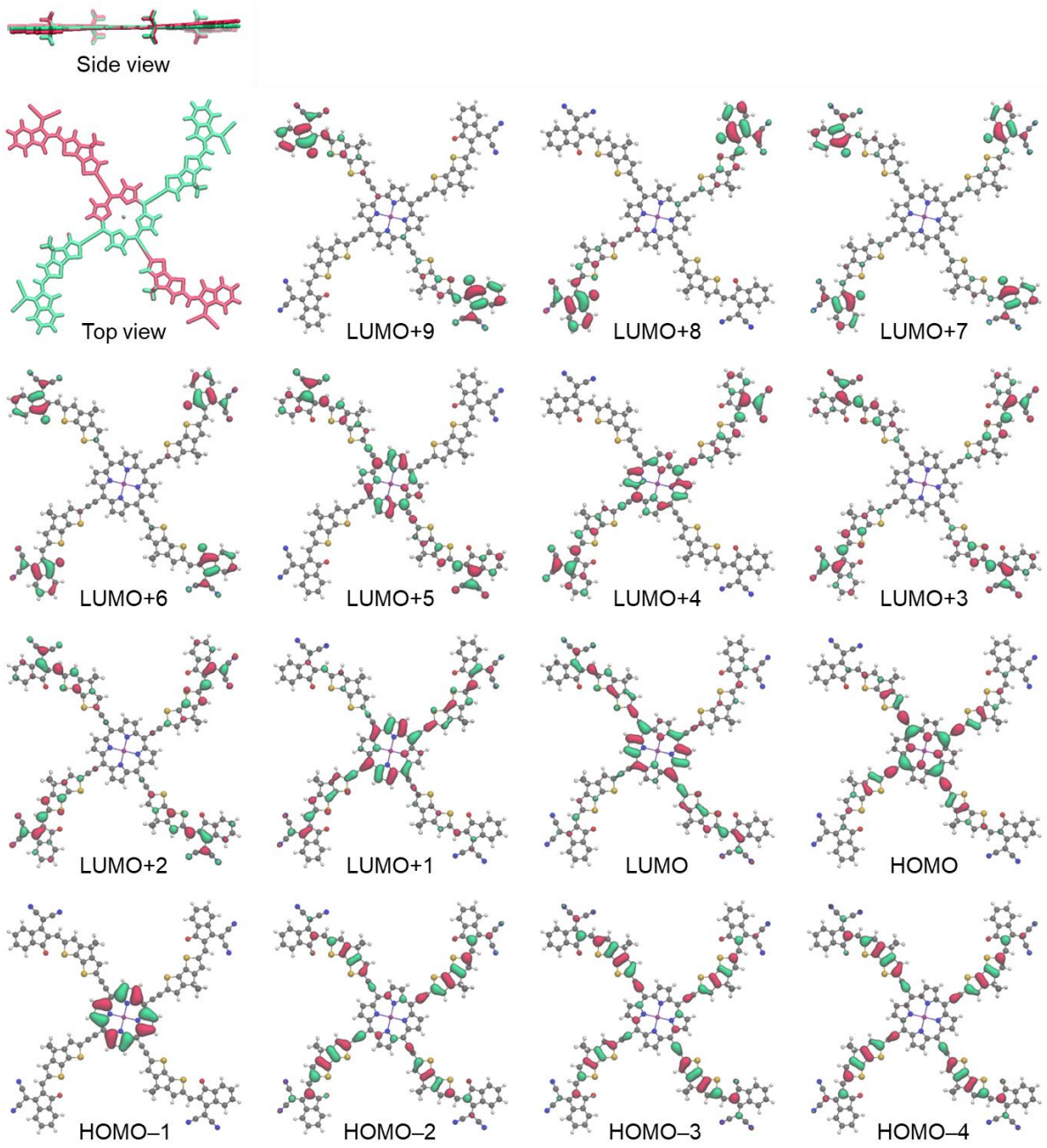

Figure A4. Superimposed geometry-optimized structures of Por4IC (top left), as calculated in gas phase (green structure) and using PCM with toluene as solvent (red structure). Optically accessible frontier orbitals describing the electronic ground state of Por4IC in toluene